The Dissertation Committee for Puneet Kohli Certifies that this is the approved version of the following dissertation:

Fundamental Understanding of the Physics and Modeling of Boron Source/Drain Extension Evolution During CMOS Device Fabrication

Committee:

_____

Sanjay Banerjee, Supervisor

_____

Amitabh Jain, Co-Supervisor

_____

Dim-Lee Kwong

_____

Michael Becker

_____

Chih-Kang Shih

Fundamental Understanding of the Physics and Modeling of Boron Source/Drain Extension Evolution During CMOS Device Fabrication

by

Puneet Kohli, B.E. ; M.S.

Dissertation

Presented to the Faculty of the Graduate School of

The University of Texas at Austin

in Partial Fulfillment

of the Requirements

for the Degree of

Doctor of Philosophy

The University of Texas at Austin

December, 2003

Acknowledgements

I would first like to thank my advisor, Professor Sanjay Banerjee for his support and encouragement during my years at University of Texas at Austin. The academic atmosphere in which extensive collaboration is possible has been a very special part of my experience working under his tutelage and I appreciate it.

I would also like to thank Dr. Amitabh Jain, my co-supervisor, for his continued interest and guidance through the course of my research. I have greatly benefitted from his insight and experience.

I extend my sincere thanks to Professor Scott Dunham for introducing me to process modeling, and that too in a very enjoyable and rewarding manner.

I am indebted to Professors Dim-Lee Kwong, Michael Becker, Chih-Kang Shih for agreeing to serve on my committee and providing constructive comments.

I would like to acknowledge that this work has been supported in part by Texas Instruments, Semiconductor Research Corporation, and the Texas Advanced Technology and Research Program.

I would like to thank Dr. S. Chakravarthi, a friend and a critic, for his valuable feedback.

My heartfelt gratitude to my colleagues at International Sematech for their support while I was writing this dissertation.

I would like to convey special thanks to all my friends and colleagues for making my graduate school experience very enjoyable and memorable.

My sincere thanks to Akbar for his love and support.

This work is dedicated to my parents, my sister, and my friends, Bala and Jay, for their continued love and support during all these years.

Fundamental Understanding of the Physics and Modeling of Boron Source/Drain Extension Evolution During CMOS Device Fabrication

Publication No. _____

Puneet Kohli, Ph.D.
The University of Texas at Austin, 2003

Supervisor(s): Sanjay K. Banerjee, Amitabh Jain

Improvements in the integrated circuit performance over the past three decades have been mainly possible by the downward scaling of device dimensions. Device scaling requires that all lateral and vertical dimensions of the transistor be scaled. In the last decade, in order to continue conventional scaling of the source/drain junctions, the semiconductor industry has relied heavily on decreasing the implant energy, and also on minimizing the thermal budget of the activation anneal. With Transient Enhanced Diffusion less pronounced for low implant energies and sharper anneal temperature profiles, interactions of dopant atoms and point defects with surface films and interfaces are becoming of paramount importance in determining the concentrations of dopants and point defects, and therefore the resulting device structures. A nitride spacer with an underlying deposited TEOS oxide, that behaves as a convenient etch stop layer, is a popular choice for sidewall spacer in modern CMOS process flows. In this work

the effect of the silicon nitride spacer process on the B profile in silicon and the related dose loss of B from the Si into the silicon dioxide has been investigated. This is reflected as a dramatic decrease in the junction depth. The influence of the nitride spacer chemistry on B dose loss from the Si has also been investigated. The different nitride chemistries result in different B dose loss. A new model that predicts B junction depths and dose loss during fabrication of ultra-shallow junctions has been developed. A study of the interactions of dopant atoms and silicon point defects with silicon oxide films during annealing for ultra-shallow junction formation has been included. A new method for activation of source/drain junctions by microwave annealing has been proposed.

Table of Contents

List of Tables

List of Figures

Chapter 1

Introduction

In the semiconductor industry the most dominant device used today is the Si based metal oxide semiconductor field effect transistor (MOSFET). Improvements in the computer industry over the past 30 years have relied heavily on the ability to increase the speed of the silicon MOSFET through the downward scaling of all vertical and lateral dimensions of the transistor [1]. The scaling of the device dimensions not only leads to faster devices but also allows larger and more complex circuits to be implemented on a smaller area. However, scaling the dimensions of the source and drain regions decreases the amount of free charge and can result in an unacceptable increase in device resistance. Therefore, in order to scale down the MOS transistor the active dopant concentrations in the source, drain and channel regions must increase while the vertical and lateral dimensions are decreased. For the source and drain regions, a highly abrupt, high concentration profile is needed for low device resistance. The maximum doping concentration is extremely important, since higher dopant charge permits shallower junctions while still maintaining low sheet resistance. Equally important is the abruptness of the source/drain regions. These regions must be highly abrupt to permit current to spread out quickly once it enters these regions [1].

The main technique in forming shallow junctions is to use low energy ion implantation combined with rapid thermal anneal (RTA)/Spike anneal. Decreasing the implant energy puts the excess Si interstitials closer to the surface. The surface acts as an efficient sink for the interstitials, thus reducing transient enhanced diffusion (TED), which results from the interaction of excess interstitials with the dopant atoms. For implant energies below 1 keV, TED can be nearly eliminated. Increasing the ramp rate of anneal, too, has greatly reduced TED effects. With TED less pronounced for low implant energies and sharper anneal temperature profiles, surface reactions and related processes emerge to dominate the formation of ultra-shallow junctions. Interactions of dopant atoms and point defects with surface films and interfaces are becoming of paramount importance in determining the concentrations of dopants and point defects, and therefore the resulting diffusion profiles [2]. Also it has been reported that because the dopants reside so close to the surface after implantation, they out-diffuse from the Si lattice into the process chamber or diffuse into the screen oxide [2]. More recently, large amounts of "dose loss" have been observed at the Si/SiO_2 interface. It is not uncommon for 50% of a shallow implant dose to be trapped and remain electrically inactive at this interface [3]. The resulting increase of series resistance becomes a problem when the channel length shrinks below 0.25μm. In principle one might simply implant more dopants, but the dopants migrate in all directions and an increased dose means more diffuse (not abrupt) profiles [4]. Also the duration of TED increases with implant dose and energy, although the instantaneous enhancement is usually almost independent of implant

conditions. Electrically inactive dopant atoms can appear well below solid solubility limits during TED [4]. Increased implant dose also translates into longer implant times and therefore reduced throughput.

1.1 Boron Source/Drain Extension Formation

After the Field Oxide Isolation the Well and Transistor Channel implants are done. Following it the Gate Oxidation, Gate Deposition, and Gate Patterning are performed, respectively. Polysilicon oxidation is then carried out to heal the corners and prevent any shorts. With the gate in place, and with oxide (screen oxide) on the source/drain regions, patterning for the source/drain extension implant is done. Boron source/drain extension implant follows. Similar patterning steps are required to form N-type source/drain extension in a CMOS process flow. Each patterning step is followed by a clean to get rid of the photo resist completely. A low temperature anneal is carried out at this stage to prevent enhanced diffusion during subsequent low temperature sidewall spacer deposition processes. Also this anneal flushes out the excess interstitials to the surface and thereby limits the highly doped drain (HDD) B profile diffusion during the final high temperature activation anneal. Next a sidewall spacer is formed. Oxide spacers in deep sub-half micron technology are limited by poor conformity of deposited oxides, trenching in the field oxide, and occurrence of shunts between gate and drain/source, due to the salicidation step. Nitride spacer with a deposited tetraethoxysilane (TEOS) oxide pad, that behaves as a convenient etch stop layer, allows overcoming these difficulties and helps obtain a reduced short channel effect [5]. After the spacer is formed the deep source drain implants are done

with appropriate patterning and implants. The final high temperature activation anneal follows next. Self-aligned silicide formation completes the front end processing of the CMOS. So, the source/drain extension B implant profile is subjected to various cleans associated with the patterning steps for various implants, followed by an anneal (950^{o}C spike), followed by sidewall spacer formation (TEOS followed by Nitride deposition), and finally the high temperature activation anneal (1050^{o}C spike).

Figure 1-1 shows typical B (implanted as BF_2) diffusion profiles for source/drain extension for the 130nm technological node that we obtained at Texas Instruments. The figure contrasts the profiles after full flow vs. implant and anneal only. We can see that the full flow that includes cleans and the spacer process in addition to the implant and anneal results in a shallower profile with a much-reduced dose of B (3.08E14/cm^2 vs. 4.35E14/cm^2). The calculated sheet resistance goes higher as the profile is not only shallower but also has a reduced maximum active dopant concentration. The average conductivity values {calculated as the inverse of the product of R_s (Calculated) and X_j (at 1E18/cm^3)} for the full flow profile vs. implant and anneal only profile are 530 and 591, Siemens/cm respectively. This tells us that the trade off of dose loss in terms of reduced X_j in the case of full flow is not desirable. Besides, the abruptness value (decay length between concentration of 1E19/cm^3 and 1E18/cm^3) for the full flow profile (7.4nm/decade as opposed to 6.0nm/decade) also reveals a poor junction in terms of the capacitance between the gate and source/drain. Clearly, the cleans and spacer process impact the dopant diffusion in terms of the junction depth,

junction abruptness and junction conductivity. The theme of this research is to gain a fundamental understanding of the physics of B source/drain extension evolution during front end CMOS processing, and modeling it.

1.2 Organization of Thesis

This dissertation is organized as follows:

Chapter 1: Introduction.

Guided by Metal Oxide Silicon Field Effect Transistor (MOSFET) scaling rules, the junction depth (X_j) and sheet resistance (R_s) of the source/drain extension region of a MOSFET must be reduced in order to meet the requirements for future nodes. A typical process flow for source/drain extension formation is introduced. The theme of this research is to study the impact of various front-end CMOS process steps on the dopant diffusion profile in terms of the junction depth, junction abruptness and junction conductivity.

Chapter 2: Interactions of B dopant atoms and silicon point defects with SiO_2 films during annealing for ultra-shallow junction formation.

In this chapter we present an investigation of the effect of oxide thickness on the annealed B diffusion profile. Experiments were specifically designed to determine the effect of varying oxide thickness on the B diffusion profile upon annealing. The thicker the oxide during annealing, the deeper the B diffusion profile. We propose a physical model of the Si-SiO_2 system based on the interactions of B dopant atoms and silicon point defects with SiO_2 films in order to explain the experimental observations.

Chapter 3: Effect of nitride sidewall spacer process on B dose loss in ultra-shallow junction formation.

A nitride spacer with an underlying deposited TEOS oxide, that behaves as a convenient etch stop layer, is a popular choice for sidewall spacer in modern CMOS process flows. In this chapter we have investigated the effect of the silicon nitride spacer process on the B profile in silicon and the related dose loss of B from the Si into the silicon dioxide. This is reflected as a dramatic decrease in the junction depth. We find that the silicon nitride influences the concentration of H in the silicon dioxide during the final source/drain anneal. The presence of H enhances the diffusivity of B in the silicon dioxide and thereby results in a significant dose loss from the Si into the silicon dioxide. In this work we have shown this dose loss can be lowered by altering the silicon nitride stoichiometry.

Chapter 4: Fundamental characterization and modeling of the effect of different nitride sidewall spacer processes on B dose loss in ultra-shallow junction formation.

In this chapter we have investigated the influence of the nitride spacer chemistry on B dose loss from the Si. The different nitride chemistries result in different B dose loss. A new model that predicts B junction depths and dose loss during fabrication of ultra-shallow junctions is developed.

Chapter 5: Microwave annealing for ultra-shallow junction formation.

In this chapter we propose a new method for activation of source/drain junctions by microwave annealing. A study with B/BF_2 implants at ultra low energies and high doses was completed. The samples were subjected to a high

power cyclotron resonance maser, called a gyrotron, for annealing. There appears to be some evidence of electromagnetic field-aided activation. The activation levels achieved exceed the levels reported by thermal means at the corresponding temperatures, though the results are not conclusive.

Chapter 6: Conclusions and future work.

Potential applications of this work in ultrashallow junction formation and future work on the effect of nitride spacer on B dose loss and on microwave annealing investigation are suggested in this chapter.

1.3 References

1. P. Packan, MRS Bulletin, 18, June 2000.

2. S. Biesemans, S. Kubicek, K. D. Meyer, Proceedings of Challenges in Predictive Process Simulation, Germany, 17-20 Aug, 1997 (www.ihp-ffo.de/chipps/97).

3. M. Duane, presentation at NIST Characterization and Metrology workshop, March 1998.

4. J. Dabrowski, H.-J. Mussig, M. Duane, S. T. Dunham, R. Goossens, H.-H. Vuong, Advances in Solid State Physics 38, 565, 1999.

5. M. Ada-Hanifi, M. Bonis, Ch. Verove, M. T. Basso, N. Revil, M. Haond, M. Lecontellec, Proceedings of the 27th European Solid State Device Research Conference, Stuttgart, Gemany, 22-24 September 1997.

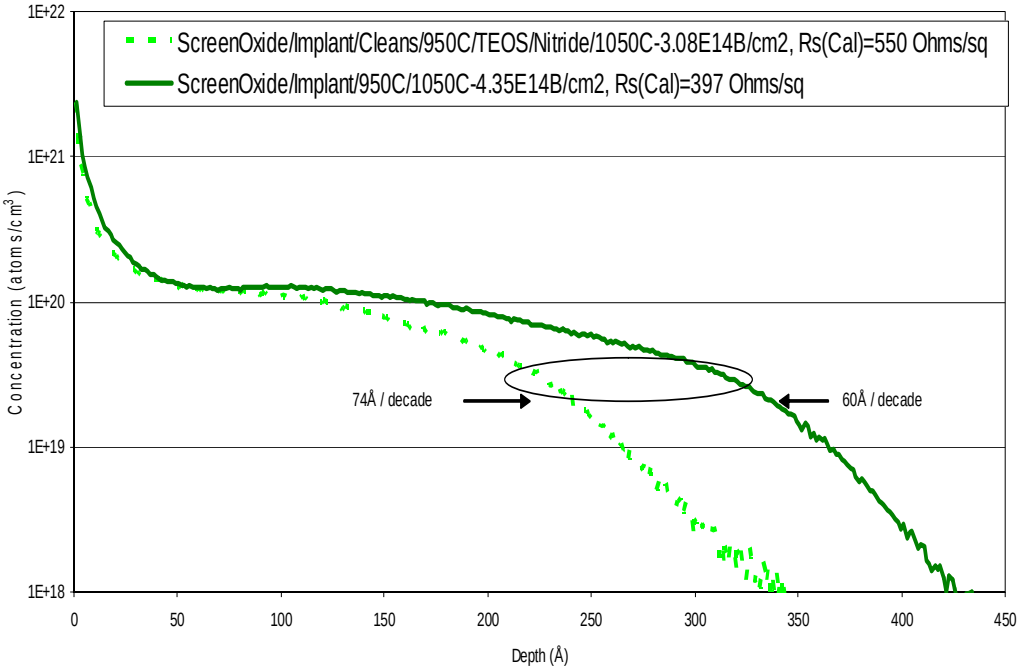

Figure 1-1. Comparison of B SIMS profile after implant and anneal, and after front-end CMOS device processing required to form source/drain extensions (implant, cleans, spacer and anneal). Clearly the front-end processing has a significant impact on the junction depth, junction gradient and junction conductivity.

Chapter 2

Interactions of B dopant atoms and Si point defects with SiO_2 films during annealing for ultra-shallow junction formation

2.1 Abstract

In this work we present an investigation of the effect of oxide thickness on the annealed B diffusion profile. Experiments were specifically designed to determine the effect of varying oxide thickness on the B diffusion profile upon annealing. The thicker the oxide during annealing, the deeper the B diffusion profile. Model of the Si-SiO_2 system based on the interactions of B dopant atoms and silicon point defects with SiO_2 films has been proposed in order to explain the experimental observations.

2.2 Introduction

In the semiconductor industry the most dominant device used today is the Si based metal oxide semiconductor field effect transistor (MOSFET). Improvements in the computer industry over the past 30 years have relied heavily on the ability to increase the speed of the Si MOSFET through the downward scaling of all vertical and lateral dimensions of the transistor. The scaling of the device dimensions not only leads to faster devices but also allows larger and more complex circuits to be implemented on a smaller area [1]. In the last decade, in order to continue conventional scaling of the source/drain junctions, the semiconductor industry has relied heavily on decreasing the implant energy, and also on minimizing the thermal budget of the activation anneal. Decreasing the

implant energy puts the excess Si interstitials closer to the surface. The surface acts as an efficient sink for the interstitials, thus reducing transient enhanced diffusion (TED), which results from the interaction of excess Si interstitials with the dopant atoms [2]. For implant energies below 1 keV, TED can be nearly eliminated. Increasing the ramp rate of anneal, too, has greatly reduced TED effects. With TED less pronounced for low implant energies and sharper anneal temperature profiles, surface reactions and related processes have started to dominate the formation of ultra-shallow junctions. Interactions of dopant atoms and point defects with surface films and interfaces are becoming of paramount importance in determining the concentrations of dopants and point defects, and therefore the resulting diffusion profiles.

Since interactions of point defects and dopant atoms play a central role in the integrated circuit fabrication processes, we present experiments that were designed to gain a fundamental understanding of the interactions of dopant atoms and the point defects with thin oxide films.

2.3 Experiment

Typically for source/drain extension formation, dopants have to be implanted through an oxide, called screen oxide. The alternative of doing the gate re-oxidation to repair the gate edge RIE damage after the implant results in unacceptable oxidation enhanced diffusion (OED) [3]. Other motivations of implanting through a screen oxide could be to avoid channeling, to avoid contamination from the implanter, and to create shallow implanted profiles by bringing the peak closer to the surface (without having to resort to ultra low

energy implants and thus avoiding energy contamination issues with ultra low energy implants).

In a typical CMOS device flow this "implanted oxide" (since dopants have been implanted through it) will see a number of cleaning process steps in order to get low particle count and metallic impurity levels. These different cleans could result in etching away varying amounts of the implanted screen oxide. Table 2-1 summarizes the effect of two typical cleans used in the industry on the implanted screen oxide thickness, as measured by transmission electron microscopy. It should be noted that these cleans are calibrated routinely in the industry to ensure very limited etching of the thermally grown oxide. However, as shown here, the same etches could cause a lot of etching of the implanted thermally grown oxides. A B dose of 1.2E15 atoms/cm^2 was implanted through a 50Å (target thickness) thermally grown oxide for all these samples. It should be noted that the starting implanted screen oxide thickness was 57Å and it is reduced to 13Å and 0Å for the Low Temperature SC1 (LTSC1) and High Temperature SC1 (HTSC1) cleans (at room temperature and 65°C), respectively. In our experiments we have tried to imitate this effect of cleans by varying the implanted screen oxide thickness prior to annealing by using well tailored etches. Therefore, besides giving a fundamental understanding of the effect of varying oxide thickness on the dopant diffusion profile, it also makes the experiments very relevant to industry.

In the experiments we carried out to determine the effect of varying oxide thickness on B diffusion, the starting material was n-type silicon with <100> crystal orientation. The wafer splits are summarized in Table 2-2.

Clean Details	**TEM Oxide thickness (Å)**
No Clean (as-implanted)	57
igh Temperature SC1 (HTSC1)	0
Low Temperature SC1 (LTSC1)	13

Table 2-1: The effect of two different cleans on the thickness of the implanted screen oxide.

Process Steps \ Wafers	Set A							Set B				
	Set AA				Set AB							
Screen (Thermal) oxide 50Å	X	X	X	X	X	X	X					
B implant	X	X	X	X	X	X	X					
BF_2 implant (into pre-damaged Si)								X	X	X	X	X
Etch Screen oxide to 30Å			X									
Etch Screen oxide to 15A				X								
Etch Screen oxide completely (0Å)					X	X	X					
Cap (RTCVD) oxide 20Å										X		
Cap (RTCVD) oxide 30Å						X						
Cap (RTCVD) oxide 40Å											X	
Cap (RTCVD) oxide 50Å							X					
Cap (RTCVD) oxide 60Å												X
1050°C spike		X	X	X	X	X	X		X	X	X	X

Table 2-2: Summary of the wafer processing conditions.

On a set of wafers, Set A, a B dose of 1.2E15 atoms/cm^2 was implanted through the 50Å thermally grown screen oxide at 1.3keV corresponding to a standard source/drain extension implant.

In a sub-set of wafers, Set AA, after B implantation the thermally grown screen oxide was etched back to different thicknesses and then the wafers were annealed. Screen oxide on one wafer was etched back to 30Å, and on another it was etched back to 15Å. For reference, one wafer in this sub-set was preserved without any screen oxide etch (50Å oxide intact). All wafers from this subset were spike annealed at 1050°C.

In another sub-set of wafers, Set AB, after B implantation, screen oxide was etched off completely and two different thicknesses of RTCVD cap oxide (30Å or 50Å) were deposited. No oxide was deposited on one wafer after etching the screen oxide. All wafers in this sub-set were spike annealed at 1050°C.

On another set of wafers, Set B, a BF_2 dose of 8E14 atoms/cm^2 was implanted at 5keV into Si. These wafers had seen a damage-generating-heavy-species implant (non-amorphizing) prior to the BF_2 implant in order to prevent any channeling. After implantation, three different RTCVD oxide thicknesses – cap oxide - were deposited on three different wafers. The first wafer had a 20Å oxide, the second had 40Å and the third had a 60Å RTCVD oxide deposited. All these wafers were then spike annealed at 1050°C.

All anneals were performed in a highly inert N_2 ambient with very low levels of oxygen (< 100 ppm) to avoid any oxidation enhanced diffusion [4].

All B profiles in Si were obtained using Secondary Ion Mass Spectroscopy (SIMS) at Texas Instruments. All samples were dipped in HF before SIMS analysis. SIMS measurements were performed using CAMECA IMS 6f magnetic sector instrument. All measurements were performed using an O_2^+ primary beam and detecting positive secondary ions. Primary oxygen beam with impact energies of 800eV was used. The angle of incidence was approximately 42 degrees. The beam current and raster size were adequate to provide about 0.5Å/s erosion rate. An oxygen backfill was applied to ensure the surface is fully oxidized during depth profiling. SIMS integrated dose values have an error of ±10% and depth resolution is up to 10Å. Some of the SIMS analysis was redone in order to confirm the results. Sheet resistance values were obtained using a four point probe and the standard deviation was less than 5% .

2.4 Results

2.4.1 *Effect of RTCVD cap oxide thickness on B diffusion* :

Figure 2-1 shows the B SIMS profiles after a 1050°C spike anneal for different thicknesses of the RTCVD cap oxide during annealing. All these samples had a B implant. The as-implanted profile is shown for comparison. The sample with the thickest RTCVD cap oxide, 50Å, results in the deepest junction depth. The sample with the 30Å RTCVD cap oxide results in a deeper junction than the sample with no oxide during annealing. The sample with no oxide during annealing results in the shallowest profile. Figure 2-2 shows the sheet resistance values for these annealed profiles with different cap oxide thicknesses during annealing.

Figure 2-3 shows the B SIMS profiles, for BF_2 implanted samples, after a 1050°C spike anneal for different thicknesses of the RTCVD cap oxide during annealing. The sample with the thickest RTCVD cap oxide, 60Å, results in the deepest junction depth. The sample with the 20Å RTCVD cap oxide results in the shallowest junction, while the sample with 40Å oxide results in a profile shallower than the sample with 60Å oxide but deeper than the sample with 20Å oxide.

2.4.2 *Effect of screen oxide thickness on B diffusion* :

Figure 2-4 shows the B SIMS profiles after a 1050°C spike anneal for different thicknesses of the screen oxide during annealing. All these samples had a B implant. The as-implanted profile is shown for comparison. As is evident the sample with the thickest oxide, 50Å, results in the deepest junction depth. The sample with the 30Å screen oxide during annealing results in a deeper junction than the sample with 15Å oxide but shallower than the sample with 50Å oxide. The sample with no oxide during annealing results in the shallowest profile. Figure 2-5 shows the sheet resistance values for these annealed profiles with different screen oxide thickness during annealing.

2.5 Discussion

It is very important to note that by etching the oxide to different thicknesses after the implant or by depositing different thicknesses of RTCVD cap oxide after the implant, all samples have identical initial dopant and damage distributions in the Si. As is evident from figures 2-1,2-3 and 2-4, the samples with thickest oxide result in deepest junctions and the samples with the thinnest

oxide result in the shallowest junctions. This trend is observed for both thermally grown screen oxide and RTCVD deposited cap oxide, as well as for B and BF_2 implants. The sheet resistance measurements shown in these figures further confirm the trend observed from the SIMS profiles for the B implanted cap as well as screen oxide cases. The sample with the deepest profile results in the lowest sheet resistance in each case. Theoretical calculations of sheet resistance based on empirical formulae from TSUPREM for the given SIMS profiles agree well with the experimental measurements.

Kasnavi et al. suggested that for B implants the dose loss is due to segregation of B into the bulk of the oxide [5]. Their model predicts that a thicker oxide would result in more bulk segregation and therefore more dose loss. It should be expected that the increased dose loss could only result in shallower (or similar, if TED was dominant) diffusion profiles. However, we clearly see that our results for different oxide thicknesses, for both cap and screen oxides as well as for B and BF_2 implants, show deeper profiles for the samples with the thicker oxides. Therefore bulk segregation and resultant B dose loss can not explain the deeper junctions with thicker oxides.

Another possible explanation could be that the outdiffusion flux of B from the oxide into the ambient is the dominant flux, and therefore the thicker the oxide the less the outdiffusion flux and hence deeper the profile. However, it needs to be noted that the integrated dose values for the diffused SIMS profiles show similar values for the profiles with different oxide thicknesses. Based on reports on B dose loss for different nitride spacer chemistries (chapter 4), experimentally

observed percentage changes in junction depth with varying amounts of percentage dose loss for similar B doses and anneals are shown in Figure 2-6 [6]. Also shown in this figure is the plot of percentage change in junction depth and corresponding percentage dose loss value for samples from our current work. Clearly our data does agree with on the prior experimental observations.

Also, in an attempt to simulate the observed junction depth differences based on B dose loss, we set the outdiffusion flux of B from oxide into the ambient to a high value and considered B flux in the oxide as the rate-limiting flux in our simulations. We found that we could match the experimentally observed differences in the junction depth with different oxide thicknesses by adjusting the B dose loss from the Si, into the oxide and then further into the ambient, but doing so resulted in perceptibly different profiles through out in the silicon. However, the experimental profiles seem identical near the surface for different oxide thicknesses and the only differences are seen towards the tail of the diffused profiles. This indicates that B dose loss due to outdiffusion might not be the reason for the observed differences in the diffused profiles for different oxide thicknesses.

High temperature SiO_2 decomposition at the oxide/Si interface has been reported in the literature [7-11]. At high temperatures and low oxygen partial pressure, SiO_2 decomposition can occur according to the reaction $Si + SiO_2 \rightarrow SiO$, where the Si substrate acts as a source of the Si for the reaction. The process could be extremely non-uniform, resulting in the nucleation and growth of voids with little overall thinning of the oxide. The decomposition of SiO_2 probably

includes the serial processes of SiO formation at the SiO_2/Si interface, SiO outdiffusion through the oxide film and evaporation of SiO. Anh et al. identified vacancy generation at the SiO_2/Si interface caused by SiO formation in thin oxide films in inert ambients at high temperatures by observing dopant diffusion and stacking fault shrinkage [12]. He found that P diffusion was retarded, as diffusion was enhanced and the shrinkage rate of pre-existing stacking faults was increased. The phenomena strongly suggests that a vacancy supersaturation and a self-interstitial undersaturation exist under thin SiO_2 layer during annealing in Ar.

Dunham et al. modeled the Si/SiO_2 system more quantitatively by considering the processes that are occurring: desorption of SiO into the gas phase, diffusion of Si across the oxide and segregation of Si interstitials at the Si/SiO_2 interface, interface recombination, and diffusion of interstitials in the substrate [2]. In his model he assumed that a constant segregation coefficient m_I relates the ratio of the concentration of Si interstitials in the Si to that in the oxide, and that there are no reactions involving interstitials in the oxide. With his model he was able to explain a broad range of data both under oxidizing and non-oxidizing conditions, and also estimate the amount of thinning that would be consistent with the interstitial undersaturation observed by Ahn. Dunham's model suggests a strong dependence on oxide thickness and that thickness dependence is matched well by a model assuming the diffusion of a Si species across the oxide.

We use a similar analysis (as Dunham et al. [2]) under conditions of interstitial supersaturation (due to implantation) and TED. Figure 2-7 illustrates schematically the concentration of active species during inert ambient annealing

for a Si/SiO_2 system under conditions of interstitial supersaturation. The effect of oxide thickness can be understood by a simple analysis of TED. It has been experimentally observed that the B diffusivity enhancement during TED is nearly independent of the B implant damage for initial stages and after some time period, T, the enhancement goes away[13,14]. This would imply that the excess interstitial concentration is approximately fixed during the early stages of TED and after some time it comes down to the equilibrium value. Reports by Eaglesham et al. revealed {311} defects as the actual source of the interstitials during TED[15].

Let C_I^{peak} be the effective interstitial solubility associated with the formation of {311} defects. Let Y be the average depth into Si from the Si/SiO_2 interface of net interstitial distribution. This depth Y could be the projected implant range for a non-amorphizing implant or the end-of-range depth for an amorphizing implant. The total dose of excess interstitials (after initial recombination) is Q. Based on a '+1' damage model, Q is equal to the implanted dose [5]. We assume after initial recombination of interstitials and vacancies (starting with a +1 interstitial dose), there are no interstitial reactions with vacancies and lattice defects in the Si and the only dominant flux of interstitials is the one towards the surface. To simplify our analysis further we assume that the concentration of the SiO species at the SiO_2/ambient interface is zero. Now we can assume a steady state flux balance at the SiO_2/Si interface between the flow of Si interstitials from the substrate, recombination at the interface and flow into oxide:

$$[D_I^{Si} . \{C_I^{peak} - C_I^{Si}\}] / Y = [\sigma . \{C_I^{Si} - C_I^{*}\}] + [(D_I^{SiO2} .\{ C_I^{Si} / m_I \}) / X] \quad \text{(Eq.1)}$$

where C_I^* is the interstitial concentration under equilibrium conditions, X is the oxide thickness, σ is the interface recombination velocity for interstitials, D_I^{Si} is the diffusivity of the interstitials in Si, D_I^{SiO2} is the diffusivity of excess Si in SiO_2, and m_I is the segregation coefficient for interstitials between Si and oxide. Further, we can estimate the TED time, T (= Dose/Flux), as the time taken for all the excess interstitials to escape out of the system as:

$$T = Q / [(D_I^{Si} \{C_I^{peak} - C_I^{Si}\}) / Y]$$

$$= Q / ([\sigma . \{C_I^{Si} - C_I^{*}\}] + [(D_I^{SiO2} .\{ C_I^{Si} / m_I \}) / X]]) \quad \text{(Eq.2)}$$

Ignoring the recombination flux (negligible interface recombination when implanted dose is much higher than the number of interface traps) :

$$T = Q / [(D_I^{SiO2} .\{ C_I^{Si} / m_I \}) / X] \quad \text{(Eq.3)}$$

During TED the interstitial supersaturation is C_I^{peak} / C_I^*, so the amount of excess diffusion expected during TED is given by :

$$\sqrt{(DT)}_{TED} = \{ D_B^* . f_I . [C_I^{peak} / C_I^*] . T \}^{0.5}$$

$$= \{ D_B^* . f_I . [C_I^{peak} / C_I^*] . (Q / [(D_I^{SiO2} .\{ C_I^{Si} / m_I \}) / X]) \}^{0.5}$$

$$= \{ D_B^* . f_I . [C_I^{peak} / C_I^*] . [(Q . m_I) / (C_I^{Si} . D_I^{SiO2})] . X \}^{0.5} \quad \text{(Eq.4)}$$

where D_B^* is the B diffusivity under equilibrium conditions and f_I is the fraction of B diffusion associated with interstitial mechanism.

This formalism clearly shows that thicker the oxide (X) more the B diffusion. This model therefore explains why we would observe a deeper junction for a thicker oxide.

For a more accurate analysis we ran simulations by considering transient diffusion/recombination in the silicon, the as-implanted B SIMS profile and a '+1' damage model. However, one of the major barriers to such modeling is that the reported values for parameters such as interstitial diffusivity, Si atom diffusivity in oxide, and interstitial segregation coefficient between Si/SiO_2 vary over several orders of magnitude [2]. The effect of the decomposition of thin oxide films can be captured by understanding that the phenomenon drives the interstitial concentration at the interface to values below the equilibrium concentrations. In our simulations we fixed the C_I/C_I^* at the interface to different values in order to match the profiles. For thin films, the Si flux in the oxide being very high could result in high degrees of interstitial undersaturation. Figure 2-8 shows the simulated profiles and SIMS profiles for the different screen oxide thicknesses. Simulated B diffusion profiles show good agreement with the SIMS profiles. The C_I/C_I^* values at the interface for the simulations for different oxide thicknesses are shown in figure 2-9. In our case it should be noted that the model was calibrated assuming that the 50Å screen oxide results in no interstitial undersaturation at the interface. This assumption makes it possible for us to quantify the thickness effect on the CI/CI* undersaturation (as shown in figure

2-9). It seems to be a reasonable assumption considering that the differences in junction depth diminish going from 30Å to 50Å oxide (as compared to the differences observed between 15Å and 30Å screen oxide profiles).

In these experiments, B profile for the BF_2 implant case is always shallower than the B implant case (comparing Fig. 2-1 and Fig. 2-3). It has been reported before that in forming shallow junctions, B and BF_2 implants with similar as-implanted profiles behave quite differently. BF2 implants result in shallower junctions, significant dose loss and high activation [5]. Both, the damage due to implanting the larger BF_2 molecule and the presence of F, seem to change the effective diffusivity of B [5].

Comparing the B diffusion profiles for samples with 50Å screen oxide and 50Å RTCVD cap oxide, it is evident that the RTCVD cap oxide results in a higher dose loss from the Si than the screen oxide during annealing. The integrated dose numbers are as different as 5.4E14 atoms/cm^2 and 7.8E14 atoms/cm^2 for the RTCVD cap oxide and screen oxide samples, respectively. The same trend is observed between the RTCVD oxide and screen oxide for the other thicknesses as well. It is expected that the RTCVD oxide will results in a higher dose loss into the oxide since the deposited oxide has no B to start with while the screen oxide receives substantial B dose during implantation. So for the RTCVD cap oxide it could be expected that more B would be lost due to segregation into the oxide. However, our simulations show that the differences that could be expected based on segregation are much smaller than those observed experimentally. Kohli et al. have reported the presence of high levels of H in the as-deposited oxides [6].

Many reports in literature have discussed enhanced B diffusion in the oxides due to the presence of H [16-19]. While it is believed that the H could diffuse out of the deposited oxides into the ambient upon annealing, it might still result in highly enhanced B diffusion in the initial phase of annealing.

It is interesting to note in figure 2-1 that the profile with no oxide results in the shallowest junction. However, the sheet resistance value is the same as that of the sample with 30Å cap despite a shallower X_j. Looking carefully at the profile it can be seen that the concentration of B is higher (between 100Å and 170Å into Si) for the sample with no oxide as compared to samples with the cap. This would explain why the sheet resistance values are similar between the 30Å cap oxide and no oxide cases even though the no oxide case has a lower Xj. The shallower diffusion profile indicates that the bare Si serves as a much more effective interstitial sink than the RTCVD cap oxide/Si interface. Clearly, a bare silicon surface results in the shallowest junction without compromising the sheet resistance.

2.6 Summary

We have studied the effect of varying oxide thickness on the B diffusion profile. Thinner oxides result in shallower junctions. A bare silicon surface is most desirable for low sheet resistance ultra-shallow junction formation. We have successfully modeled the effect of oxide thickness on junction depth. The model takes into account the segregation of excess Si between the oxide and the Si substrate and diffusion of that excess Si in the oxide.

2.7 References

1. P. Packan, MRS Bulletin, 18, June 2000.
2. S. Dunham, J. Appl. Phys., Vol 71, No. 2, 685, 1992.
3. R. Lindsay, et al., Proceedings Ultra Shallow Junctions 2001, 255, 2001.
4. M. Miyake, J. Appl. Phys., Vol 57, No. 6, 1861, 1985
5. R. Kasnavi, et al. Mat. Res. Soc. Symp. Vol. 610, B4.3, 2000.
6. P. Kohli, et al., (to be published) J. Va. Sci. Technol., Jan 2004.
7. R. Tromp, et al. Phys Rev lett. 55, 2332, 1985.
8. K. Hofmann, et al. Appl. Phys. Lett. 49, 1525, 1986.
9. K. Hofmann, et al. J.Electrochem. Soc. 134, 240, 1987.
10. G. W. Rubloff, et al. Phys. Rev. Lett. 58, 2379, 1987.
11. M. Liehr, et al. J.Va. Sci. Technol. A 5, 1559, 1987.
12. S. T. Ahn, Ph.D. Thesis, Stanford University, 1988.
13. R. Angelucci et al. J. Electrochem. Soc. 134, 3130, 1987.
14. P. A. Packan, Ph.D. Thesis, Stanford University, 1991.
15. D. J. Eaglesham et al. Appl. Phys. Letts. 70 (24), 3281, 1997.
16. R. Fair, IEEE Electron Device Letters, Vol. 17 (5), 242, 1996.
17. Y. Shacham-Diamand, W. G. Oldham, J. Elect. Mater., 15, 229, 1986.
18. T. Aoyama et al., J.J.Appl. Phys. Vol. 38, 2381, 1999.
19. R. B. Fair, IEDM Tech. Digest, 85, 1995.

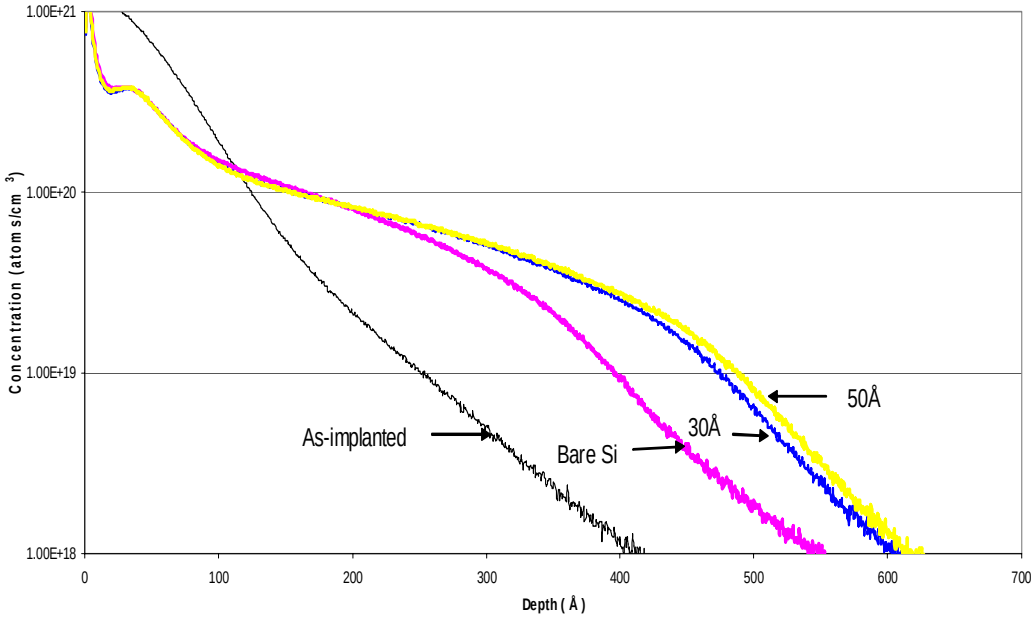

Fig. 2-1. Boron SIMS profiles in Si showing the effect of cap oxide thickness on B diffusion profile. B was implanted through a 50Å screen oxide and then etched away completely. Different thicknesses of cap oxide were deposited. Thicker oxide during annealing gives deeper junction.

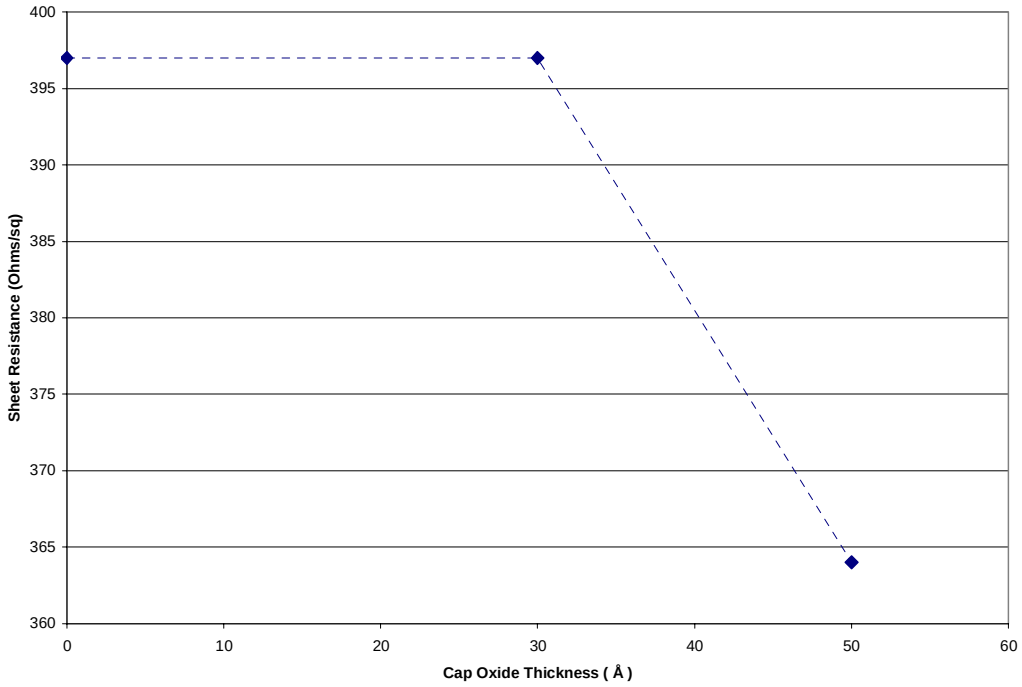

Fig. 2-2. Effect of cap oxide thickness on sheet resistance. The trend corroborates SIMS profiles as shown in Fig. 2-1.

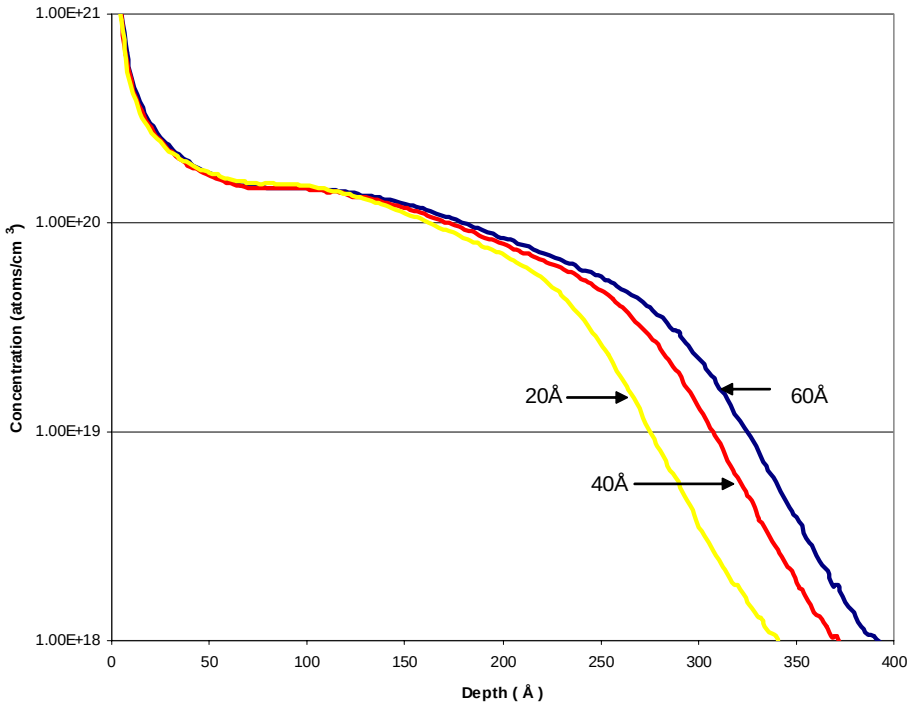

Fig. 2-3. Boron SIMS profiles in Si showing the effect of cap oxide thickness on B diffusion profile. BF_2 was implanted into bare silicon. Different thicknesses of cap oxide were deposited. Thicker oxide during annealing gives deeper junction.

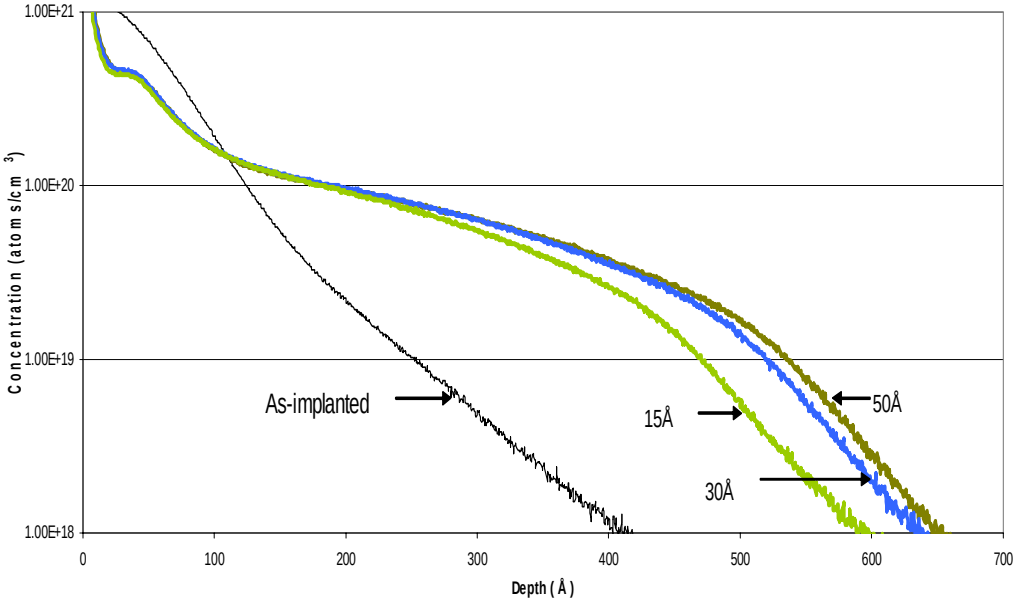

Fig. 2-4. Boron SIMS profiles in Si showing the effect of screen oxide thickness on B diffusion profile. B was implanted through a 50Å screen oxide and then etched to different thicknesses. Thicker oxide during annealing gives deeper junction.

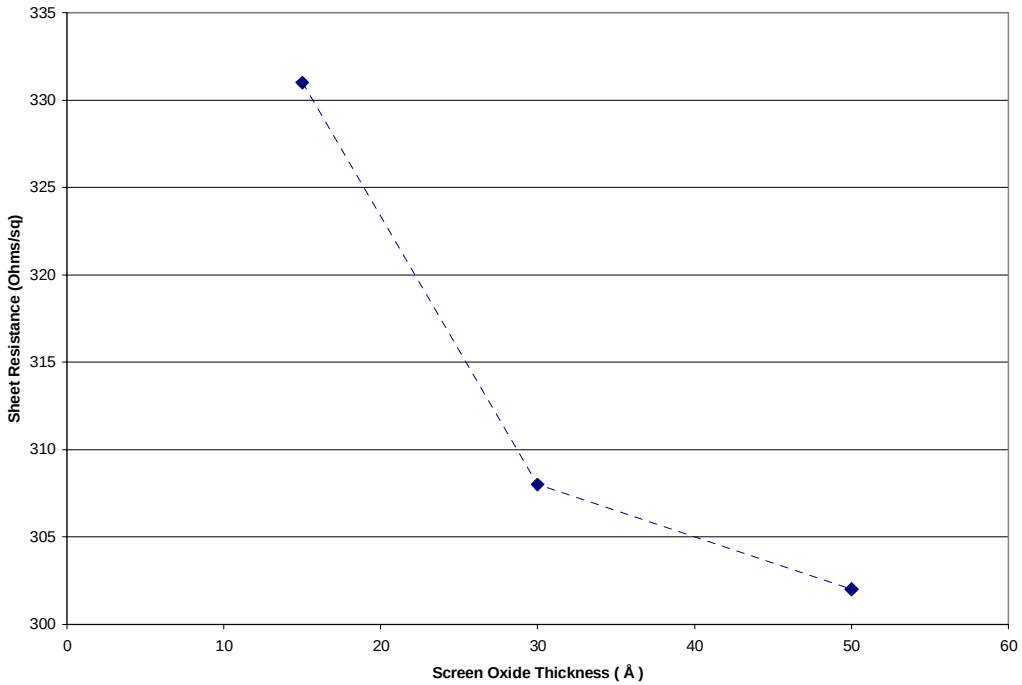

Fig. 2-5. Effect of cap oxide thickness on sheet resistance. The trend corroborates SIMS profiles as shown in Fig. 2-4.

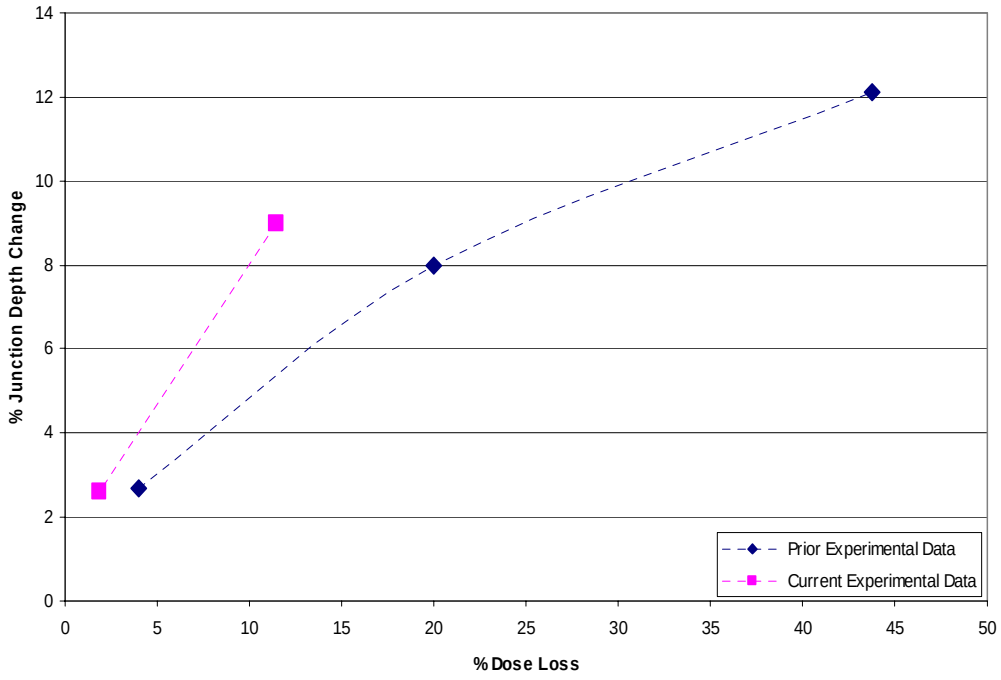

Fig. 2-6. Percentage dose loss vs. percentage change in junction depth for current experiments and prior dose loss related experiments. Clearly the current experimental data does not agree with the prior dose loss data.

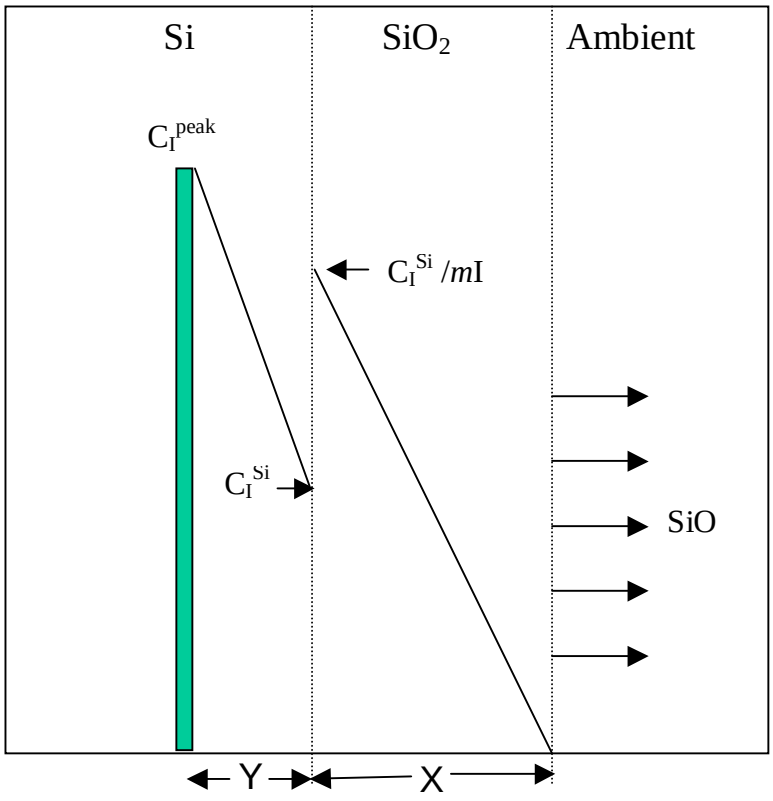

Fig. 2-7. Schematic illustration of the concentrations of reacting/diffusing species during inert ambient annealing of thin oxide films.

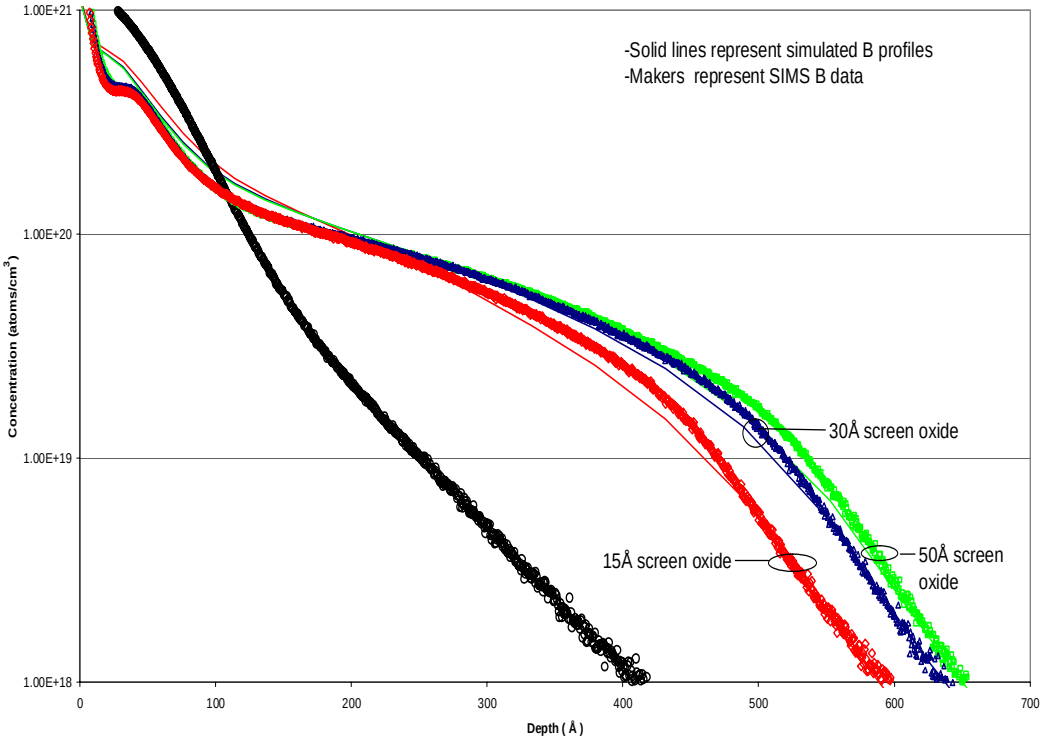

Fig. 2-8. Comparison between model and data for diffusion of B under different screen oxide thicknesses during annealing in an inert ambient.

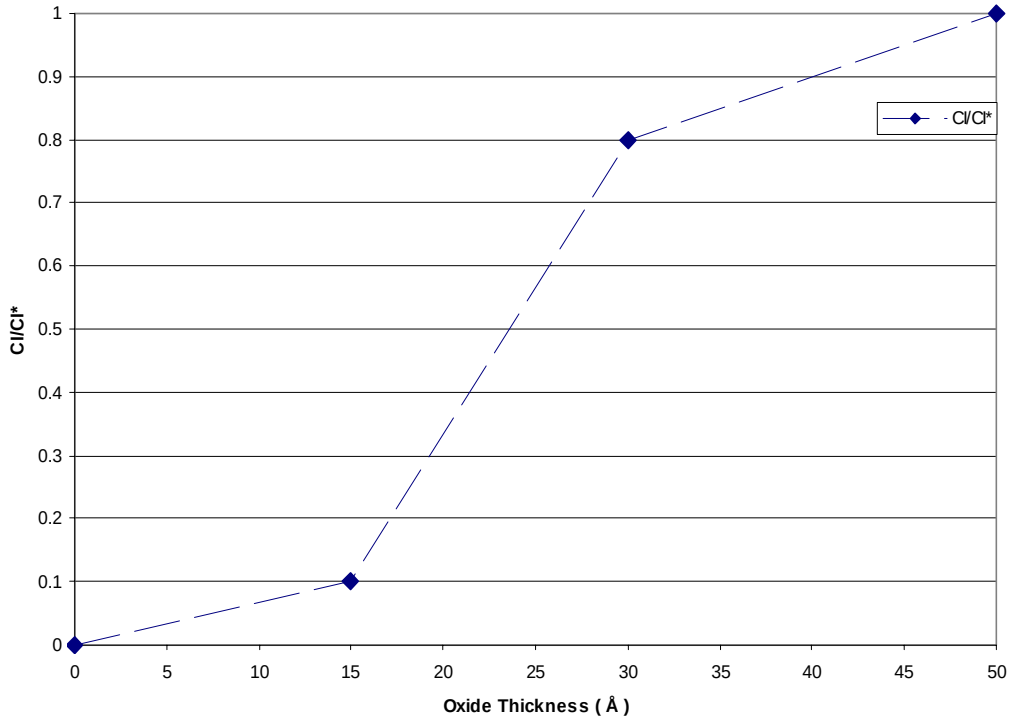

Fig. 2-9. Interstitial undersaturation vs. Oxide thickness as based on simulations shown in Fig. 2-8.

Chapter 3

Effect of nitride sidewall spacer process on boron dose loss in ultra-shallow junction formation

3.1 Abstract

A nitride spacer with an underlying deposited TEOS oxide, that behaves as a convenient etch stop layer, is a popular choice for sidewall spacer in modern CMOS process flows. In this work we have investigated the effect of the silicon nitride spacer process on the boron profile in silicon and the related dose loss of B from the Si into the silicon dioxide. This is reflected as a dramatic decrease in the junction depth. We find that the silicon nitride influences the concentration of hydrogen in the silicon dioxide during the final source/drain anneal. The presence of H enhances the diffusivity of B in the silicon dioxide and thereby results in a significant dose loss from the Si into the silicon dioxide.

3.2 Introduction

Improvements in the integrated circuit performance over the past three decades have been mainly possible by the downward scaling of device dimensions. Device scaling requires that all lateral and vertical dimensions of the transistor be scaled. In the last decade, in order to continue conventional scaling of the source/drain junctions, the semiconductor industry has relied heavily on decreasing the implant energy, and also on minimizing the thermal budget of the

activation anneal. Decreasing the implant energy puts the excess interstitials closer to the surface. The surface acts as an efficient sink for the interstitials, thus reducing transient enhanced diffusion (TED), which results from the interaction of excess interstitials with the dopant atoms. For implant energies below 1 keV, TED can be nearly eliminated. Increasing the ramp rate of anneal, too, has greatly reduced TED effects. With TED less pronounced for low implant energies and sharper anneal temperature profiles, surface reactions and related processes emerge to dominate the formation of ultra-shallow junctions. Interactions of dopant atoms and point defects with surface films and interfaces are becoming of paramount importance in determining the concentrations of dopants and point defects, and therefore the resulting device structures [1].

In the standard CMOS process flow, sidewall spacer is widely used to self align the deep source/drain from the shallow source/drain extension. Oxide spacers in deep sub-micron technology are limited by trenching in the field oxide, and occurrence of shorts between gate and drain/source, due to the salicidation step. Silicon nitride spacer (from now on we will refer to silicon nitride as nitride and silicon dioxide as oxide) with an underlying deposited tetraethoxysilane (TEOS) oxide that behaves as a convenient etch stop layer, overcomes these difficulties [2]. The aim of this work is to analyze the effect of nitride spacer on the B dose loss from the Si into the overlying implantation oxide and TEOS oxide.

3.3 Experiment

The experimental procedure was designed for standard VLSI source/drain extension formation with nitride spacer in the CMOS device flow as shown in figure 3-1. The starting material was *n*-type Si with <100> crystal orientation. A 50Å thermal oxide was grown on all the wafers. The wafers were then subjected to a B (or BF_2) implant at 1.3keV (or 6keV BF_2) and a B dose of 1.2E15 atoms/cm^2. Wafers that received the BF_2 implant had received a pre-damage implant of 3E13 Sb/cm^2 at 30keV to reduce B channeling. All wafers were subjected to a 950˚C spike anneal. A 150Å thick TEOS oxide layer was then deposited at 650˚C as part of the sidewall spacer process. Next a 300Å thick RTCVD nitride layer was deposited by flowing silane and ammonia at 700˚C. A nitride layer thickness of 1100Å instead of the 300Å thickness was deposited on some samples. Furthermore, for some samples during the nitride deposition step, no reaction gases were made to flow (only N_2 purge). This was to subject the wafers to the same thermal budget without actually depositing any nitride. Finally wafers were subjected to the source/drain spike anneal at 1050˚C. Some wafers were not subjected to the final anneal. Three different nitride deposition processes were employed with different flow rates of ammonia and silane, but the same thermal budget was used.

Also, some samples were prepared with 1500Å oxide. Some of these samples had thermally grown oxide, while others had a TEOS based deposited oxide, in order to study the diffusivity of B in oxide. A B dose of 5E13atoms/cm^2 was implanted at 18keV into the 1500Å thick oxide samples. Further, on some of

these wafers 2000Å RTCVD nitride was deposited. Nitride of this thickness enables comparison of two extreme conditions. Wafers both with and without the nitride, were annealed at 1050˚C for 11 seconds. Some wafers were not annealed to serve as reference.

The other set of wafers are deposited with 1200Å thick TEOS oxide, and then with or without 300Å thick nitride. Next the wafers were subjected to 1050˚C spike anneal. Some wafers were not subjected to anneal to serve as reference. These samples enable a study of hydrogen loss from the oxide upon annealing, using the NRA technique described below.

All B profiles in Si and in the oxide were obtained using Dynamic Secondary Ion Mass Spectroscopy (DSIMS) at Texas Instruments. Dynamic SIMS measurements were performed using CAMECA IMS 6f magnetic sector instrument. All measurements were performed using an O_2^+ primary beam and detecting positive secondary ions. Primary oxygen beam with impact energies of 800eV and 500eV were used. The angles of incidence were approximately 42 and 46 degrees, respectively. The beam current and raster size were adequate to provide about 0.5Å per second erosion rate. For bare Si samples, an oxygen backfill was applied to ensure the surface is fully oxidized during depth profiling. For the sample with oxide no oxygen backfill was used to identify oxide/substrate interface and minimize sputtering rate change in the Si substrate. Electron flood gun charge neutralization was used for the oxide samples. SIMS integrated dose values have an error of ±10% and depth resolution is up to 10Å.

H profiles in the oxide were obtained using Nuclear Reaction Analysis (NRA) at the State University of New York, Albany. This method makes use of the nuclear reaction:

$$^{15}N + {}^{1}H \rightarrow {}^{12}C + {}^{4}He + \text{gamma-ray}$$

The sample to be analyzed is bombarded with ^{15}N at or above the resonant energy (6.385 MeV) and the number of characteristic gamma rays produced in the target is measured with a scintillation detector [3]. When the sample is bombarded with ^{15}N at the resonance energy, the gamma-ray yield is proportional to H on the surface of the sample. When the sample is bombarded with ^{15}N above the resonance energy, there are negligible reactions with the surface H. However, as the ^{15}N ions penetrate the sample, they lose energy and reach the resonance energy at some depth. Now the gamma-ray yield is proportional to H at this depth. Fourier Transform Infrared Spectroscopy was also used to analyze the H content in the nitride films. Sheet resistance values were obtained using a four-point probe and the standard deviation was less than 5%.

3.4 Results

Effect of presence of nitride on B diffusion profile: Figure 3-2 shows identical B diffusion profiles in the Si/TEOS oxide stack right before the final source/drain activation anneal for samples with and without nitride. These samples were implanted with B. It is important to note that both samples were subjected to the same thermal budget, irrespective of whether nitride was deposited on top of the TEOS or not. Samples implanted with BF_2 into pre-damaged Si also show identical profiles for samples with and without the nitride,

before the final anneal at 1050˚C. Therefore, the nitride deposition (and not the thermal budget associated with it) does not influence B diffusion.

Figures 3-3 and 3-4 show the B diffusion profiles for both the samples with and without the nitride after the 1050˚C spike, for B and BF_2 implant cases, respectively. For both B and BF_2 implant cases, after the final activation anneal, samples with the nitride show lower retained B dose in Si than those without the nitride. So during the 1050˚C spike, the presence of nitride on top of TEOS oxide seems to influence the final B diffusion profile. Samples with the nitride on top of TEOS show lower B concentration at each depth in Si and consequently shallower junctions (~100Å in B implanted case and ~140Å in BF_2 implanted case) in Si compared to samples without the nitride. However, the B concentration in the TEOS oxide is higher at all depths for the samples with the nitride compared to the samples without the nitride. It is clear from the profiles that the reduction in junction depth in the presence of nitride comes along with a lower B peak concentration.

In these experiments, B diffusion profiles for the BF_2 implant case are always shallower than the B implant case (compare Fig. 3-3 and Fig. 3-4). We found from transmission electron microscopy (TEM) that a dose of 1.2E15 atoms/cm^2 BF_2 implanted into pre-damaged Si through a 50Å thermally grown oxide results in an amorphous Si layer thickness of 112Å. Upon annealing, this amorphous layer regrows by solid phase epitaxy. The only damage remaining after the initial stages of annealing is the end-of-range damage. For the B implant there is an abundance of interstitials even after the first stages of annealing. The

amount of damage, particularly interstitials in the case of B, dictates the enhancement of B diffusivity and also the amount of immobile B clustered in boron-interstitials complexes (BICs). Besides damage, the presence of F also changes the effective diffusivity of B [4].

Effect of presence of nitride on B diffusion in thermal and TEOS oxide: Figure 3-5 shows the three B diffusion profiles in TEOS oxide for different processing conditions. The as-implanted profile of B in TEOS oxide does not show any measurable broadening even after relatively long high temperature anneal at 1050˚C for 11seconds. However, with the nitride present the same profile shows measurable diffusion. It is the presence of nitride on top of the TEOS oxide that influences the B diffusivity during the high temperature anneal. For samples with thermal oxide instead of the TEOS oxide, the three profiles corresponding to the processing conditions of the profiles in Figure 3-4 look identical. The presence of the nitride seems to substantially enhance the diffusivity of the B in the oxide in the case of TEOS oxide, while it does not seem to influence the B diffusivity in the case of thermal oxide.

Atomic Concentration (%)	C	N	O	Si
NitridE1	0.61	46.15	5.16	48.08
NitridE2	0.8	45.85	5.84	47.51
NitridE3	0.66	43.27	6.22	49.85

Table 3-1: XPS results for the three different nitrides deposited by varying the flow rate of ammonia and silane during deposition.

Effect of nitride stoichiometry and thickness variation: Figures 3-6 shows B diffusion profiles in Si/TEOS stack after final source/drain anneal for three different nitride stoichiometries for B implanted samples. The three different nitride stoichiometries were obtained by varying the flow rates (ratio as well as total gas flow rate) of NH_3 and SiH_4. The total thermal budgets involved in the nitride deposition for the three different nitride stoichiometries, for the same nitride thickness, were made identical. Figure 3-6 also shows the B diffusion profile for B implant after annealing without a nitride. The XPS results for the three nitrides have been summarized in Table 3-1. Nitride 1 has the highest concentration of N while Nitride 3 has the least N concentration. All four B profiles were identical right before the 1050˚C anneal. However, during annealing different nitrides seem to influence B diffusion in different ways. Boron concentration in Si, after the final anneal, is highest for NitridE1 followed by Nitride 2 and then Nitride 3; while the B concentration in the TEOS oxide is highest for Nitride 3 followed by Nitride 2 and then Nitride 1. It is important to note that during DSIMS analysis for different processing conditions we observed B in the TEOS oxide but found no measurable amount of B in the nitride. It is apparent that different nitrides influence the amount of B dose loss from the Si into the TEOS oxide differently, and therefore resulting in different junction depths and B peak concentrations. Figure 3-7 shows B diffusion profiles in Si for two different nitride thicknesses. The thicker nitride evidently results in higher dose loss from the Si into the oxide. The total thermal budgets involved for the recipes resulting in different deposition thicknesses were identical with the actual

deposition times being different. In addition to the nitride chemistry it is apparent that the nitride thickness also influences the B diffusion profile.

3.5 Discussion

From figures 3-3 and 3-4 it is evident that the presence of the nitride influences the oxide in a way that it results in higher B dose loss from the Si into the TEOS oxide. From the B profiles in figure 3-5, one understands that the presence of nitride on the TEOS oxide enhances the B diffusivity in the oxide. Assuming simple Fickian diffusion, the B diffusion profile in the TEOS oxide in the presence of nitride can be modeled by increasing the B diffusivity in oxide by a factor of 2000.

In order to understand the effect of nitride we profiled N in the TEOS oxide. Our results from Time-of-flight SIMS as well as DSIMS showed very similar levels of N in the TEOS oxide both with and without the presence of nitride after the 1050˚C anneal. Recent reports have discussed the effect of stress due to thin films on B diffusion in Si. However, we noted before that while B implanted TEOS oxide sample showed enhanced B diffusion during anneal in the presence of nitride, the thermal oxide sample implanted with B did not show any B enhanced diffusion during annealing even in the presence of nitride. The stress values obtained using wafer bow measurements with the nitride were of the order of 1E10 dynes/cm^2 tensile. According to the literature [5], much higher stress values would be required to change the B diffusivity by a factor of 2000, as seen for the B implanted TEOS sample with nitride. Also, different nitride chemistries

(which will be discussed elsewhere) result in very similar values of stress; however, they result in very different B diffusion profiles.

Extensive reports in the literature have discussed the nitride acting as a source of H that diffuses in the underlying oxide during nitride deposition and/or during annealing [6,7]. This H is believed to form H-related defects in the oxide, which lower the B diffusion activation energy in the oxide [8]. Nitride FTIR measurements before and after anneal in Figure 3-8 show that both peaks corresponding to wave numbers for Si-H bond and N-H bond decrease in intensity after the nitride has been annealed, indicating out-diffusion of H from the nitride during annealing.

Figure 3-9 shows the H profiles obtained by NRA in the TEOS oxide with and without nitride, after anneal. The H profile for as-deposited TEOS oxide is also shown. It is important to note that the H levels in the as-deposited TEOS are very high. Instead of the nitride acting as source of H and thereby increasing the H concentration in the underlying oxide upon annealing, we find that nitride seems to be acting as a barrier for the H out-diffusion from the underlying TEOS during annealing. The H concentration in the TEOS after annealing is much higher (3.5E21atoms/cm^3) if the nitride is present during annealing as compared to the H concentration in the TEOS after annealing without nitride. Figure 3-10 shows the H concentrations in the TEOS and thermal oxide, for samples corresponding to the processing conditions indicated in figure 3-5. It is interesting to note that the H concentration for as-deposited TEOS is very high while that of as-grown oxide is very low. After annealing, the H concentration in TEOS oxide

decreases both with and without the nitride. For thermal oxide with the nitride, upon annealing we find an increase in H concentration. This indicates the possibility of nitride acting as a source of H. However, for TEOS the out-diffusion flux of H from the TEOS seems to be the dominant one. We believe it is the high H concentration during anneal in the presence of nitride that causes enhanced B diffusion. Also it appears that below a certain threshold value of H, no enhancement of B diffusivity is observed (as in the case of TEOS annealed without nitride).

We know that the H concentration in as-deposited TEOS oxide is very high and that upon annealing this H out-diffuses from the oxide directly into the ambient if there is no nitride present, or through the nitride into the ambient if nitride is present. We believe that H diffusion through the nitride is the rate-limiting step since the presence of nitride results in higher retained H in the oxide. The higher concentration of H in the TEOS oxide due to the presence of nitride, results in increase in B dose-loss from Si into the oxide. This B dose loss reduces the extent of B diffusion in Si by reducing the concentration-dependent diffusivity. This model also explains the experimental observation of more dose loss into the oxide in the presence of thicker nitride. Since H diffusion through the nitride is the rate-limiting step, a thicker nitride would result in less H out diffusion from the TEOS oxide for the same anneal. This implies that a thicker nitride would result in a higher retained H concentration in the TEOS oxide, resulting in a greater enhancement of B diffusivity and thereby more B dose loss from the Si into the oxide, as is experimentally observed. The variation of nitride

stoichiometry possibly influences the diffusivity of H through the nitride, and thereby results in different H concentrations in the TEOS oxide upon annealing for the different stoichiometries. However, NRA profiling did not show any significant differences in H concentration in the TEOS for the three different stoichiometries studied here. Therefore, we believe optimizing the nitride stoichiometry is important to obtain desirable ultra-shallow junctions.

3.6 Summary

An investigation of the influence of the nitride spacer on B dose loss from the Si into the oxide has been done. We showed that the as-deposited TEOS oxide has very high concentration of H. This H diffuses out readily upon annealing. However, the presence of nitride acts as a diffusion barrier for the out-diffusing H, resulting in high concentration of retained H in the TEOS even after annealing. The presence of this high level of retained H causes an enhancement of B diffusivity in the oxide and thereby enhances the amount of B dose loss into the oxide from the Si. It is imperative to optimize the sidewall spacer stoichiometry and thickness in order to form very conductive shallow junctions.

3.7 References

1. S. T. Dunham, IEDM Tech. Digest, 501, 1998.
2. M. Ada-Hanifi et al., Proceedings of the 27th European Solid State Device Research Conference, Stuttgart, Germany, 1997.
3. W. A. Lanford and M. J. Rand, J. Appl. Phys., 49 (4), 2473, 1978.
4. R. Kasnavi et al., Mat. Res. Soc. Symp. Vol. 610, B4.3, 2000.
5. M. Aziz, Defect and Diffusion Forum, 153, 1998.
6. S. Tokitoh, et al., IRPS Technical Digest, 307, 1997.
7. S. Inaba, et al., IEEE Transactions on Electron Devices, Vol. 46, 6, 1999.
8. R. Fair, IEEE Electron Device Letters, Vol. 17 (5), 242, 1996.

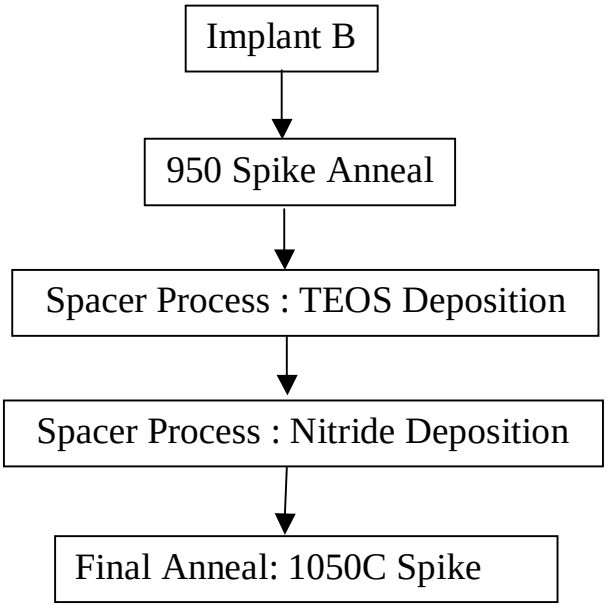

Figure 3-1: Experimental procedure for standard VLSI *p*-MOS source/drain extension formation with nitride sidewall spacer.

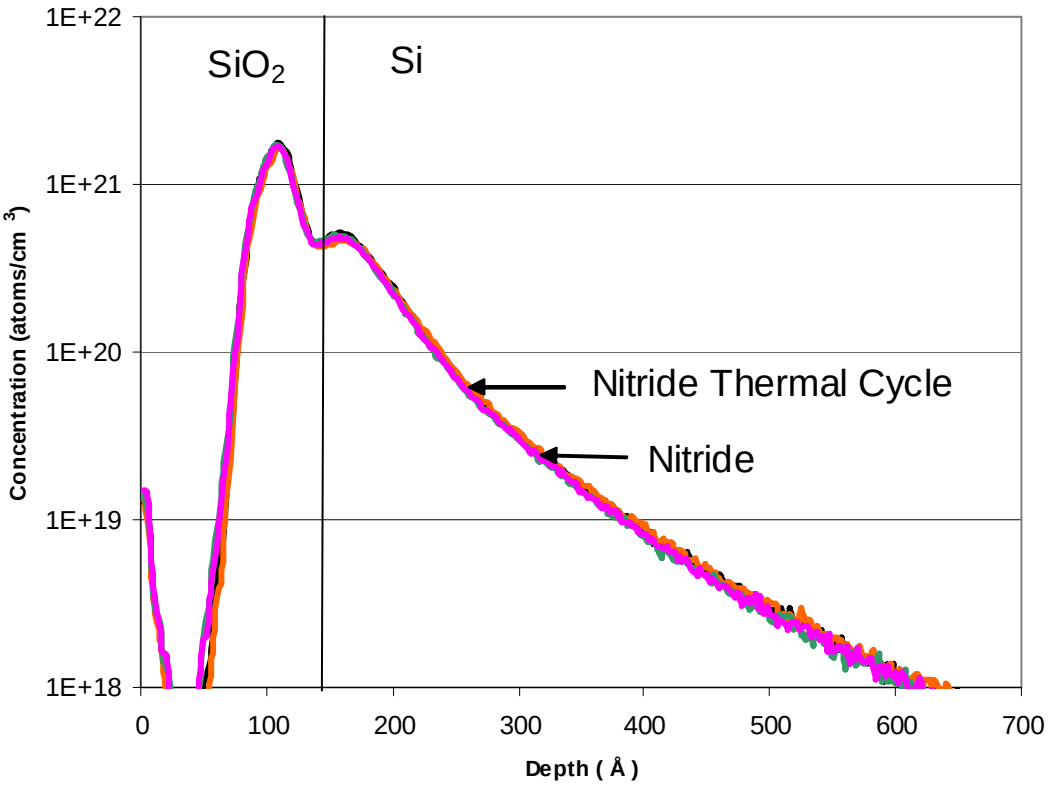

Figure 3-2: B diffusion profiles before 1050˚C spike anneal are identical for both the samples with and without the nitride. B was implanted in these samples.

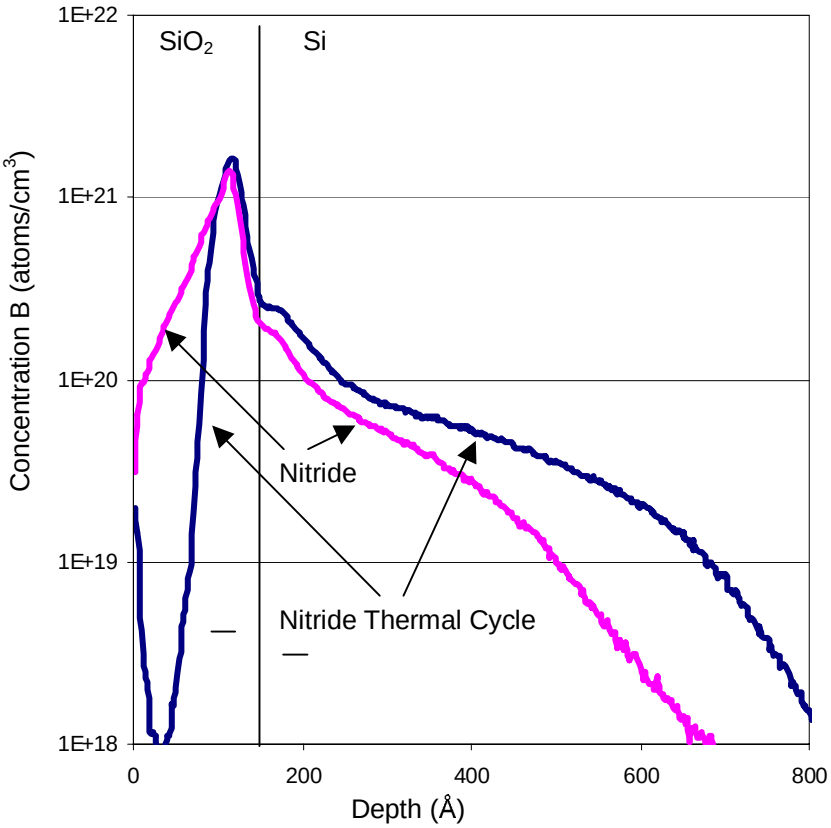

Figure 3-3: B diffusion profiles after 1050˚C spike anneal. In the presence of nitride less B is retained in Si (and more B is lost into the oxide) as compared to the nitride thermal cycle case. B was implanted in these samples.

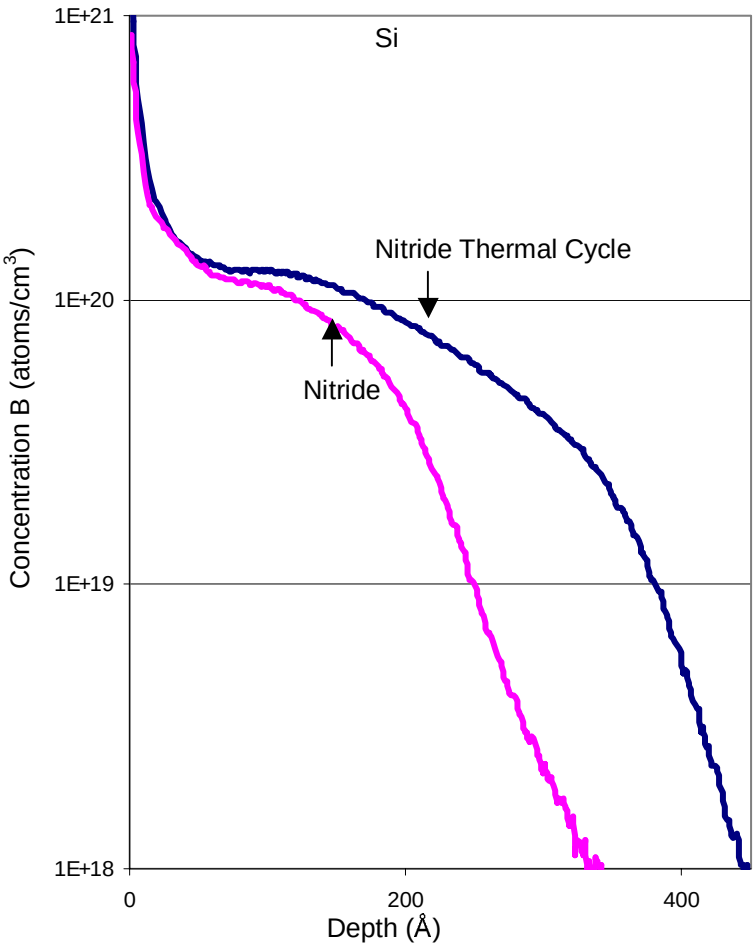

Figure 3-4: B diffusion profiles after 1050˚C spike anneal. In the presence of nitride less B is retained in Si (and more B is lost into the oxide) as compared to the nitride thermal cycle case. BF_2 was implanted in these samples.

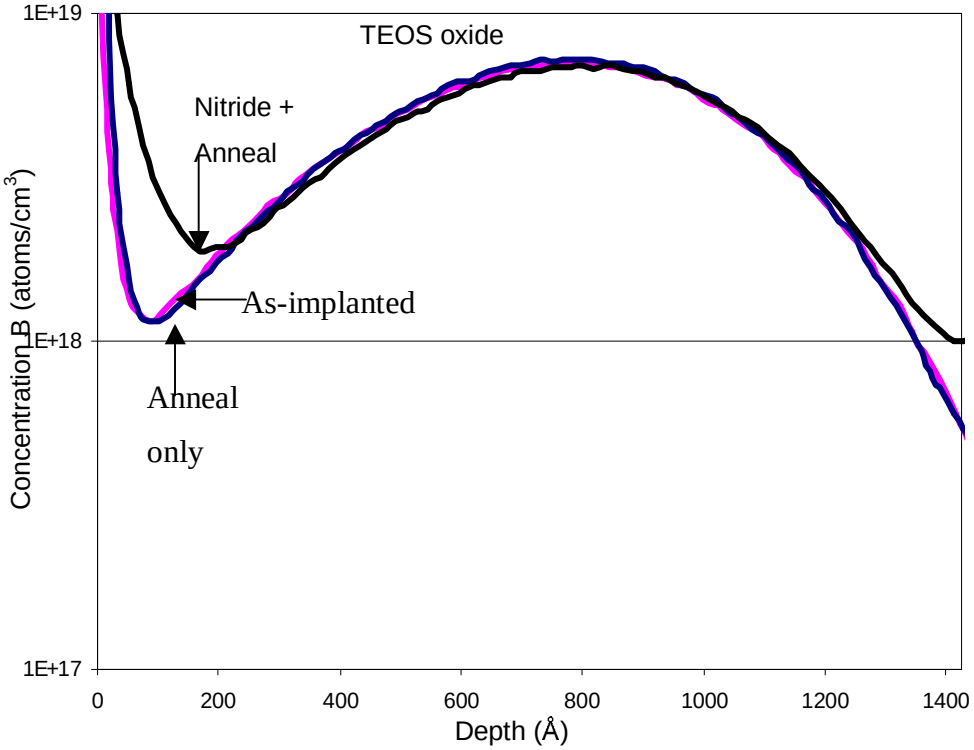

Figure 3-5: B diffusion profiles in TEOS oxide after anneal. In the presence of nitride, B diffuses faster. The B annealed profile without the nitride is identical to the as-implanted profile.

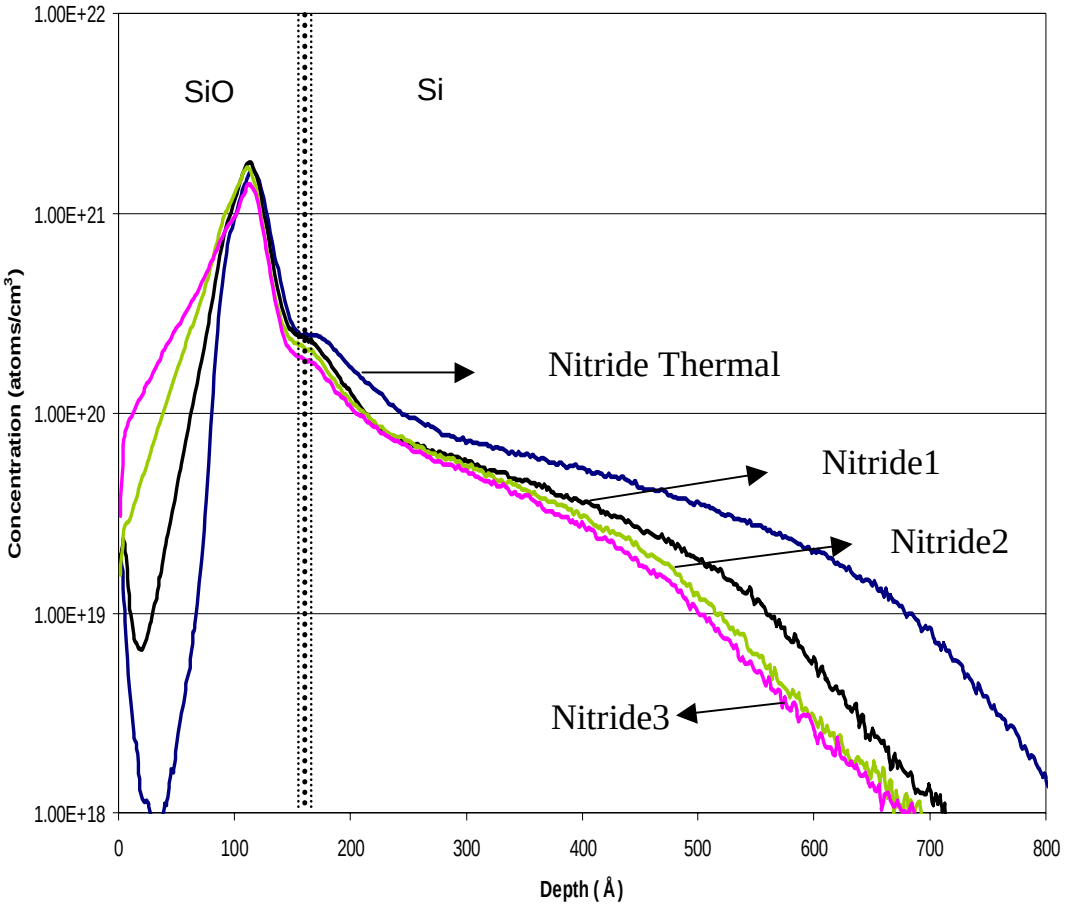

Figure 3-6: Effect of nitride stoichiometry on B diffusivity in oxide and B profile in Si. Nitride 1 seems to retain most B dose in the Si without any susbstantial trade off in junction depth.

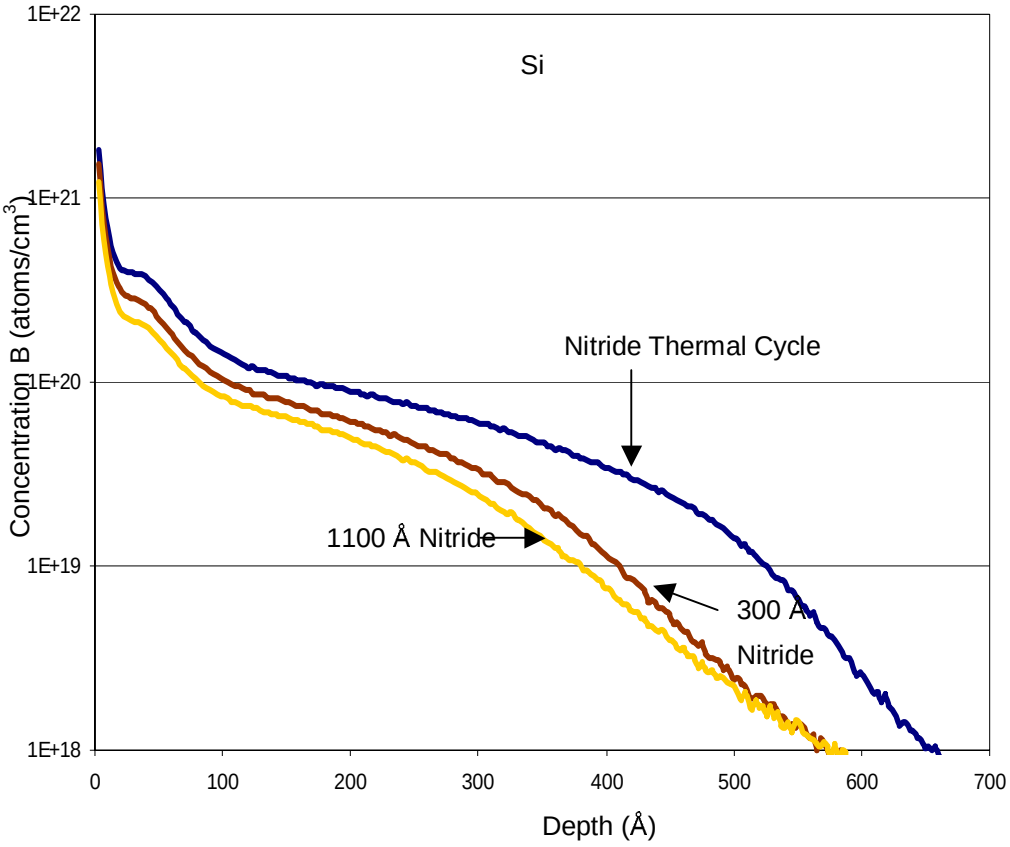

Figure 3-7: Effect of nitride thickness on B dose loss. Thicker film results in more B dose loss from Si into oxide.

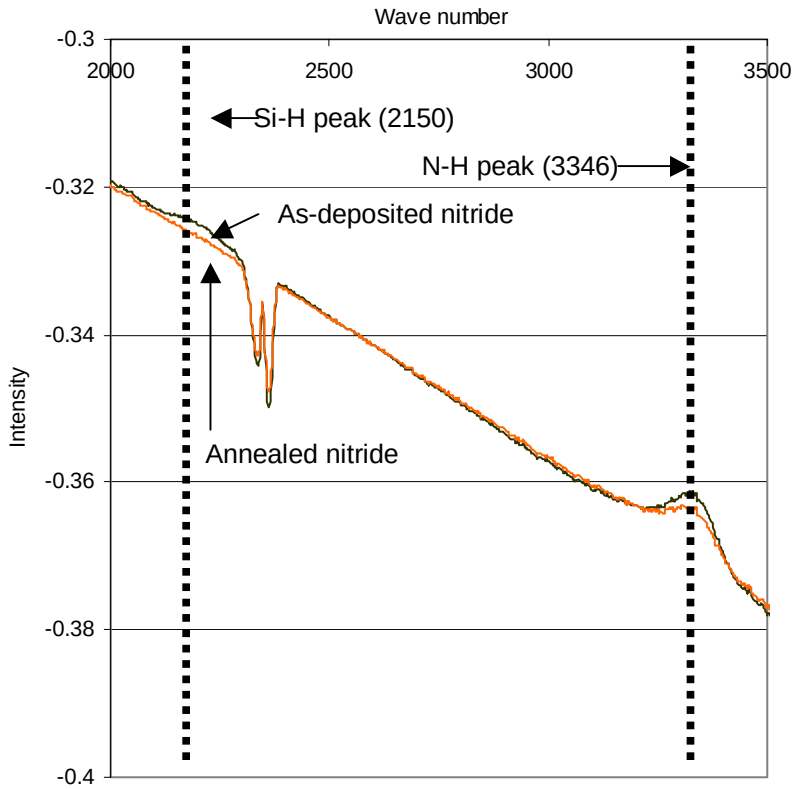

Figure 3-8: FTIR data showing decrease in both H associated peaks in nitride upon annealing. H out-diffuses from the nitride film upon annealing.

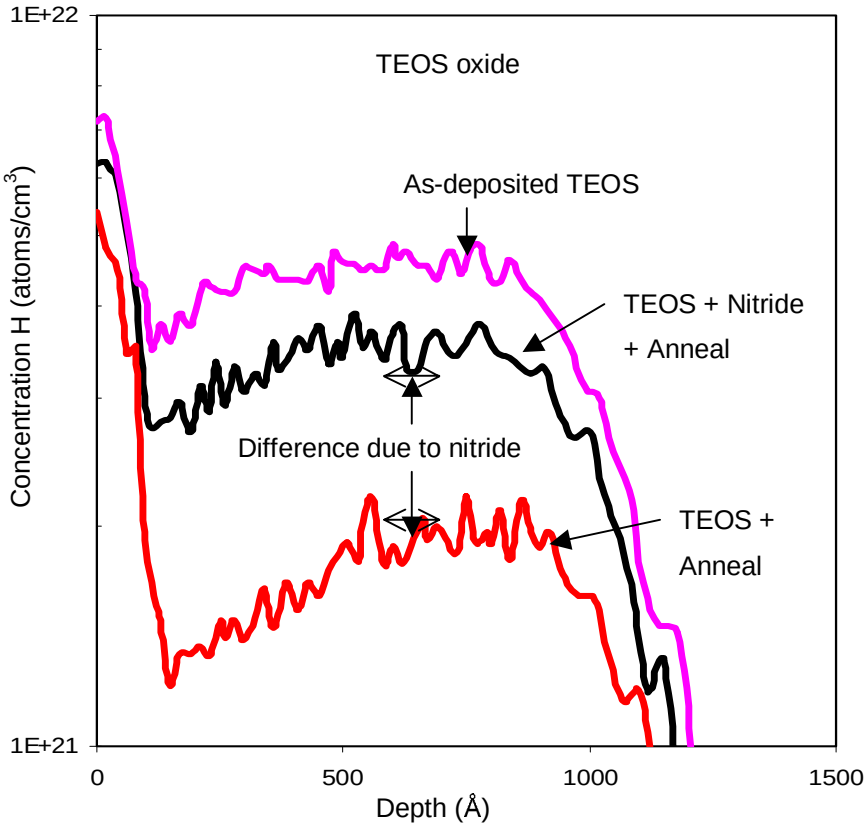

Figure 3-9: NRA H data showing as-deposited TEOS oxide has high levels of H. Nitride acts as a barrier for H out-diffusion.

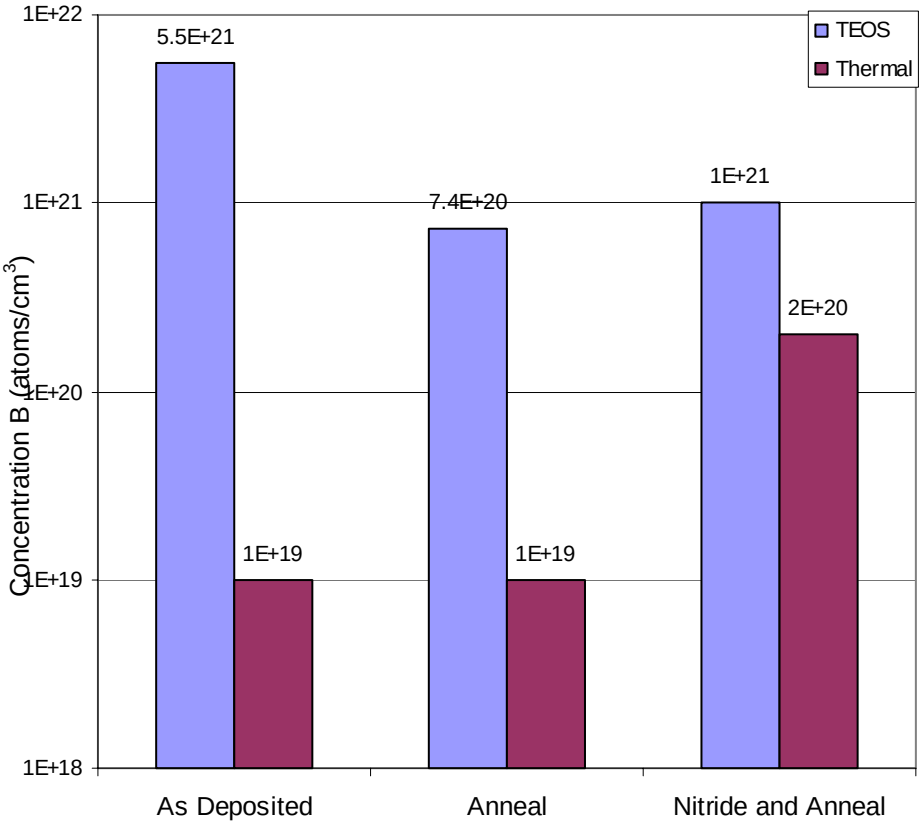

Figure 3-10: NRA H data showing in the case of TEOS oxide, nitride acts as a diffusion barrier for H, while in the case of thermal oxide nitride acts as a source of H during annealing.

Chapter 4

Fundamental characterization and modeling of the effect of different nitride sidewall spacer processes on boron dose loss in ultra-shallow junction formation

4.1 Abstract

A nitride spacer with an underlying deposited TEOS oxide, that behaves as a convenient etch stop layer, is a popular choice for sidewall spacer in modern CMOS process flows. In this work we have investigated the effect of the silicon nitride spacer process chemistry on the boron profile in silicon and the related dose loss of B from Si into silicon dioxide. This is reflected as a dramatic change in the junction depth, junction abruptness and junction peak concentration for the different nitride chemistries. We find that the silicon nitride influences the concentration of hydrogen in the silicon dioxide and the different nitride chemistries result in different concentrations of hydrogen in the silicon dioxide during the final source/drain anneal. The presence of H enhances the diffusivity of B in the silicon dioxide and thereby results in a significant dose loss from the Si into the silicon dioxide. In this work we show that this dose loss can be minimized and the junction profile engineered by choosing the desirable nitride chemistry.

4.2 Introduction

The rapid pace of improvements in the semiconductor industry has resulted principally from the exponential scaling down of device dimensions-both

lateral and vertical, since both the speed and the number of transistors per unit area increase as device dimensions are decreased. In the last decade, in order to continue conventional scaling of the source/drain junctions, the semiconductor industry has relied heavily on decreasing the implant energy, and also on minimizing the thermal budget of the activation anneal. However, with transient enhanced diffusion (TED) being less pronounced for low implant energies and sharper anneal temperature profiles, surface reactions and related processes are starting to dominate the formation of ultra-shallow junctions [1]. Recent work by Kohli et al has emphasized the importance of interactions of dopants with silicon nitride spacer layers on ultra-shallow junction formation [2]. They investigated the influence of silicon nitride spacer (from now on we will refer to silicon nitride as nitride and silicon dioxide as oxide) with an underlying deposited tetraethoxysilane (TEOS) oxide on B dose loss from the Si into the oxide. They showed that the as-deposited TEOS oxide has very high concentration of H. This H diffuses out readily upon annealing. However, the presence of nitride acts as a diffusion barrier for the out-diffusing H, resulting in high concentration of retained H in the TEOS even after annealing. The presence of this high level of retained H causes an enhancement of B diffusivity in the oxide[2-6] and thereby enhances the amount of B dose loss into the oxide from the Si. In this work we study the effect of different nitride chemistries on the hydrogen concentration in the oxide after annealing and the corresponding B dose loss.

4.3 Experiment

The experimental procedure was designed for standard source/drain extension formation with nitride spacer in the complimentary metal oxide semiconductor (CMOS) device flow, as shown in figure 4-1. Figure 4-2 shows the schematic representation of the CMOS structure to illustrate the different capping layers after source/drain extension implants in a standard CMOS process flow. After the source/drain extension implants, Si is first capped with a TEOS oxide layer (oxide1) followed by a nitride layer. For thin nitride spacer layer, the nitride deposition is followed by another oxide layer (oxide2) in order to obtain the desired thickness (in our case 800Å) of the sidewall spacer. Two different nitride chemistries were used in this work - BisTertiaryButylAminoSilane (BTBAS) and DiChloroSilane (DCS). In both chemistries NH_3 is the reacting gas. The deposition cycle for BTBAS chemistry is at 550°C for 2hrs and for DCS chemistry it is at 740°C for 1hr.

The starting material was *n*-type Si with <100> crystal orientation. On the first set of wafers, Set A, a 50Å thermal oxide was grown. The wafers were then subjected to a B (or BF_2) implant at 1.3keV (or 6keV BF_2) and a B dose of 1.2E15 atoms/cm^2. Wafers that were subjected to the BF_2 implant received a pre-damage implant. Pre-damage implant prevents dopant channeling. All wafers were subjected to a 950˚C spike anneal. A 150Å thick TEOS oxide layer was then deposited at 650˚C as part of the sidewall spacer process. Next a BTBAS nitride (300Å) or DCS nitride (800Å or 300Å) layer was deposited. For some samples during the nitride deposition step, no reaction gases were made to flow (only N_2

purge). This was to subject the wafers to the same thermal budget as BTBAS or DCS nitride without actually depositing any nitride. Finally wafers were subjected to the source/drain spike anneal at 1050˚C. Some wafers were not subjected to the final anneal to serve as a reference (as indicated in Table 4-1). For the two different DCS nitride thickness (300Å and 800Å) recipes the thermal budgets were very similar.

Another set of wafers, Set B, was deposited with 1200Å thick TEOS oxide, and then with or without, 300Å thick BTBAS nitride or 800Å DCS nitride. Next the wafers were subjected to 1050˚C spike anneal. Some wafers were not subjected to an anneal to serve as a reference (as indicated in Table 4-1). These samples enable a study of hydrogen loss from the oxide upon annealing, using the NRA technique described below.

The wafer splits for sets A and B are shown in Table 4-1.

Process Steps \ Wafers	Set A												Set B			
B implant	X	X	X	X	X	X	X	X	X	X						
BF_2 implant (into pre-damaged Si)											X	X				
TEOS 150Å	X	X	X	X	X	X	X	X	X	X	X	X				
TEOS 1200Å													X	X	X	X
BTBAS 300Å		X		X							X				X	
BTBAS Thermal Cycle			X		X											
DCS 300Å								X								
DCS 800Å						X			X			X				X
DCS Thermal Cycle							X			X						
1050°C spike				X	X			X	X	X	X	X		X	X	X

Table 4-1. Summary of wafer processing conditions.

PMOS devices were fabricated on a set of wafers, Set C, with either a 800Å DCS nitride spacer or a dual layer spacer - 300Å BTBAS followed by 500Å RTCVD oxide. Besides the spacer process, all other processing for these wafers was identical, and similar to standard PMOS device process flow.

Hydrogen profiles in the oxide were obtained using Nuclear Reaction Analysis (NRA) at the State University of New York, Albany. This method makes use of the nuclear reaction:

$$^{15}N + {}^{1}H \rightarrow {}^{12}C + {}^{4}He + \text{gamma-ray}$$

The sample to be analyzed is bombarded with ^{15}N at or above the resonant energy (6.385 MeV) and the number of characteristic gamma rays produced in the target is measured with a scintillation detector [3]. When the sample is bombarded with ^{15}N at the resonance energy, the gamma-ray yield is proportional to H on the surface of the sample. When the sample is bombarded with ^{15}N above the resonance energy, there are negligible reactions with the surface H. However, as the ^{15}N ions penetrate the sample, they lose energy and reach the resonance energy at some depth. Now the gamma-ray yield is proportional to H at this depth.

All B profiles in Si and in the oxide were obtained using dynamic Secondary Ion Mass Spectroscopy (DSIMS) at Texas Instruments. Dynamic SIMS measurements were performed using a CAMECA IMS 6f magnetic sector instrument. All measurements were performed using an O_2^+ primary beam and detecting positive secondary ions. Primary oxygen beam with impact energy of 800eV was used. The angle of incidence was approximately 42 degrees. The beam current and raster size were adequate to provide about 0.5Å per second

erosion rate. For bare Si samples, an oxygen backfill was applied to ensure the surface is fully oxidized during depth profiling. SIMS integrated dose values have an error of ±10% and depth resolution is up to 10Å. All B profiles in oxide were obtained using time-of-flight SIMS. Nitrogen and C profiles were also obtained for some samples by dynamic SIMS. Wafer bow measurements were also made. Sheet resistance values were obtained using a four-point probe and the standard deviation was less than 5%.

4.4 Results and Discussion

4.4.1 *Effect of presence of BTBAS nitride on B diffusion profile*

The target BTBAS nitride thickness was 300Å. Figure 4-3a and 4-3b show the B diffusion profiles in the Si and the TEOS oxide stack, respectively, right before the final source/drain activation anneal (for samples implanted with B). It is important to note that both samples were subjected to the same thermal budget, irrespective of whether nitride was deposited on top of the TEOS or not. Furthermore, we found that the B profile in both Si and TEOS oxide stack was not affected by the nitride deposition thermal budget. BTBAS deposition is a very low temperature process (550°C/2hrs) and it could therefore be expected that there is no conspicuous dopant movement in Si or the TEOS oxide stack during the BTBAS nitride dep/BTBAS thermal cycle only. Figures 4-4a and 4-4b show the B diffusion profiles in Si and TEOS oxide stack respectively, for samples with and without the BTBAS nitride after the 1050˚C spike. After the final activation anneal, samples with the nitride show lower retained B dose in Si than those without the BTBAS nitride. So during the 1050˚C spike, the presence of BTBAS

nitride on top of TEOS oxide seems to influence the final B diffusion profile. Samples with the BTBAS nitride on top of TEOS show a lower B concentration over most of the profile in Si and consequently shallower junctions in Si compared to samples without the BTBAS nitride. However, the B concentration in the TEOS oxide is higher along most of the depth in Si for the samples with the BTBAS nitride compared to the samples without the BTBAS nitride. It is clear from the profiles that the reduction in junction depth in the presence of BTBAS nitride comes along with a lower B concentration in Si.

Figure 4-5 shows the H profiles obtained by NRA in the TEOS oxide with and without BTBAS nitride, after anneal. The H profile for as-deposited TEOS oxide is also shown. It is important to note that the H levels in the as-deposited TEOS are very high. Instead of BTBAS nitride acting as a source of H and thereby increasing the H in the underlying oxide upon annealing, we find that BTBAS nitride seems to be acting as a barrier for the H out-diffusion from the underlying TEOS during annealing. The H concentration in the TEOS after annealing is much higher (2.6E21 atoms/cm^3) if the nitride is present during annealing as compared to the H concentration in the TEOS after annealing without nitride (1.9E21 atoms/cm^3). It is the high H concentration during anneal in the presence of BTBAS nitride that causes enhanced B diffusion [2].

4.4.2 *Effect of presence of DCS nitride on B diffusion profile*

The target DCS nitride thickness was 800Å. Figures 4-6a and 4-6b show the B diffusion profiles in the Si and the TEOS oxide stack, respectively, right before the final source/drain activation anneal for samples implanted with B. It is

important to note that the two samples marked “DCS nitride” and “DCS thermal”, were subjected to the same thermal budget, irrespective of whether DCS nitride was deposited on top of the TEOS oxide or not. The third sample marked “TEOS only” shows the B profile in both Si and TEOS oxide stack right before the DCS nitride deposition/DCS thermal cycle. Unlike BTBAS nitride, DCS nitride deposition is not a very low temperature process (740°C/1hr). Figures 4-6a and 4-6b show that there is conspicuous dopant movement in Si during the nitride deposition/nitride thermal cycle, with respect to the starting profile (marked “TEOS only”). From other experiments (not presented here), we believe that similarly processed samples which have received 950°C spike anneal before the TEOS and nitride deposition cycles, are close to equilibrium during the TEOS and nitride deposition cycles (TED is over during the 950°C spike). Therefore, it is likely that the diffusion witnessed in the sample marked “DCS thermal” is close to equilibrium B diffusion at such temperatures. It is, however, interesting to note that the B diffusion profile for the sample subjected to DCS nitride deposition is shallower that the profile for the sample subjected to DCS thermal cycle only. Also the B profile in TEOS oxide stack for the sample with the DCS nitride is more diffused than the profile that is subjected to DCS thermal cycle only. This implies that for the sample with the DCS nitride, B diffusion is enhanced in the TEOS oxide stack which leads to some dose loss from the Si into the oxide during the nitride deposition itself, thus resulting in a shallower profile than what one would expect due to the thermal cycle only. Figures 4-7a and 4-7b show the B diffusion profiles in Si and TEOS oxide stack, respectively, for both the samples

with and without the DCS nitride after the 1050˚C spike. After the final activation anneal, samples with the DCS nitride show lower retained B dose in Si than those without the DCS nitride. Although the profiles before the final anneal for samples with DCS nitride and with DCS thermal cycle only showed some difference in the total integrated dose value, the difference observed after the final anneal at 1050°C is more than an order of magnitude. So during the 1050˚C spike, the presence of DCS nitride on top of TEOS oxide influences the final B diffusion profile. Samples with the DCS nitride on top of TEOS show lower B concentration over most of the profile in Si and consequently shallower junctions in Si, compared to samples without the DCS nitride. However, the B concentration in the TEOS oxide is higher at all depths for the samples with the DCS nitride compared to the samples without the DCS nitride. It is clear from the profiles that the reduction in junction depth in the presence of DCS nitride comes along with a lower B concentration along most of the profile depth. The average conductivity of the junctions (calculated as the inverse of the product of sheet resistance and junction depth) indicates formation of a lower conductivity junction in the presence of DCS nitride. These trends are similar to what is observed in the case of BTBAS nitride and also what has been reported in the case of RTCVD nitride [2].

Figure 4-8 shows the H profiles obtained by NRA in the TEOS oxide with and without DCS nitride, after anneal. The H profile for as-deposited TEOS oxide is also shown. Once again, we find that nitride seems to be acting as a barrier for the H out-diffusion from the underlying TEOS during annealing. The H

concentration in the TEOS after annealing is much higher (3.73E21 atoms/cm^3) if the nitride is present during annealing as compared to the H concentration in the TEOS after annealing without nitride (1.9E21 atoms/cm^3).

Figure 4-9 shows the effect of DCS nitride thickness on the B dose retained in the Si. As reported before [5], the thicker the nitride the more the B dose loss from Si into oxide. However, the change in integrated dose values while going from 800Å to 300Å is relatively small (<5%) and therefore the thickness effect can be viewed as a secondary effect.

4.4.3 *Comparison of different nitride chemistries on B diffusion profiles*

Boron diffusion data with RTCVD nitride after 1050°C spike anneal has been reported in chapter 3. Figure 4-10 shows the final annealed profiles obtained with and without nitride for BTBAS, DCS and RTCVD nitride. It is evident (as has been discussed before for each of these nitrides) that the presence of nitride results in shallower junctions. BTBAS nitride results in the highest retained dose in the Si followed by DCS nitride and RTCVD nitride, respectively. Figure 4-11 shows the peak H concentration in TEOS after 1050°C spike for the different nitrides. BTBAS nitride that results in the highest retained B dose in Si and therefore the least B dose loss from Si into oxide shows the lowest H peak concentration, whereas RTCVD nitride which shows the least retained B dose in Si shows the highest H peak concentration in TEOS after the final anneal. These observations correlate well with the dose loss model proposed in chapter 3. Based on our observations BTBAS seems to be a less effective barrier to H out diffusion

from the TEOS into the ambient through the nitride compared to DCS or RTCVD nitride.

The stress values obtained using wafer bow measurements with the nitride (DCS\BTBAS\RTCVD) were of the order of 1E10 dynes/cm^2 tensile. According to the literature [7], much higher stress values would be required to change the B diffusivity in order to be able to match the B profiles in the oxide in the presence of nitride. Also, it is important to note that different nitride chemistries result in very similar values of stress; however, they result in very different B diffusion profiles. In order to understand the effect of nitride we profiled N in the TEOS oxide (and C in addition to N in the case of BTBAS, since BTBAS chemistry has C). Our results from DSIMS showed very similar levels of N (and C) in the TEOS oxide both with and without the presence of nitride after the 1050˚C anneal. We therefore believe that it is indeed the high concentration of H in the TEOS in the presence of nitride that results in enhanced B diffusivity in the TEOS oxide and the related B dose loss.

The integrated dose values for the profiles obtained with the nitride thermal cycles for BTBAS, DCS or RTCVD nitride, show very similar values. It is interesting to note that the gradient/abruptness of the profiles obtained with and without nitride are very similar for each nitride. This probably implies that the thermal budget associated with the nitride deposition dictates the abruptness of the final B diffusion profile. Furthermore, since BTBAS results in the most abrupt profile and DCS results in the most gradual profile, it is probable that lower the

thermal budget of the nitride deposition higher the gradient of the diffusion profile.

Figure 4-12 shows the B diffusion profiles obtained for samples, in which BF_2 was implanted into Sb

pre-damaged Si, with 300Å BTBAS and 800Å DCS nitride spacer processes. Once again, as we had observed for B implanted samples, we find that BTBAS nitride results in a much higher retained B dose in Si than DCS nitride. Also the B profile obtained with BTBAS nitride is more abrupt. In other experiments (not discussed here) in which we deposited 500Å oxide after 300Å BTBAS deposition (in order to obtain a spacer thickness of 800Å as in DCS nitride case), we found that the oxide deposition (oxide2 in figure 4-1) did not affect the final annealed B diffusion profile in any conspicuous manner. In figure 4-13 we compare the PMOS device performance for the two different nitride spacer processes – one 800Å DCS nitride and the other 300Å BTBAS nitride followed by 500Å oxide. The devices with BTBAS nitride spacer show higher saturation currents as would be expected from a highly conductive (high concentration) and more abrupt source/drain extension.

4.5 Modeling

A model to explain the effect of sidewall nitride spacer process on source/drain extension formation is discussed below. A diffusion model for H in the source/drain spacer is developed and combined with a model for B diffusion. The model is first calibrated to H out-diffusion data obtained from NRA and then to diffusion data from SIMS. Experimentally observed changes in junction depth

with variations in sidewall nitride spacer chemistry are explained by this model. The model can be applied to TCAD process/device simulations for effective optimization of complex front-end processes.

4.5.1 *Proposed Model*

Figure 4-2 shows the schematic representation of the CMOS structure to illustrate the different capping layers after source/drain extension implants in a standard CMOS process flow. Figure 4-14 represents a schematic illustration of the models and interactions considered in this work. Primarily, we model the diffusion of H through various spacer layers (oxide1/nitride/oxide2) and its effect on B diffusion in Si and oxide. As has been suggested in literature [2] and also in this work, deposited oxides contain large amount of H. This H is highly volatile and out-diffuses readily. A nitride on top of oxide acts as a barrier to the out-diffusing H. Due to the differences in composition, different nitrides lead to different concentrations in the oxide (oxide1) after final source/drain anneal. Higher concentrations of H in oxide enhance B diffusion in oxide resulting in an increase in dose-loss of B from Si into the oxide. This reduces the extent of B diffusion in Si as observed by experimental data.

We assume diffusion of both H and B in oxides is mediated by only a neutral species. This assumption enables us to exclude ionic charge balance. We further assume that the B diffusion in oxide obeys Fick's laws. It has been reported that the B diffusion in oxide increases in the presence of H [2-6]. In order to incorporate the effect of H on the B diffusivity in oxide (D_B^{Ox}) we assume that

B reacts with the H in the oxide to form a fast diffusing species BH_n , with a diffusion coefficient D_{BHn}^{Ox} , according to the reaction –

$$B + nH <=> BH_n \qquad \text{(Eq.1)}$$

Dunham and Wu[8], as well as Mathiot and Pfister[9] have treated similar cluster formations between dopant atoms and point defects in order to explain diffusivity enhancements seen in heavily doped materials.

Assuming that B and H are in dynamic equilibrium with BH_n, we can write

$$C_{BHn} = K_{eq} .C_B.(C_H)^n \qquad \text{(Eq.2)}$$

Where K_{eq} is the equilibrium constant for the reaction between B, H and BH_n.

We know that total B concentration is equal to the sum of free B concentration (C_B) and B concentration in BH_n (C_{BHn}). Therefore,

$$d(C_B + C_{BHn}) / dt = D_B^{Ox} [d^2 (C_B) / dx^2] + D_{BHn}^{Ox} [d^2 (C_{BHn}) / dx^2]$$

$$= D_B^{Ox} [d^2 (C_B) / dx^2] + D_{BHn}^{Ox} [d^2 (K_{eq} .C_B.(C_H)^n) / dx^2] \qquad \text{(Eq.3)}$$

Since H is diffuses rapidly and results in an almost flat profile, we can approximate the second derivative of H concentration with respect to x to be zero.

Then,

$$d(C_B + C_{BHn}) / dt = D_B^{Ox} [d^2 (C_B) / dx^2] + D_{BHn}^{Ox} . Keq .(C_H)^n . [d^2 (C_B) / dx^2] \qquad \text{(Eq.4)}$$

Furthermore let us assume $D_{BHn}^{Ox} = a. D_B^{Ox}$, where "a" is a constant. Then we can rewrite Eq. 4 as

$$d(C_B + C_{BHn}) / dt = D_B^{Ox} [d^2 (C_B) / dx^2] + a.D_B^{Ox}. Keq .(C_H)^n . [d^2 (C_B) / dx^2]$$

Therefore the effective diffusion coefficient of B in oxide can be written as

$$D_B^{Eff} = D_B^{Ox} \{ 1 + [(C_H)^n / (C_H^{ref})^n]\} \qquad \text{(Eq.5)}$$

Where $(C_H^{ref})^n = 1 / (Keq . a)$, and is assumed to be a constant.

We model B diffusivity in oxide as :

$$D_B^{Eff} = D_B^{Ox} \{ 1 + [C_H/C_H^{ref}]^n\} \qquad \text{(Eq.6)}$$

Where D_B^{Ox} is the diffusivity of B in pure oxides, and C_H is the concentration of H in oxide. C_H^{ref} and n are empirical fitting parameters.

Kohli et al. have proposed that the rate of out-diffusion of H through the nitride is the rate limiting step [2]. The effect of different nitride chemistries on the rate at which H out-diffuses from the oxide1 is captured by modeling the transfer of H across the oxide/nitride interface as :

$$J_H = h [C_H^{Ox} – (C_H^{Nit} / m_{seg})]$$

where m_{seg} is the segregation coefficient of H between oxide and nitride, and h is the transfer coefficient. m_{seg} and h are empirical fitting parameters which are tuned for different nitride chemistries.

4.5.2 *Model Verification*

Hydrogen diffusion parameters are estimated by calibrating to H out-diffusion data obtained by NRA. Figure 4-15 shows comparison of the model to out-diffusion of H from an uncapped oxide into the ambient. In this work we consider the effect of two different nitride chemistries, namely, BTBAS and RTCVD. Both of these have a very low thermal budget (as opposed to DCS

nitride) and no visible dopant diffusion is observed during the deposition. In other words, the B profiles right before the final anneal look quite similar for these two nitride chemistries. Figure 4-16 looks at the effect of changing only the nitride process on H out-diffusion during the final anneal. Hydrogen segregation between the oxide and the nitride capture these differences well in the model.

A B-Si interstitial cluster model calibrated to inert anneals, Figure 4-17, is used as a reference for B diffusion in Si. Comparison of the model to B profiles is shown in Figures 4-18 – 4-21. Figure 4-18 shows model calibration representing effect of BTBAS nitride. As we observed in Figure 4-16, BTBAS is a less effective barrier against H diffusion. Hence, the dose loss and reduction in junction depth is minimal. Figure 4-19 shows the effect of the BTBAS on the boron profile in oxide1 as measured by TOF-SIMS. An enhancement in the B diffusivity is observed after the 1050°C spike anneal and is captured by the model. Figure 4-20 shows model calibration representing effect of RTCVD nitride. RTCVD nitride is a more effective barrier to H out-diffusion. Hence, this leads to increased dose loss of B into the oxide from the Si resulting in shallower junctions and with lower B concentrations compared to BTBAS nitride (Fig. 4-21).

4.6 Summary

An investigation of the influence of the nitride spacer chemistry on B dose loss from the Si into the oxide has been done. We showed that the as-deposited TEOS oxide has very high concentration of H. This H diffuses out readily upon annealing. However, the presence of nitride acts as a diffusion barrier for the out-

diffusing H, resulting in higher concentration of retained H in the TEOS even after annealing. The presence of this high level of retained H causes an enhancement of B diffusivity in the oxide and thereby enhances the amount of B dose loss into the oxide from the Si. However, different nitride chemistries result in different concentration of H in the TEOS upon annealing and therefore different B dose loss. BTBAS nitride, by acting as the least effective barrier for H out-diffusion from the TEOS, relative to DCS and RTCVD nitride, results in the highest retained B dose in Si and therefore results in most conductive source/drain junctions. The MOSFET I_{on}-I_{off} values show BTBAS to be the most desirable chemistry. A new model that predicts B junction depths and dose-loss during fabrication of ultra-shallow junctions has been developed.

4.7 References

1. S.T. Dunham, IEDM Tech. Digest, 501, 1998.
2. P. Kohli, et al., (to be published) J. Va. Sci. Technol., Jan 2004.
3. Y. Shacham-Diamand, W. G. Oldham, J. Elect. Mater., 15, 229, 1986
4. T. Aoyama, et al., J.J.Appl. Phys. Vol. 38, 2381, 1999.
5. R. B. Fair, IEDM Tech. Digest, 85, 1995.
6. R. Fair, IEEE Electron Device Letters, Vol. 17 (5), 242, 1996.
7. M. Aziz, Defect and Diffusion Forum, 153, 1998.
8. S. T. Dunham, C. D. Wu, J. Appl. Phys. Vol. 78 (4), 2362, 1995.
9. D. Mathiot, J. C. Pfister, J. Appl. Phys. Vol. 66 (2), 970, 1989.

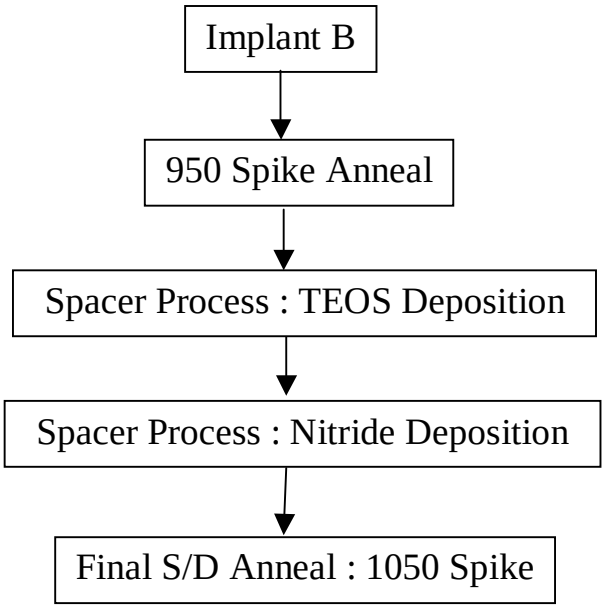

Figure 4-1: Experimental procedure for standard VLSI *p*-MOS source/drain extension formation with nitride sidewall spacer.

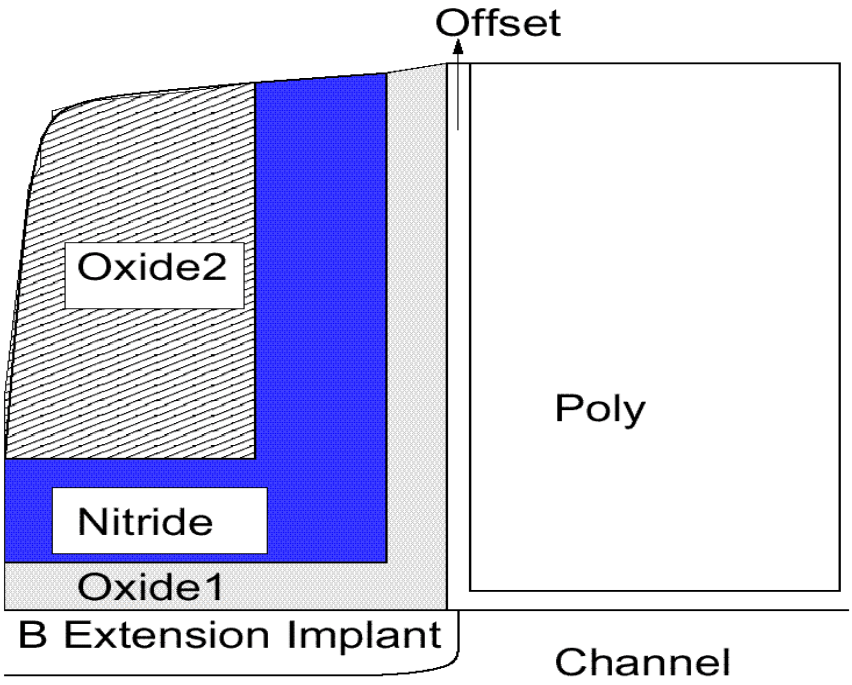

Figure 4-2 : Schematic illustration of various spacer layers during the formation of source/drain extension.

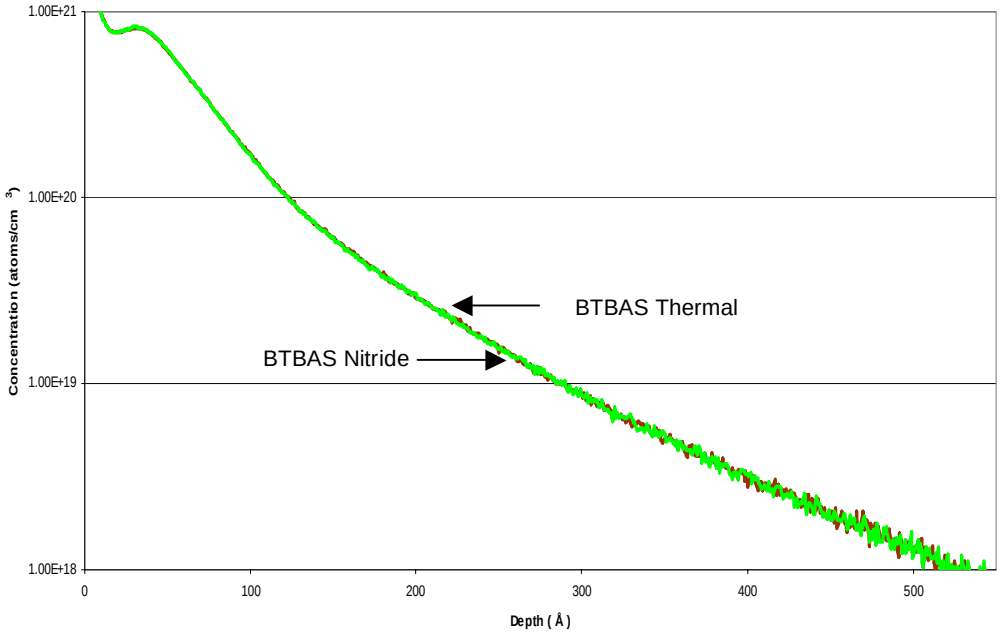

Figure 4-3(a): B diffusion profiles in Si (from DSIMS) before 1050°C anneal are identical for samples with and without BTBAS nitride. It is important to note that both samples are subjected to the same thermal budget irrespective of whether BTBAS nitride is deposited or not.

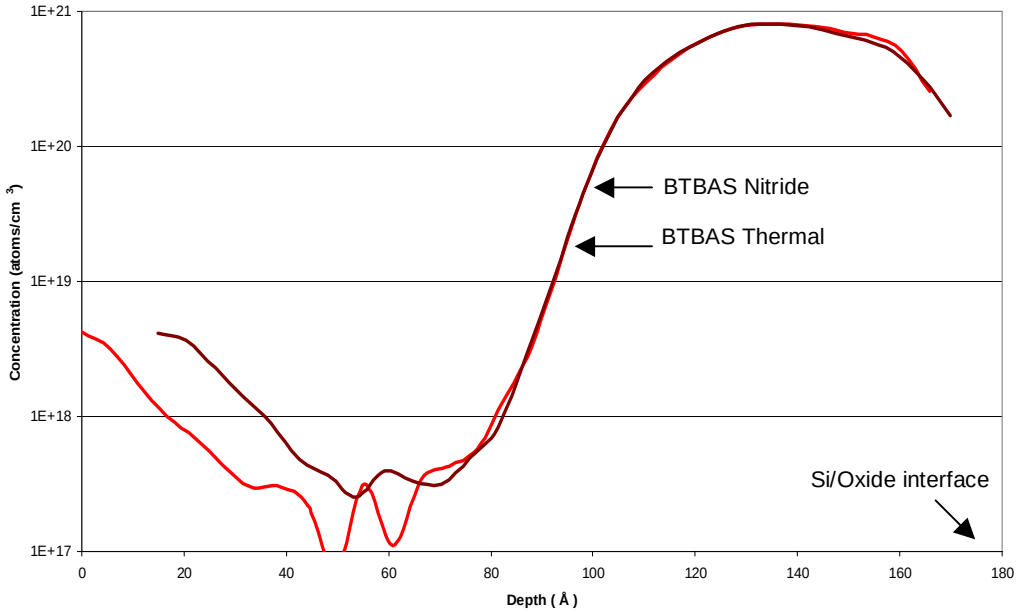

Figure 4-3(b): B diffusion profiles in TEOS oxide stack (from TOF SIMS) before 1050°C anneal are identical for samples with and without BTBAS nitride. It is important to note that both samples are subjected to the same thermal budget irrespective of whether BTBAS nitride is deposited or not.

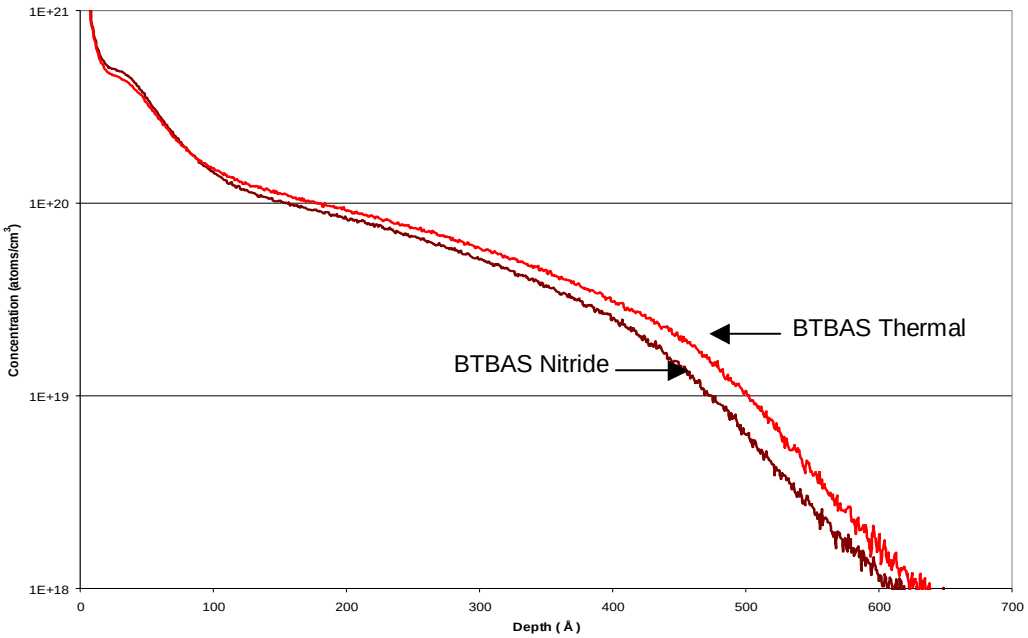

Figure 4-4(a): B diffusion profiles in Si after 1050°C anneal (from DSIMS). In the presence of BTBAS nitride less B is retained in Si.

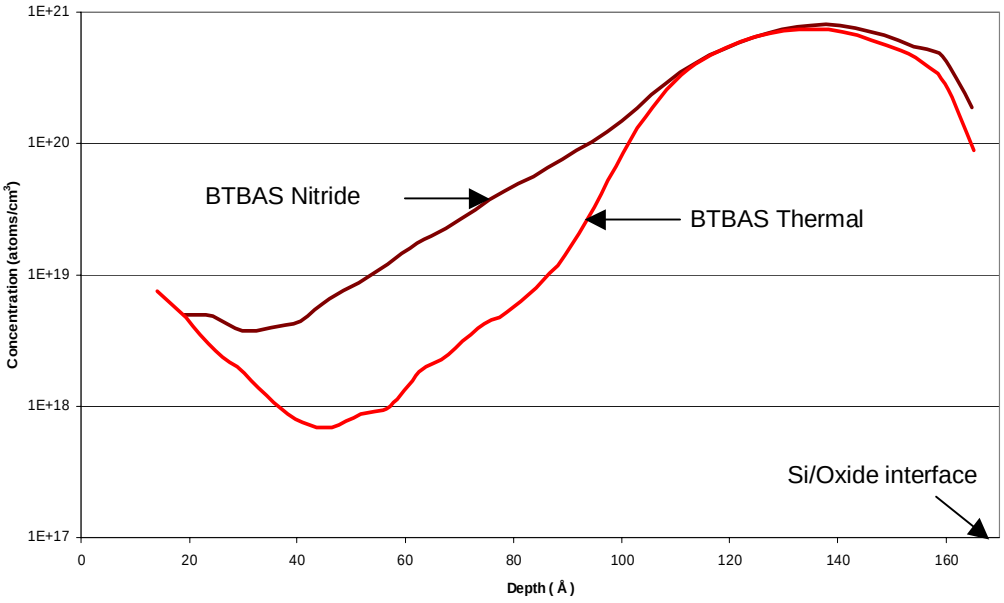

Figure 4-4(b): B diffusion profiles in TEOS oxide stack after 1050°C anneal (from TOF SIMS). In the presence of BTBAS nitride B diffusivity is enhanced in the oxide resulting in higher dose of B in the oxide.

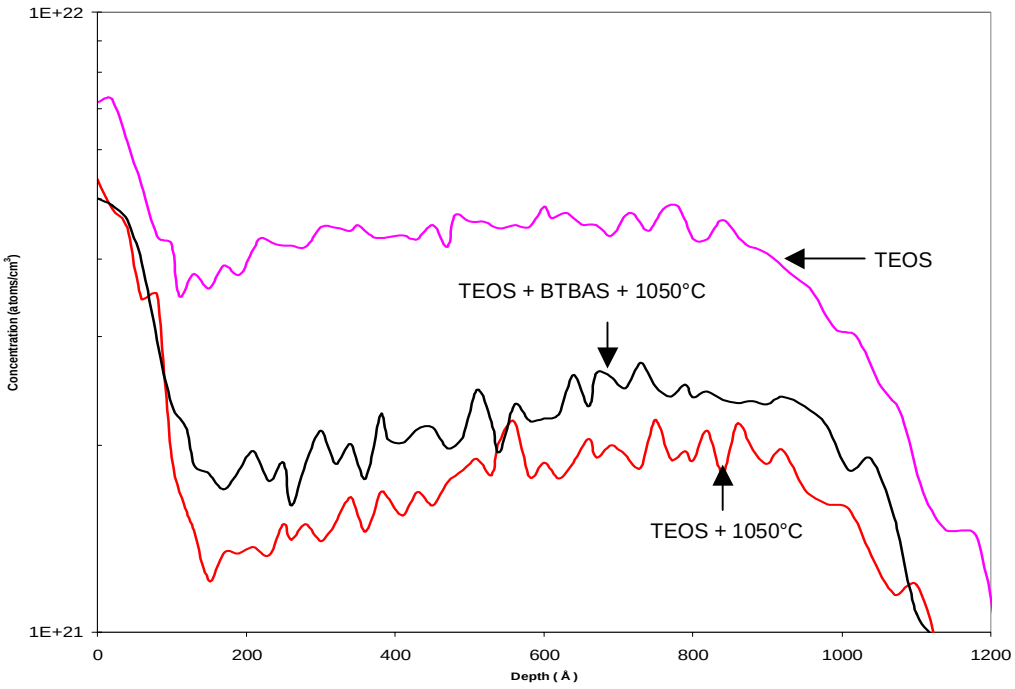

Figure 4-5: H profiles (from NRA) showing as-deposited TEOS oxide has high levels of H. BTBAS nitride acts as a barrier for H out-diffusion.

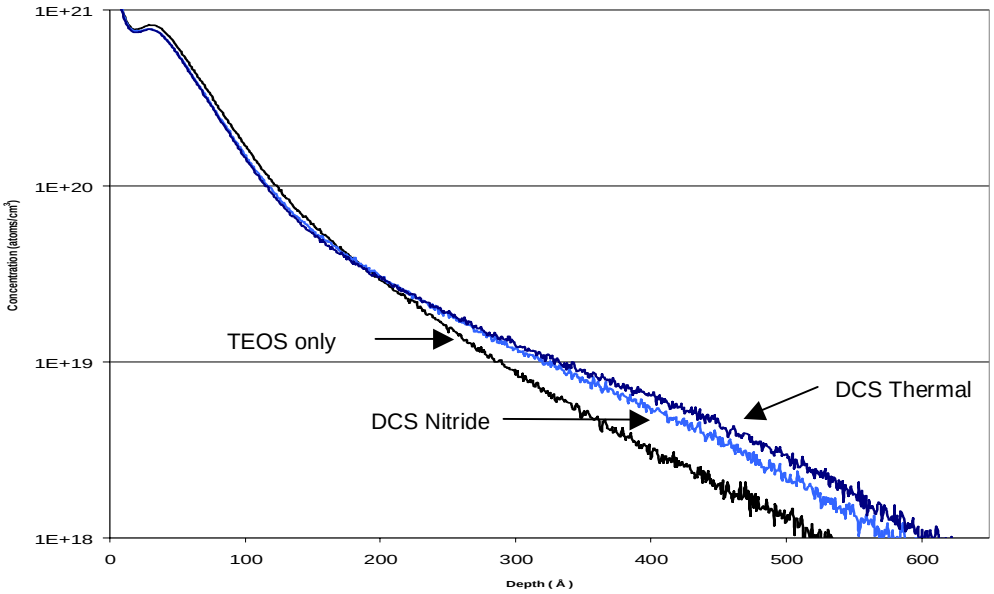

Figure 4-6(a): B diffusion profiles in Si (from DSIMS) before the final 1050°C anneal for samples with and without DCS nitride. The B profile after TEOS deposition is shown as a reference. Conspicious dopant movement in Si during DCS nitride deposition or DCS thermal cycle is observed.

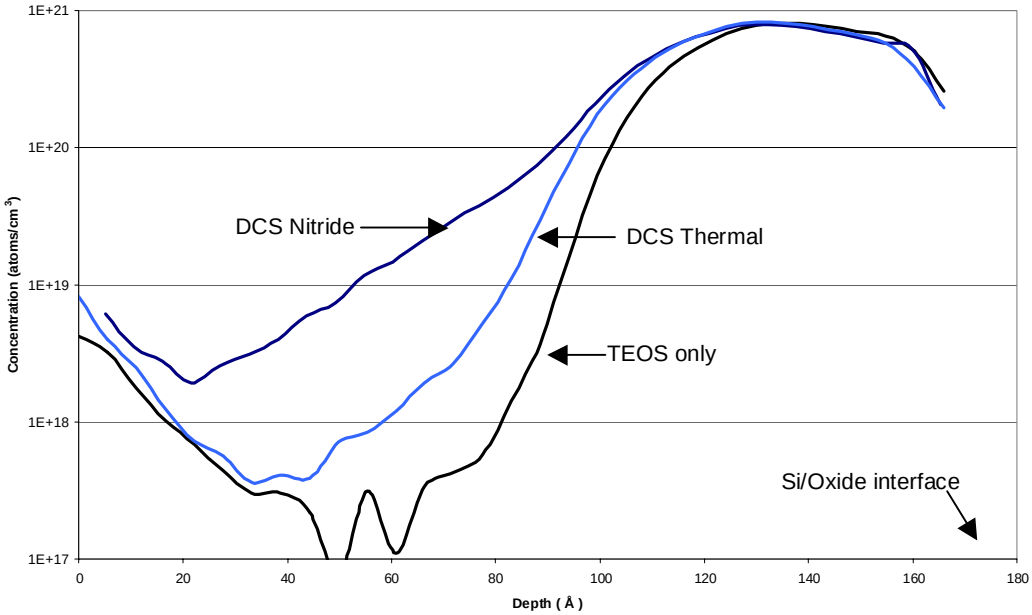

Figure 4-6(b): B diffusion profiles in TEOS oxide stack (from TOF SIMS) before the final 1050°C anneal for samples with and without DCS nitride. The B profile after TEOS deposition is shown as a reference. Conspicious dopant movement in TEOS oxide stack during DCS nitride deposition or DCS thermal cycle is observed.

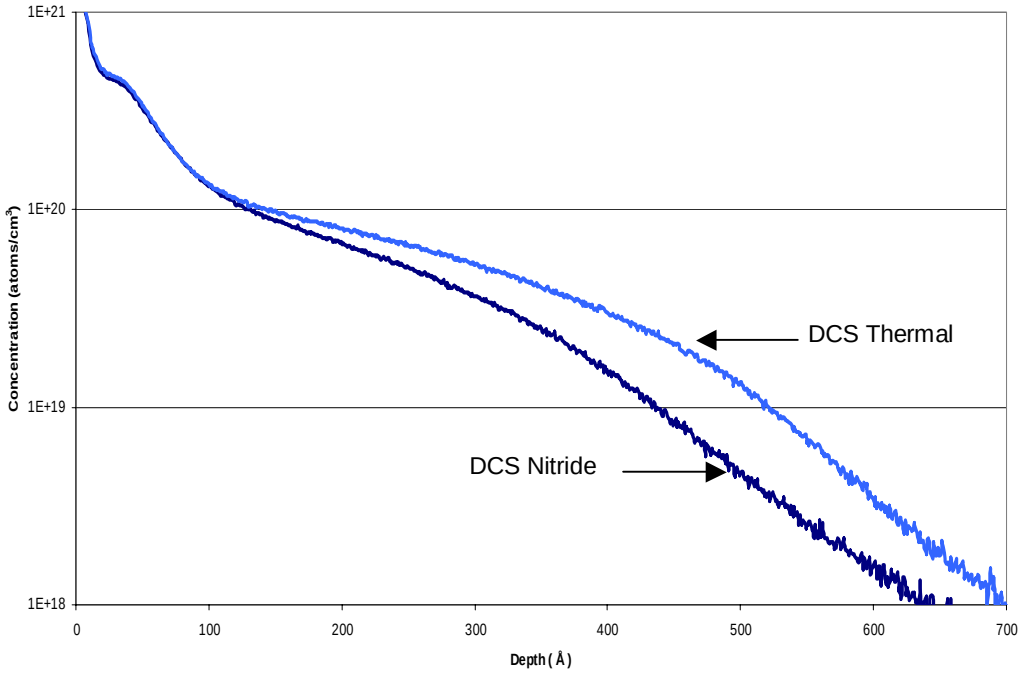

Figure 4-7(a): B diffusion profiles in Si (from DSIMS) after 1050°C anneal (from TOF SIMS). In the presence of DCS nitride less B is retained in Si.

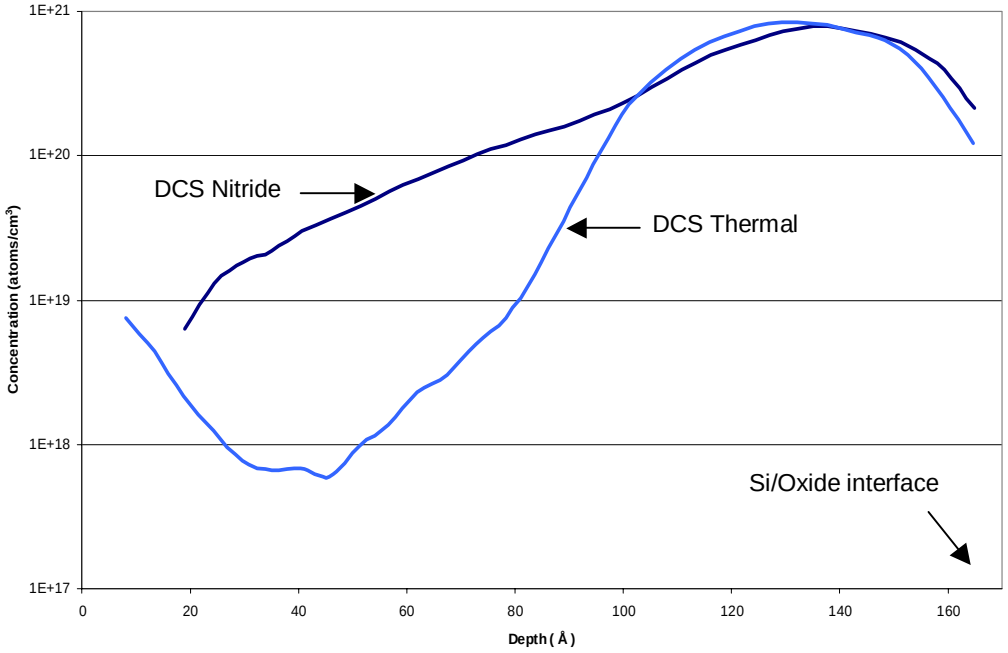

Figure 4-7(b): B diffusion profiles in TEOS oxide stack after 1050°C anneal (from TOF SIMS). In the presence of DCS nitride B diffusivity is enhanced in the oxide resulting in higher dose of B in the oxide.

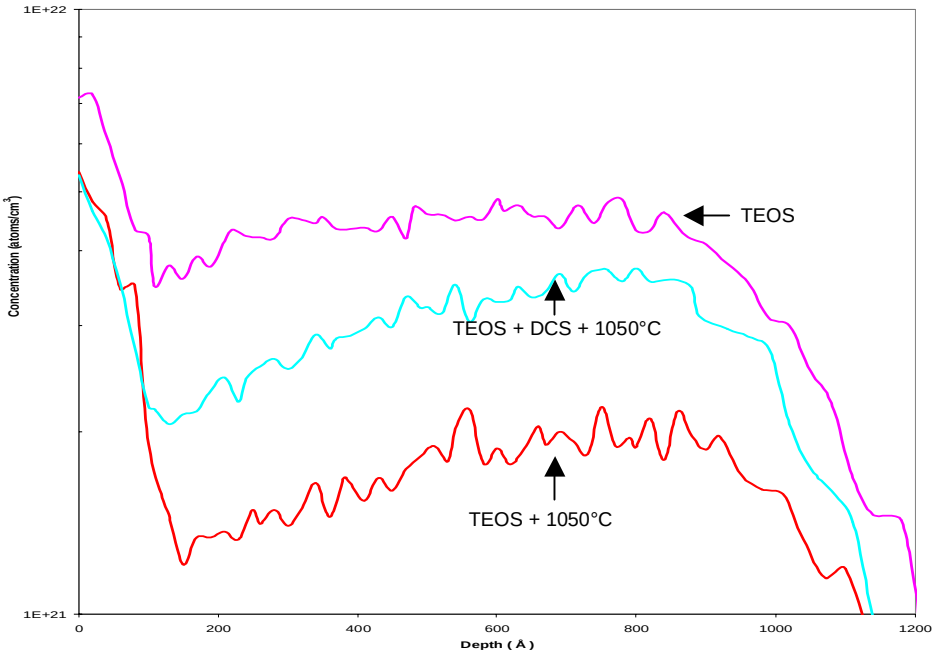

Figure 4-8: H profiles (from NRA) showing as-deposited TEOS oxide has high levels of H. DCS nitride acts as an effective barrier for H out-diffusion.

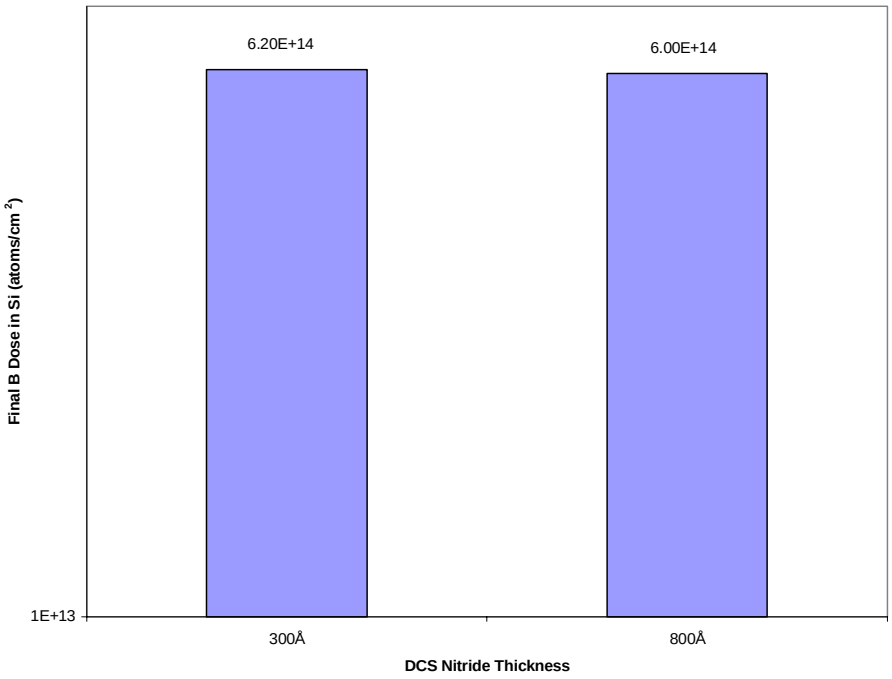

Figure 4-9: Effect of varying DCS nitride thickness on the retained B dose in Si. Thicker nitride films result in lesser retained B dose.

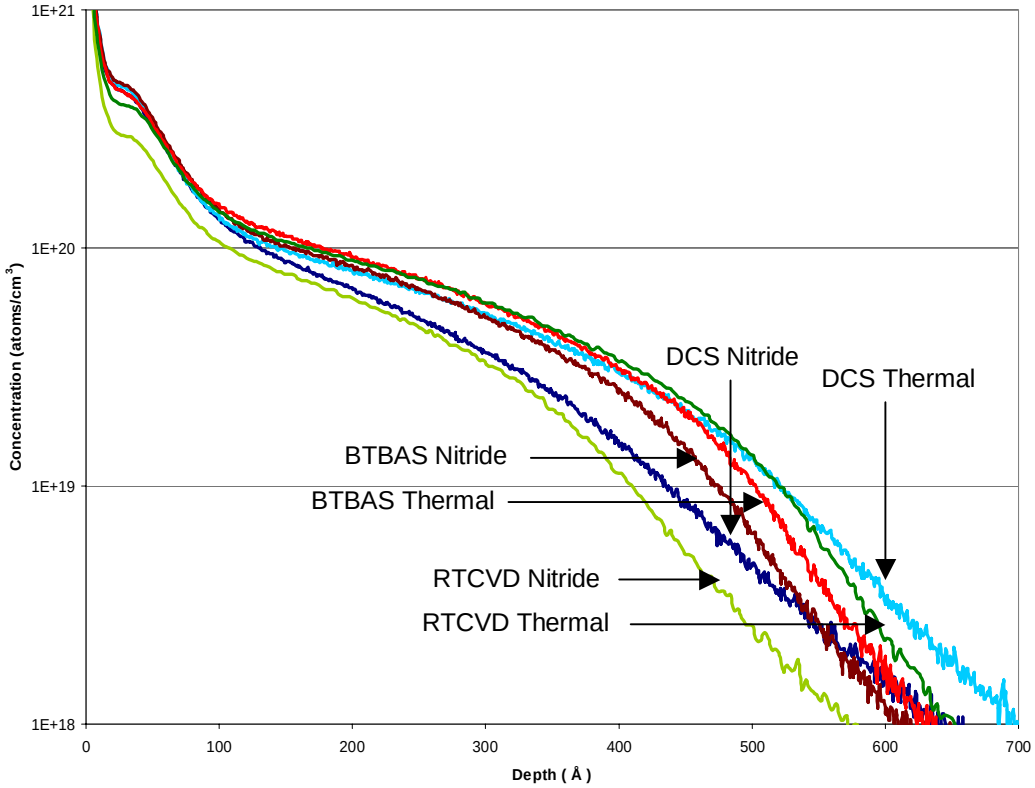

Figure 4-10: Comparison of final annealed B junctions in Si (from DSIMS) formed using BTBAS, RTCVD or DCS nitride spacer process. Also shown are the final annealed B profiles in Si obtained without nitride deposition. BTBAS nitride results in the highest retained B dose in Si.

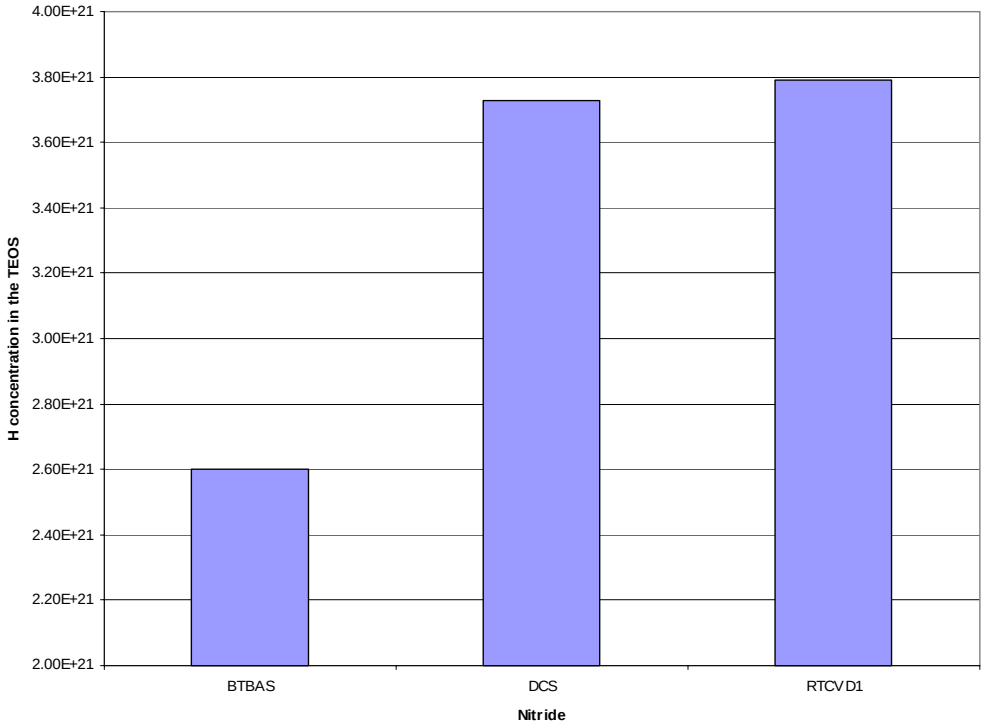

Figure 4-11: H concentration in the TEOS oxide stack after 1050°C anneal for BTBAS, DCS, and RTCVD nitride. BTBAS nitride results in the lowest concentration of H in the TEOS oxide. RTCVD nitride acts as the most effective barrier for H out-diffusion.

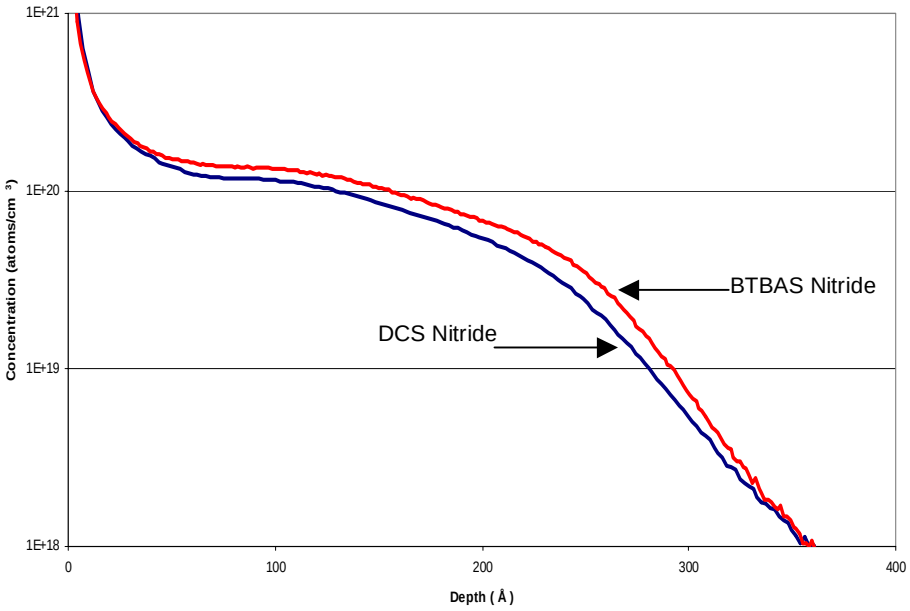

Figure 4-12: Comparison of final annealed B junctions in Si (from SIMS) formed either by DCS or BTBAS nitride. BF_2 was implanted into pre-damaged Si in these samples.

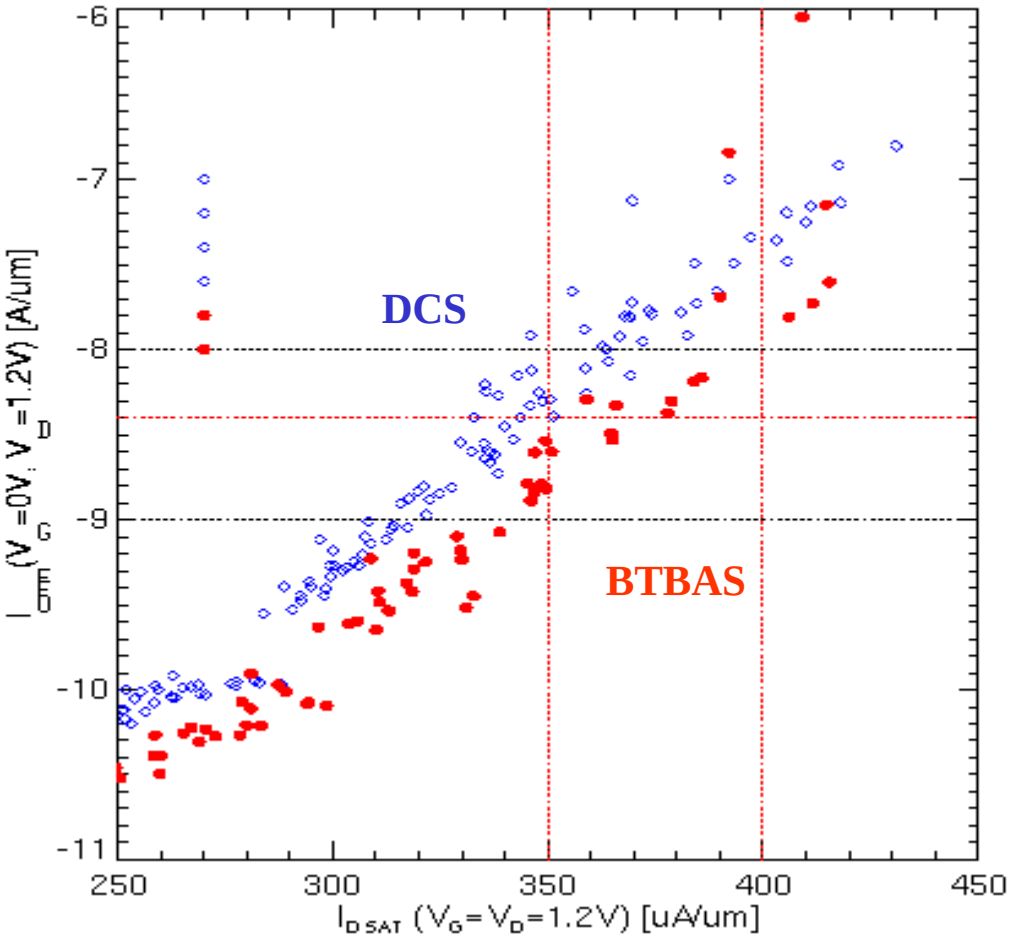

Figure 4-13: Comparison of PMOSET I_{on}- I_{off} data for devices fabricated using BTBAS or DCS nitride spacer process.

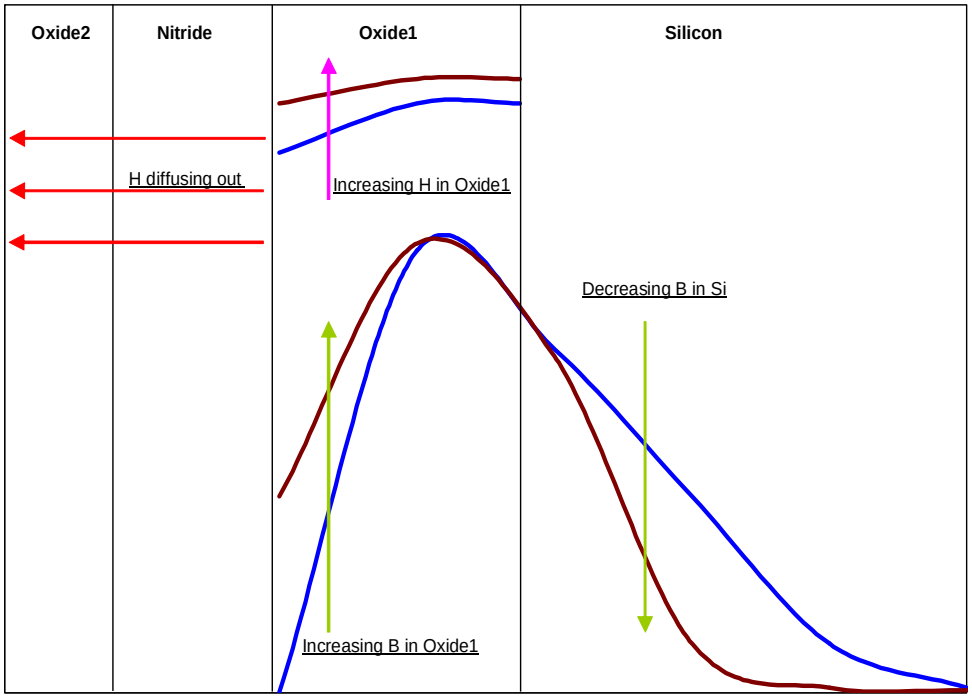

Figure 4-14: Schematic illustration of the H model and B diffusion in oxide. The presence of H in oxide enhances the B diffusivity in oxide.

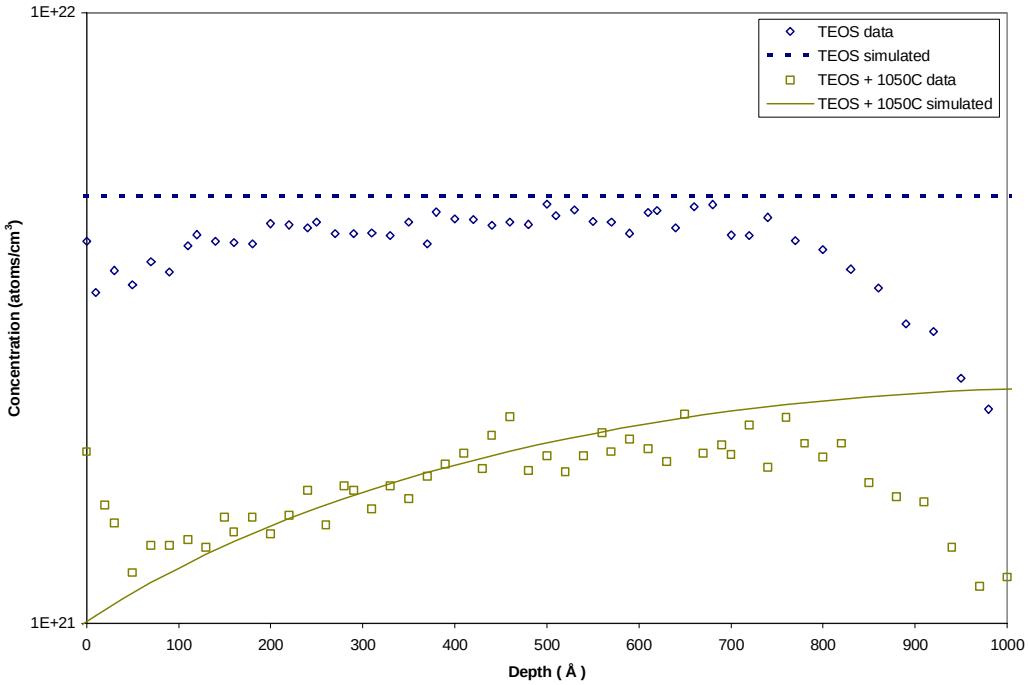

Figure 4-15: Comparison of experimental H profiles (from NRA) to simulations illustrating H out-diffusion from oxide into the ambient.

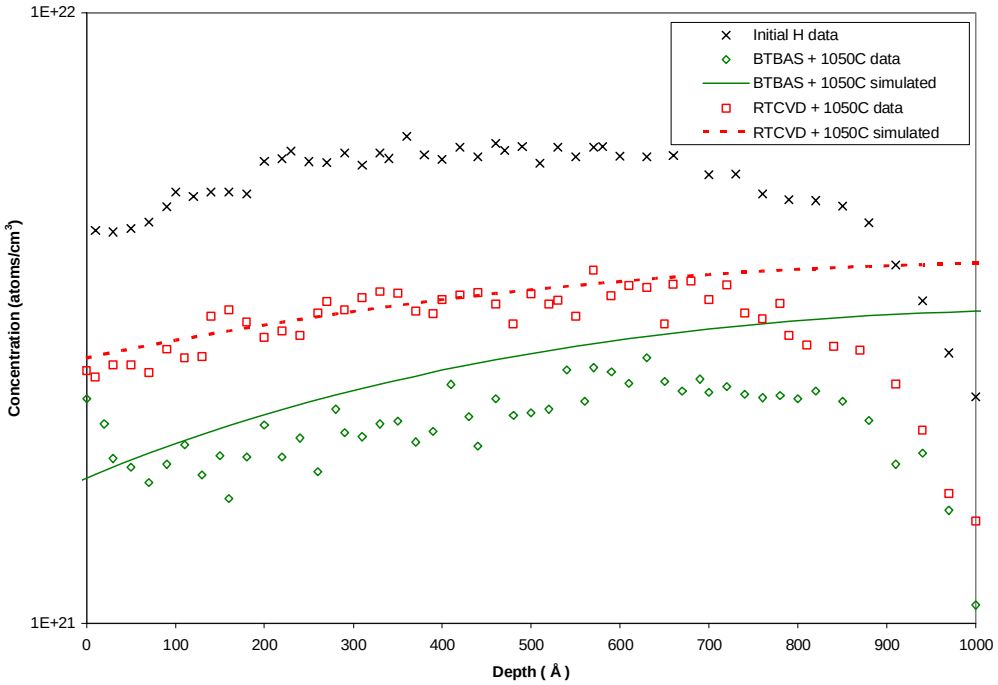

Figure 4-16: Comparison of experimental H profiles (from NRA) to simulations for an oxide capped with either BTBAS nitride or RTCVD nitride. The wafers undergo a 1050°C spike anneal after the nitride deposition. The retained H is higher in the case of RTCVD nitride.

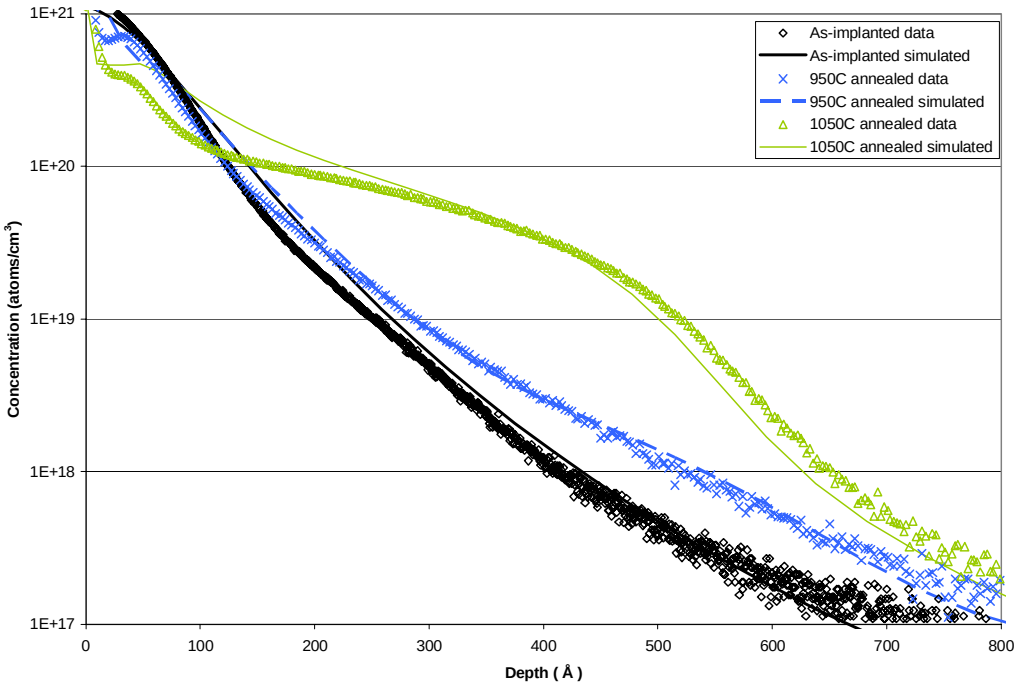

Figure 4-17: Comparison of simulations to experimental B profiles in Si (from SIMS) after 950°C or 1050°C anneal. The wafers do not undergo a nitride spacer process.

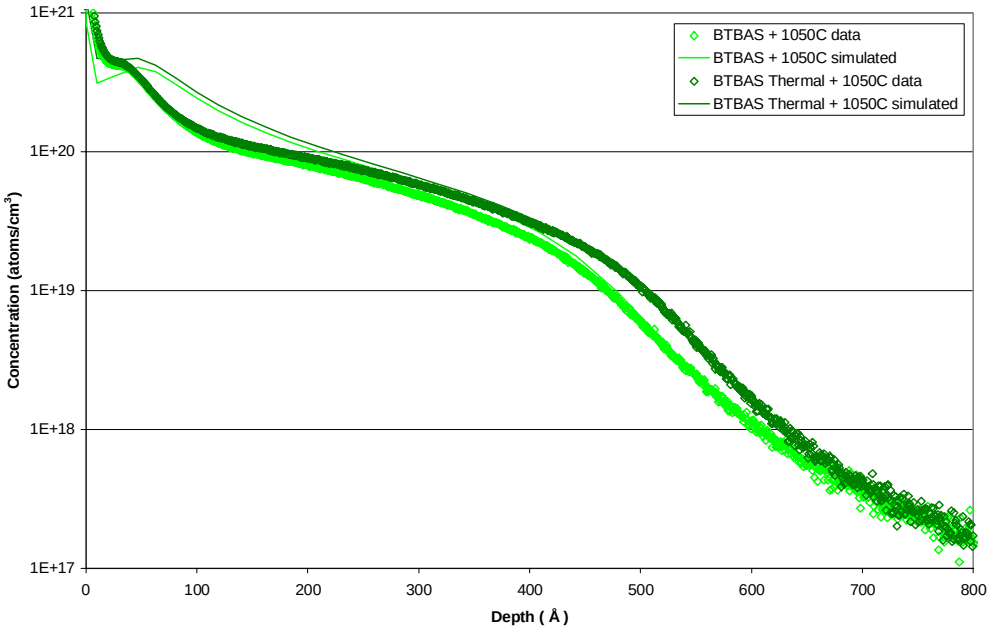

Figure 4-18: Comparison of simulations to experimental B profiles in Si (from SIMS) after a 1050°C anneal. The wafers undergo a BTBAS nitride deposition after the TEOS oxide deposition. The reference wafer undergoes the thermal budget of the BTBAS nitride process with no actual deposition.

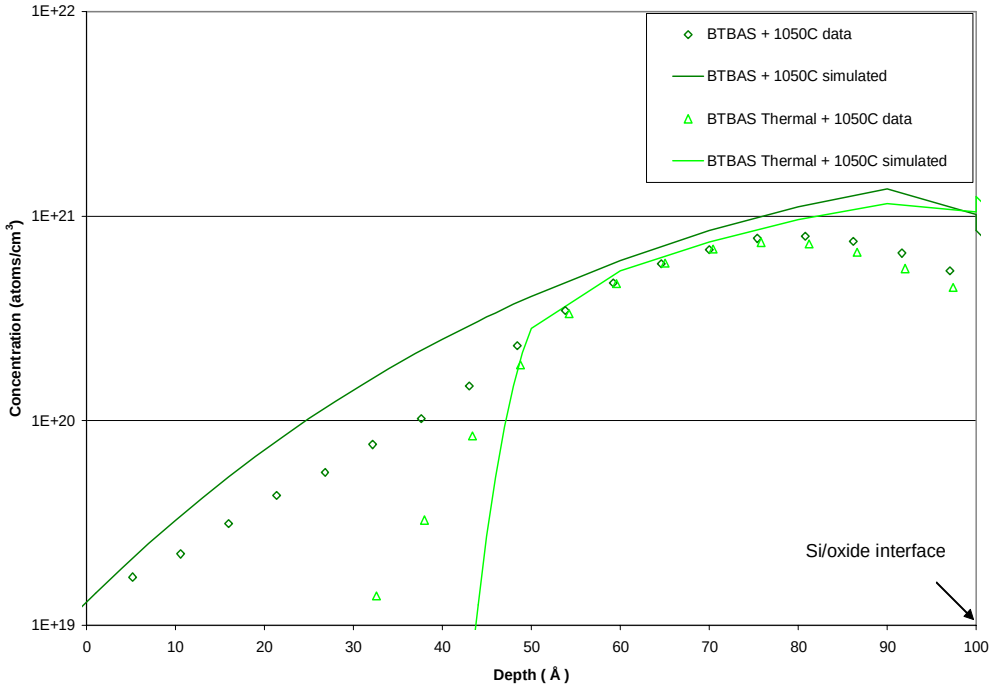

Figure 4-19: Experimental B profiles in TEOS oxide (from TOF SIMS) after the 1050°C anneal for samples from fig. 4-18 show impact of the BTBAS nitride deposition process. The model compares well with the data. Note that the actual slope from TOF SIMS data may not be quantitatively accurate but serves as a good semi-quantitative measure.

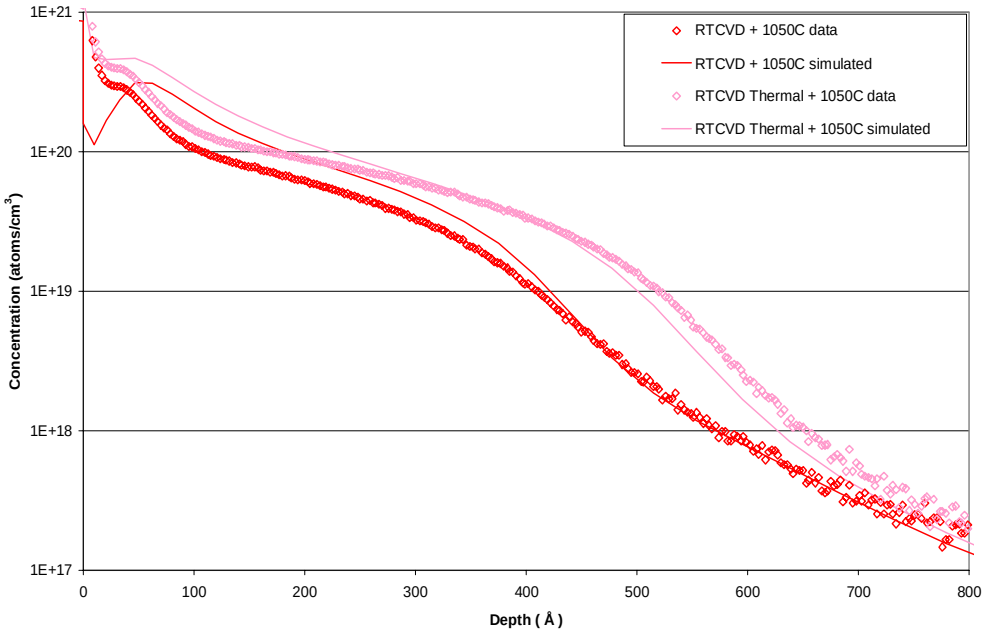

Figure 4-20: Comparison of simulations to experimental B profiles in Si (from SIMS) after the 1050°C anneal. The wafers undergo a RTCVD nitride deposition after the TEOS deposition. The reference wafer undergoes the thermal budget of the RTCVD nitride process with no actual nitride deposition.

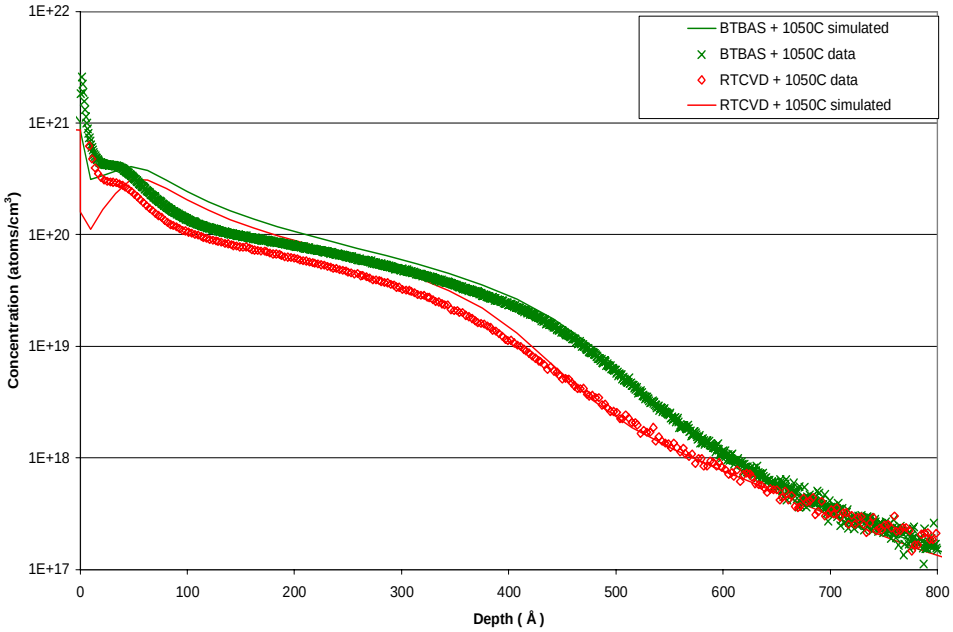

Figure 4-21: Comparison of B junctions formed using either a BTBAS nitride or a RTCVD nitride. The RTCVD nitride results in higher H concentration in the TEOS oxide leading to more B dose loss and a degraded junction.

Chapter 5

Microwave annealing for ultrashallow junction formation

5.1 Abstract

We propose a new method for activation of source/drain junctions by microwave annealing. A study with B/BF_2 implants at ultralow energies (300/500 eV) and high doses (1E15/5E15cm^{-2}) was completed. The samples were irradiated by a high power microwave source, called a gyrotron, for annealing. There appears to be some evidence of electromagnetic field-aided activation. The activation levels achieved exceed the levels reported by thermal means at the corresponding temperatures. Secondary ion mass spectroscopy was used to examine the impurity profile after ion implantation and diffusion. Spreading resistance profiling was used to examine the activated dopant profile.

5.2 Introduction

Two of the most important metrics that should be considered in evaluating the efficacy of any doping and annealing technology for the source/drain extension regions of a MOSFET are junction depth and sheet resistance (which depends on dopant activation) [1]. It is becoming increasingly clear that simply reducing the energy of conventional beam line implants, and the thermal budget of rapid thermal annealing (RTA) is not sufficient to achieve low resistance source/drain junctions. Transient enhanced diffusion (TED) of B (and to a lesser extent As) and B-enhanced diffusion as the doping in the source/drain regions is increased, to reach the low source/drain series resistance targets, is important. The

critical importance of control of the annealing ambient is emphasized by the observation of oxidation-enhanced diffusion of B and As [2].

The upper limit of active dopant concentration that can be achieved conventionally is limited by solid solubility. This is especially problematic for acceptors, where the highest solid solubility, (active peak concentration for B ~ 1E20/cm^3 at 950^o –1000^o C) is too low. It is important therefore, to examine doping and annealing techniques that could potentially exceed this concentration. The junction leakage current specifications (~ 1nA/cm^2) may be relaxed somewhat as the power supply voltages are reduced, because the threshold voltages of the MOSFET must also be reduced to meet the drive current specifications. The subthreshold leakage current is orders of magnitude greater than the source/drain leakage currents.

In this work we discuss the formation of low sheet resistance source/drain extension junctions by ultralow energy high dose implants and microwave annealing. This work is based on the fact that the energy of electromagnetic radiation can be coupled to a crystalline lattice, or even to a damaged crystalline lattice [3]. A possible coupling of the electromagnetic radiation with a local oscillator formed by the molecular configuration including the impurity may activate the dopant.

5.3 Experiment

An experimental design matrix (Table 5-1) with B/BF_2 implants at ultralow energies (300/500eV) and high doses (1E15/5E15cm^{-2}) was completed. The substrates used were 200mm n-type <100> silicon wafers, preamorphised by

a 1E15cm^{-2} Si implant at 10keV in order to reduce channeling of B. Implants were done on the HF-etched and preamorphised wafers in deceleration mode with extraction energy of 2keV for all implants, which were subsequently decelerated to 300/500 eV. Reducing the implantation energy is expected to reduce two contributions to the junction depth: the projected range of the dopant implant, Rp, as well as the TED of the dopant resulting from implantation damage which is located close to the surface. TED occurs during activation and typically becomes the dominant contribution to the junction depth when Rp is reduced to depths of the order of 10nm [4]. Due to beam current issues BF_2 was implanted instead of B for energies lower than 300 eV.

A novel source of concentrated energy, a microwave beam, was used for annealing in an effort to achieve dopant activation above the equilibrium solid solubility, with minimal diffusion. The gyrotron is a high-power cyclotron resonance maser. The aim is to take advantage of a possible 'microwave effect', which could give rise to a low-temperature, far-from-equilibrium process leading to highly conductive p^+-n junctions.

The gyrotron beam is produced from electrons gyrating in a strong magnetic field at relativistic speeds. Electrons from an electron gun are accelerated and then introduced into a resonance chamber immersed in a magnetic field produced by powerful superconducting magnets. The gyrating electrons radiate at the gyro-frequency; this is matched to the resonance chamber producing a strongly amplified wave. The gyrotron used in our experiments operates at a frequency of around 86 GHz (wavelengths λ~3.5mm), and is capable of

generating high power densities (~1kW/cm^2). The samples were irradiated at Gyrotron Technology, Inc., Pennsylvania.

Referring to figure 5-1, the gyrotron beam is introduced through a window (1) into the annealing chamber shown schematically. The chamber is purged by means of nitrogen gas inlet (2) and outlet (3) so that annealing takes place in an inert ambient. By means of mirror systems (4), the beam is focused and directed at the semiconductor sample to be annealed (5). A pyrometric temperature measurement system (6) is used for temperature measurement. The temperature is continuously monitored and in order to change the temperature the power density of the microwave could be tuned. As the ionized impurities become substitutional in the lattice, eddy currents in the doped regions will also be induced, leading to increased localized heating [3].

Table 5-2 shows the different annealing conditions that the samples were subjected to in our experiments and the sheet resistance of the annealed samples. To examine the impurity profile of ion implantation and diffusion, secondary ion mass spectrometry (SIMS) is widely used. For measuring the junctions shallower than 20nm, the primary ion energy must be optimized and techniques such as Oxygen bleeding, which have been discussed extensively [5], used. The resultant dopant profiles were measured using Adept-1010, quadrupole SIMS. The primary beam was O_2^+ with an energy of 700eV incident at an angle of 45^o. An oxygen leak was used in the chamber to eliminate the sputtering rate differences as one crosses the silicon-native oxide interface. Spreading resistance profile (SRP) measurements were done to measure the active carrier concentrations.

5.4 Results and Discussion

Figures 5-2 and 5-3 show a comparison between the simulated UT-MARLOWE and measured SIMS profiles for B and BF_2 implants, respectively. The integrated dose, as obtained from SIMS, matches relatively well with the dose calculated from UT-MARLOWE profiles for all B implants at 300/500eV. However, there is a huge difference in doses between the UT-MARLOWE prediction (2.13E15/cm^2) and the SIMS measurement (0.59E15/cm^2) for the 5E15BF2/cm^2 implant at 300eV.

The sputtered dose of silicon, as per UT-MARLOWE simulations, is low (about 1/10 of implant dose); so it is not likely that Si sputtering can account for the entire B dose loss. The simulations also show that the F dose at the surface exceeds the Si surface density, perhaps thereby changing the surface properties drastically. A large number of scattering events between B and F, B and B, and F and F, none of which are accounted for in UT-MARLOWE, can be expected. Similar reports on high dose P and As have suggested that for light atoms other dopant loss mechanisms such as re-sputtering and back-scattering must be considered [6].

A look at the SIMS and SRP profiles (figures 5-4 and 5-5 respectively) reveals that the concentrations of B that go into solution for the given anneals are much higher than the thermodynamic equilibrium solubility limits at the corresponding temperatures (760-780^oC). At annealing temperatures of 800^oC, peak active dopant concentrations up to 3E18cm^{-3} have been reported [7]. The levels of active dopant concentrations (2E19/cm^3-1E20/cm^3) seen with microwave

anneals at such low temperatures might perhaps be as a result of some kind of electromagnetic coupling action of the gyrotron beam with both the damage and dopant atoms. Up to 40% of the implanted dose was activated.

Another interesting observation is that more the as-implanted dose, higher the peak active concentration, although the annealed profiles might have similar retained doses. With the B implants one can clearly see that higher the implant energy/implant dose, deeper the junctions. However, the BF_2 implants at 300eV (equivalent B energy of 66eV) do not follow the same implant energy-junction depth relation as B implants. Despite much lower equivalent B implant energy in the 300eV BF_2 implants at doses of 1E15/cm^2 and 5E15/cm^2, the profiles are deeper than the 300eV B implant at a dose of 1E15/cm^2. The role of the Si surface in the annihilation of point defects has been studied for ultrashallow p+/n junctions [8]. The presence of F doses higher than the Si surface density in the case of an implanted BF_2 dose of 5E15/cm^2, as shown by UT-MARLOWE simulations, might make the Si surface less efficient as a sink for the removal of point defects. However, the BF_2 implants show shallower profile for the 5E15/cm^2 dose than for the 1E15/cm^2 dose, which remains unexplained.

To study the effect of microwave annealing on activation and deactivation of implanted B in Si, the anneal time was varied. Figures 5-6 and 5-7 show the effect of increase in anneal time from 15s to 30s. Pelaz et al. [7], have demonstrated a low B activation (~25%) for short anneals (<10s) that slowly increases with time up to 40% at 1000s. Our experimental results show that the peak active carrier concentrations, as measured by SRP, decrease with time

although the total activated dose increases with time (figure 5-7). A comparison between the active carrier profiles shows that the active carrier profile after the 30s anneal is twice as deep as that after the 15s anneal for both implant conditions. However, the SIMS profiles do not show a commensurate increase in the junction depths. The implants with a dose of 1E15B/cm^2 show shallower annealed profiles as compared to implants with a dose of 5E15B/cm^2 (figure 5-6). This could perhaps be explained on the basis of concentration dependence of diffusivity. The SIMS profile for the annealed sample implanted with a dose of 1E15B/cm^2 at 300eV shows the shallowest profile of all the implants because of surface proximity effects and least enhancement of diffusivity due to concentration. For both implant conditions shown in figure 5-4, the active carrier peak concentrations are higher after the 15s anneal than after the 30s anneal. It might be possible that a long anneal tends to drive the metastable system towards thermodynamic equilibrium, thus decreasing the peak active concentration.

5.5 Summary

We have proposed a novel method to activate dopants above the thermodynamic solid solubility limits. A highly abrupt, high-concentration profile is needed in the source/drain regions for device scaling. The maximum doping concentration is critical since higher charge concentrations permit shallower junctions while maintaining low resistance. By increasing the power density of the microwave, this technique might have the potential of activating the dopants to levels beyond those achievable by present RTA/Spike annealing processes, and thereby forming highly conductive junctions.

5.6 References

1. P. Kohli, et al., Journal of Electronic Materials, Vol 31, 214, 2002.
2. D. Downey, J. Liu, Materials Research Society Proceedings, Spring 1999.
3. A. Splinter, et al., US Patent 4303455.
4. A. Agarwal, et al., Mat. Sci. Semicon. Proc., 1, 17, 237, 1998.
5. S. P. Smith, et al., Proc. on 11th Int. Conf. on Ion Implantation Tech., 599 1996.
6. K. Egusa, K. Shibahara, Ion Implantation Technology Proceedings 1998.
7. L. Pelaz, et al., Applied Physics Letters, 75, 5, 662, 1999.
8. A.Sultan, S.Banerjee, Proc. on 11th Int. Conf. on Ion Implantation Tech., 615, 1996.

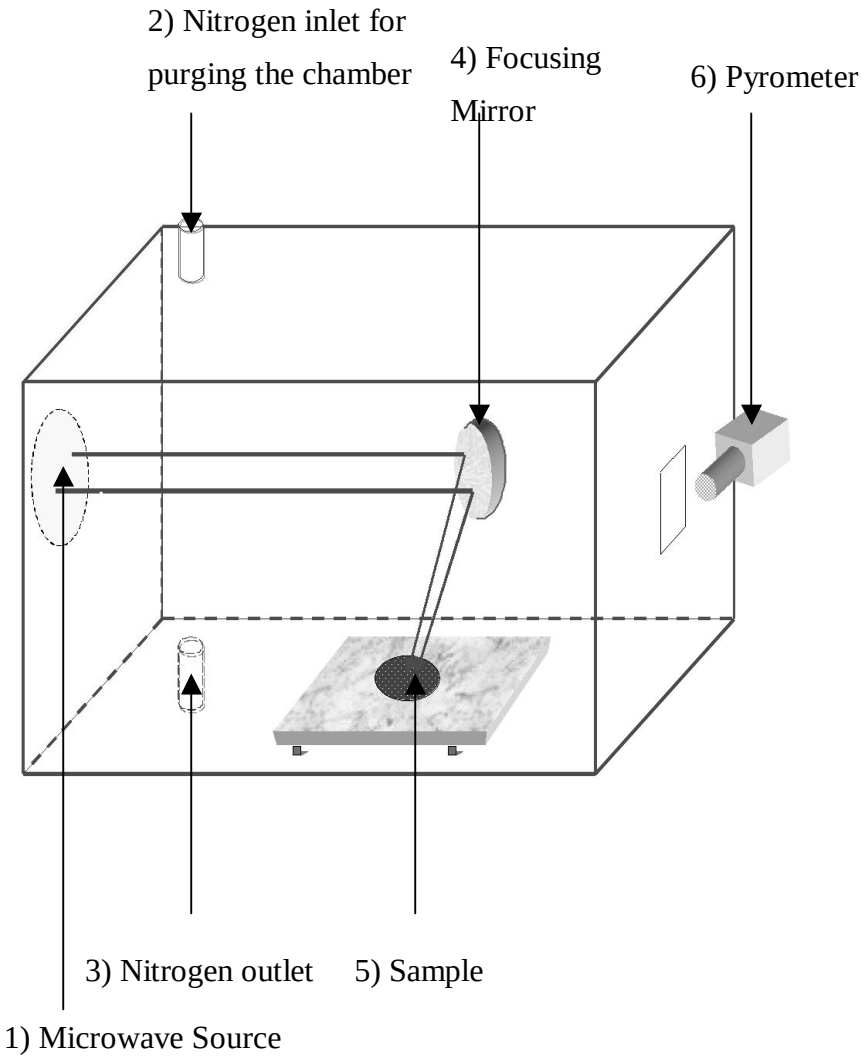

Fig 5-1. Microwave annealing setup. A novel source of concentrated energy, a gyrotron beam, is used for annealing.

Species	Dose (atoms/cm^2)	Energy (eV)
B	1E+15	300
B	5E+15	300
B	1E+15	500
B	5E+15	500
BF2	1E+15	300
BF2	5E+15	300

Table 5-1. Ultra-low energy implant matrix.

Sample	Process Time (s)	Process Temp (°C)	Sheet Resistance (Ohms/sq)
1E15B/300eV	30	760	468
5E15B/300eV	30	760	373
1E15B/500eV	30	775	496
5E15B/500eV	30	780	194
1E15BF2/300eV	30	765	1210
5E15BF2/300eV	30	780	872
1E15B/300eV	15	770	712
5E15B/300eV	15	760	N/A
1E15B/500eV	15	760	824

Table 5-2. Annealing details for the ultra-low energy implants.

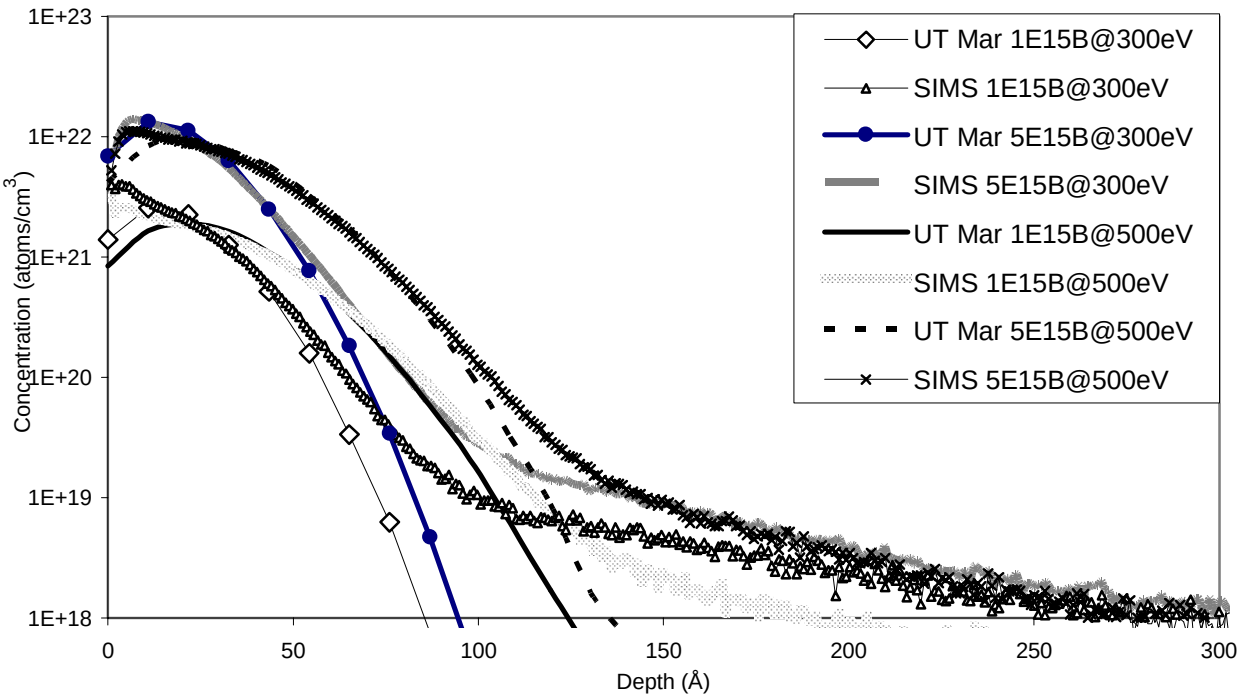

Fig 5-2. A comparison of as implanted SIMS Vs. UT MARLOWE as predicted for 1E15/5E15 atoms/cm^2 B implants at 300/500eV.

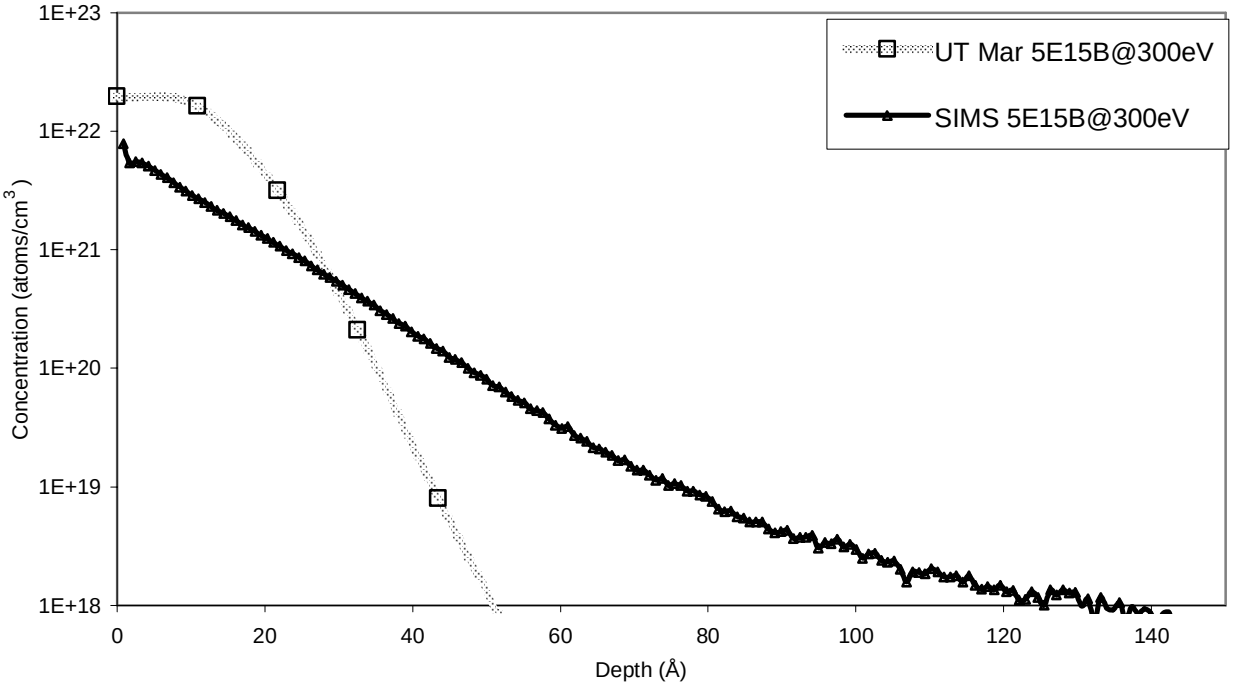

Fig 5-3. A comparison of as implanted SIMS Versus UT MARLOWE as predicted for 5E15 atoms/cm^2 BF_2 implants at 300eV.

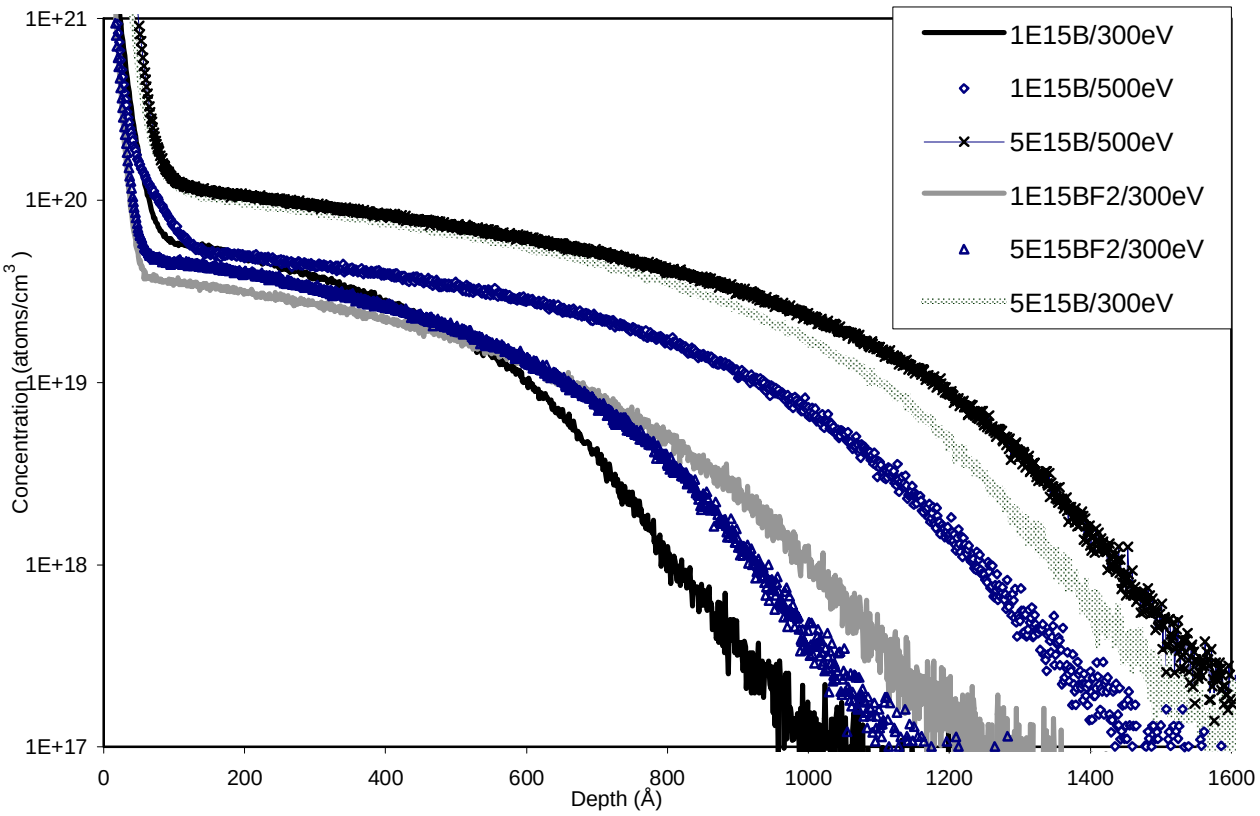

Fig 5-4. SIMS profiles of microwave annealed (30s) ultra-low energy implanted B/BF_2 samples.

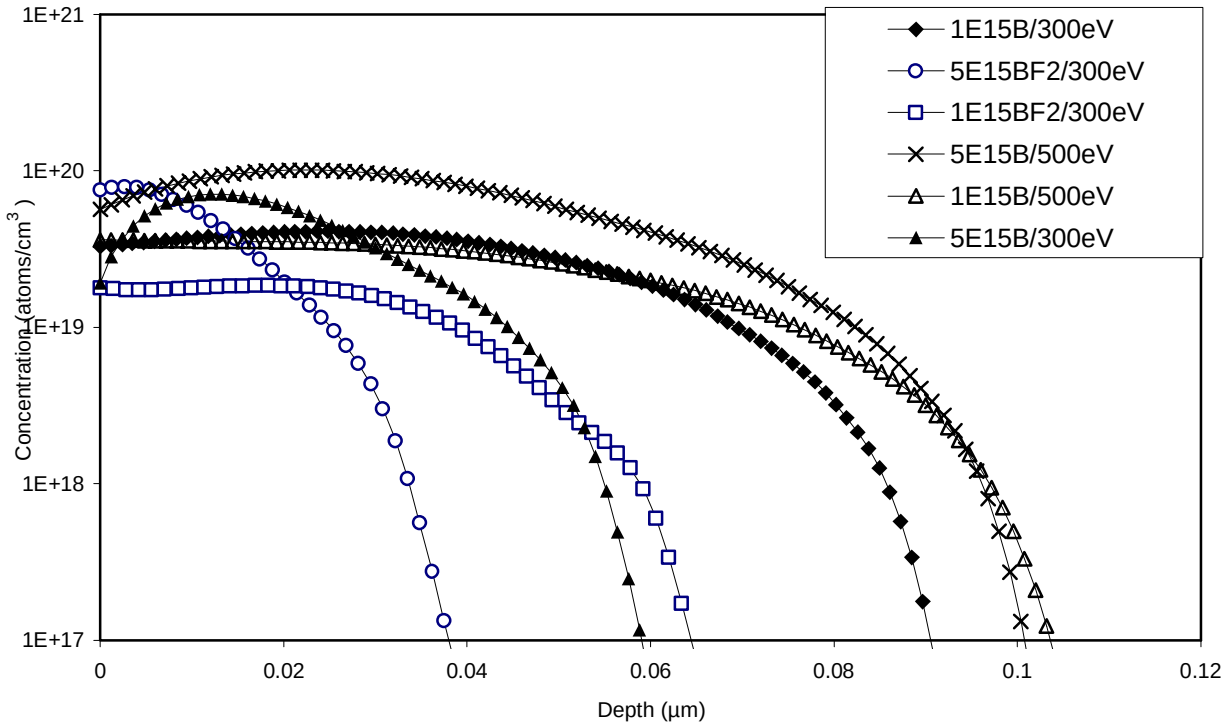

Fig 5-5. SRP profiles of microwave annealed (30s) ultra-low energy implanted B/BF_2 samples.

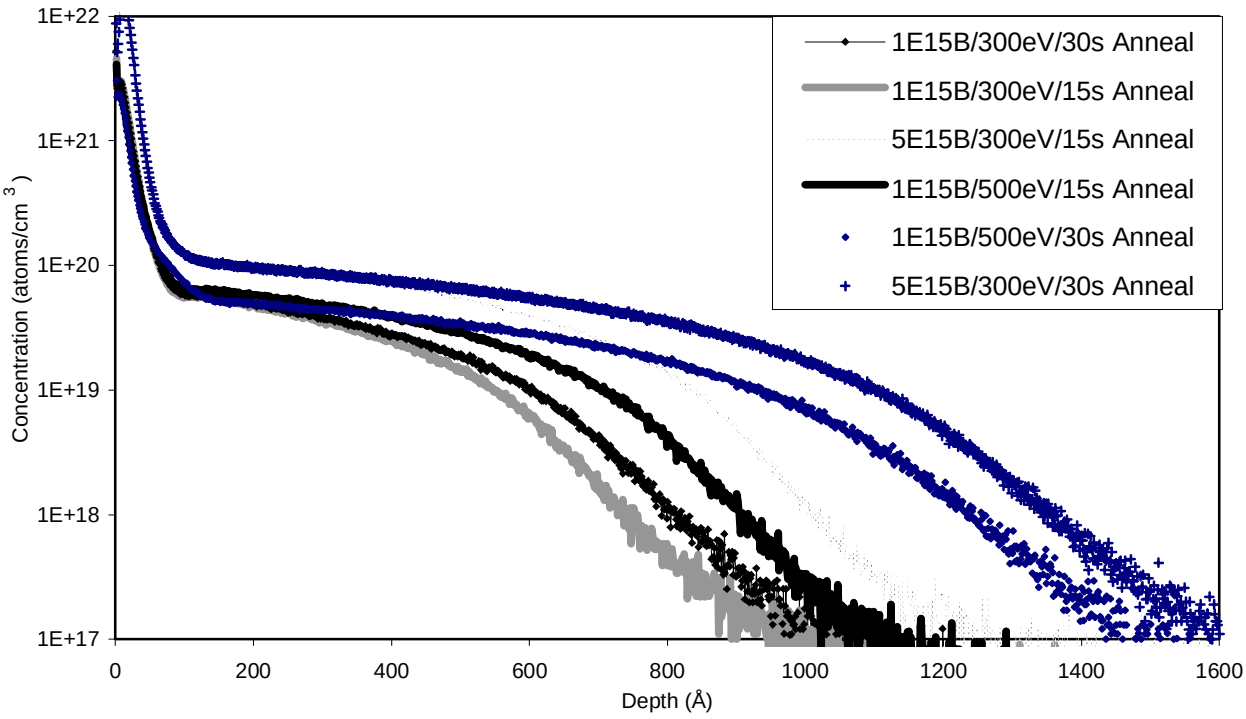

Fig 5-6. SIMS results showing the effect of anneal time (15s vs. 30s). Longer anneals diffuse B deeper, without changing the level of the plateau in the SIMS profile.

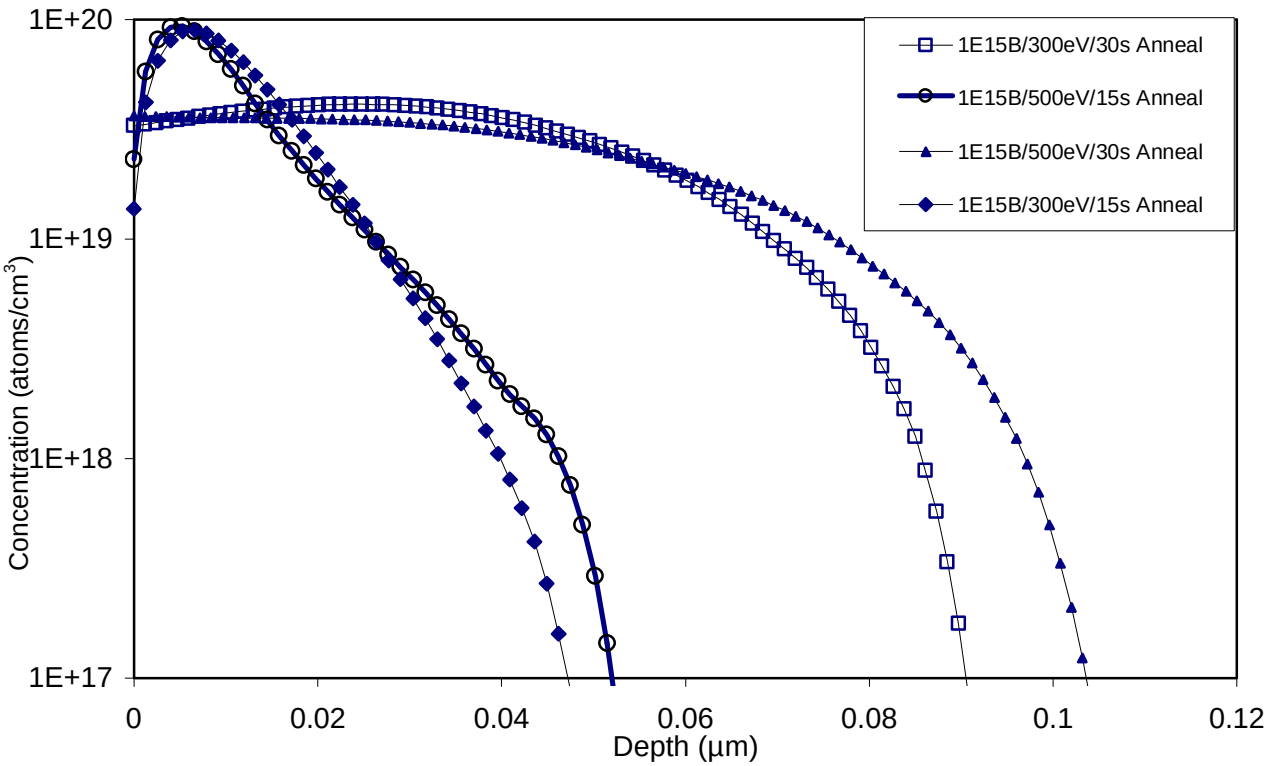

Fig 5-7. SRP analysis showing effect of anneal time (15s vs. 30s). Longer anneals decrease the peak active concentration and result in higher total activated dose.

Chapter 6

Conclusions and Future work

Our aim in this work was to understand and model the evolution of B ion implanted source/drain extension profile in silicon during the front end CMOS device fabrication.

6.1 Conclusions

The following conclusions constitute the contributions of this study –

1. It has been found that the B dopant atoms and point defects interact very strongly with thin films. Thinner silicon oxides result in shallower junctions. It has been suggested that annealing in an inert ambient results in an interstitial undersaturation at the Si/SiO_2 interface. A physical model taking into account the segregation of excess Si between the oxide and the Si substrate and diffusion of that excess Si in the oxide, has been suggested to explain the effect of oxide thickness on junction depth.

2. It has been discovered that the nitride spacer results in a B dose loss from the Si into the oxide during annealing. The as-deposited TEOS oxide has been shown to have a very high concentration of H, which diffuses out readily upon annealing. However, the presence of nitride acts as a diffusion barrier for the out-diffusing H, resulting in high concentration of retained H in the TEOS even after annealing. The presence of this high level of retained H causes an enhancement of

B diffusivity in the oxide and thereby enhances the amount of B dose loss into the oxide from the Si.

3. It has been demonstrated that the silicon nitride spacer process chemistry affects the B profile in silicon and the related dose loss of B from the Si into the silicon dioxide. This is reflected as a dramatic change in the junction depth, junction abruptness and junction peak concentration for the different nitride chemistries. It has been found that the different nitride chemistries result in different concentrations of H in the silicon dioxide during the final source/drain anneal. The different concentrations of H in the oxide result in different extents of enhancement of B diffusivity in oxide and thereby result in different amounts of dose loss of B from Si into oxide. In this work we show this dose loss can be minimized and the junction profile engineered by choosing the desirable nitride chemistry. BTBAS nitride chemistry results in the most desirable B profile, out of all the nitride chemistries considered in this work.

4. A model has been developed to explain the effect of source/drain spacer process on B source/drain extension formation. A diffusion model for H in the source/drain spacer has been suggested and combined with a model for B diffusion. The model successfully predicts the B junction depth and dose loss during fabrication of ultra-shallow junctions.

5. A novel method to activate dopants above the thermodynamic solid solubility limits has been proposed. A gyrotron beam, a source of concentrated energy, has been used for annealing in an effort to achieve dopant activation above the equilibrium solid solubility, with minimal diffusion. The aim is to take

advantage of a possible 'microwave effect', which could give rise to a low-temperature, far-from-equilibrium process leading to highly conductive p^+-n junctions. There appears to be some evidence of electromagnetic field-aided activation, though the results are not conclusive. The activation levels achieved exceed the levels reported by thermal means at the corresponding temperatures.

6.2 Suggestions for Future Work:

This work took a detailed look at the effect of different front-end process steps on the B profile. Fundamental information has been obtained on interactions of dopant atoms and point defects during these different process steps. An advanced annealing technique for ultra-shallow junction formation has been demonstrated. Some suggestions for future efforts are listed below –

1. The effect of different nitride chemistries on the H concentration in the oxide after annealing has been investigated. A study of H diffusivity through nitrides with different chemistries is an important area for future work. It is necessary to gain a fundamental understanding of the effect of different nitride parameters (chemistry, density, deposition temperature, etc) on the H diffusivity in the nitride. This work has been limited to three different nitride chemistries. The study could be further extended to more nitride chemistries. The effect of deposition temperature on the B dose loss and resultant profile is an interesting area of study.

2. An additional area of interest that becomes increasingly important as device dimensions shrink is the two-dimensional aspect of the effect of nitride

spacer on B diffusion. The lateral extent of diffusion effects may become a limiting factor in further reducing device dimensions.

3. Atomistic calculations to understand the enhancement of B diffusivity in oxide in the presence of H are required. Also, calculations for excess Si diffusivity in oxide, and segregation coefficient of excess Si atoms between oxide and Si, are needed.

4. Microwave annealing requires extensive studies. By increasing the power density of the microwave, this technique might have the potential of activating the dopants to levels beyond those achievable by present RTA/Spike annealing processes, and thereby forming highly conductive junctions.

5. Another area of interest is the segregation and diffusion properties of different oxides – thermally grown and deposited.

Bibliography

Chapter 1 References

1. P. Packan, MRS Bulletin, 18, June 2000.
2. S. Biesemans, S. Kubicek, K. D. Meyer, Proceedings of Challenges in Predictive Process Simulation, Germany, 17-20 Aug, 1997 (www.ihp-ffo.de/chipps/97).
3. M. Duane, presentation at NIST Characterization and Metrology workshop, March 1998.
4. J. Dabrowski, H.-J. Mussig, M. Duane, S. T. Dunham, R. Goossens, H.-H. Vuong, Advances in Solid State Physics 38, 565, 1999.
5. M. Ada-Hanifi, M. Bonis, Ch. Verove, M. T. Basso, N. Revil, M. Haond, M. Lecontellec, Proceedings of the 27th European Solid State Device Research Conference, Stuttgart, Gemany, 22-24 September 1997.

Chapter 2 References

1. P. Packan, MRS Bulletin, 18, June 2000.
2. S. Dunham, J. Appl. Phys., Vol 71, No. 2, 685, 1992.
3. R. Lindsay, et al., Proceedings Ultra Shallow Junctions 2001, 255, 2001.
4. M. Miyake, J. Appl. Phys., Vol 57, No. 6, 1861, 1985
5. R. Kasnavi, et al. Mat. Res. Soc. Symp. Vol. 610, B4.3, 2000.
6. P. Kohli, et al., (to be published) J. Va. Sci. Technol., Jan 2004.
7. R. Tromp, et al. Phys Rev lett. 55, 2332, 1985.
8. K. Hofmann, et al. Appl. Phys. Lett. 49, 1525, 1986.
9. K. Hofmann, et al. J.Electrochem. Soc. 134, 240, 1987.

10. G. W. Rubloff, et al. Phys. Rev. Lett. 58, 2379, 1987.
11. M. Liehr, et al. J.Va. Sci. Technol. A 5, 1559, 1987.
12. S. T. Ahn, Ph.D. Thesis, Stanford University, 1988.
13. R. Angelucci et al. J. Electrochem. Soc. 134, 3130, 1987.
14. P. A. Packan, Ph.D. Thesis, Stanford University, 1991.
15. D. J. Eaglesham et al. Appl. Phys. Letts. 70 (24), 3281, 1997.
16. R. Fair, IEEE Electron Device Letters, Vol. 17 (5), 242, 1996.
17. Y. Shacham-Diamand, W. G. Oldham, J. Elect. Mater., 15, 229, 1986.
18. T. Aoyama et al., J.J.Appl. Phys. Vol. 38, 2381, 1999.
19. R. B. Fair, IEDM Tech. Digest, 85, 1995.

Chapter 3 References

1. S. T. Dunham, IEDM Tech. Digest, 501, 1998.
2. M. Ada-Hanifi et al., Proceedings of the 27th European Solid State Device Research Conference, Stuttgart, Germany, 1997.
3. W. A. Lanford and M. J. Rand, J. Appl. Phys., 49 (4), 2473, 1978.
4. R. Kasnavi et al., Mat. Res. Soc. Symp. Vol. 610, B4.3, 2000.
5. M. Aziz, Defect and Diffusion Forum, 153, 1998.
6. S. Tokitoh, et al., IRPS Technical Digest, 307, 1997.
7. S. Inaba, et al., IEEE Transactions on Electron Devices, Vol. 46, 6, 1999.
8. R. Fair, IEEE Electron Device Letters, Vol. 17 (5), 242, 1996.

Chapter 4 References

1. S.T. Dunham, IEDM Tech. Digest, 501, 1998.
2. P. Kohli, et al., (to be published) J. Va. Sci. Technol., Jan 2004.
3. Y. Shacham-Diamand, W. G. Oldham, J. Elect. Mater., 15, 229, 1986
4. T. Aoyama, et al., J.J.Appl. Phys. Vol. 38, 2381, 1999.
5. R. B. Fair, IEDM Tech. Digest, 85, 1995.
6. R. Fair, IEEE Electron Device Letters, Vol. 17 (5), 242, 1996.
7. M. Aziz, Defect and Diffusion Forum, 153, 1998.
8. S. T. Dunham, C. D. Wu, J. Appl. Phys. Vol. 78 (4), 2362, 1995.
9. D. Mathiot, J. C. Pfister, J. Appl. Phys. Vol. 66 (2), 970, 1989.

Chapter 5 References

1. P. Kohli, et al., Journal of Electronic Materials, Vol 31, 214, 2002.
2. D. Downey, J. Liu, Materials Research Society Proceedings, Spring 1999.
3. A. Splinter, et al., US Patent 4303455.
4. A. Agarwal, et al., Mat. Sci. Semicon. Proc., 1, 17, 237, 1998.
5. S. P. Smith, et al., Proc. on 11th Int. Conf. on Ion Implantation Tech., 599 1996.
6. K. Egusa, K. Shibahara, Ion Implantation Technology Proceedings 1998.
7. L. Pelaz, et al., Applied Physics Letters, 75, 5, 662, 1999.
8. A.Sultan, S.Banerjee, Proc. on 11th Int. Conf. on Ion Implantation Tech., 615, 1996.

Vita

Puneet Kohli was born in Chandigarh, India, on July 28th, 1976. He received his Bachelor of Engineering in Metallurgical Engineering from Regional Engineering College, Trichy in 1998. In September 1998, he entered the Graduate School of The University of Texas at Austin. Since then, he has been working towards his Ph.D. degree in Electrical and Computer Engineering. During his Graduate studies, he has contributed the following technical articles:

1. P. Kohli, A. Jain, H. Bu, S. Chakravarthi, C. Machala, S. T. Dunham, and S. K. Banerjee, "Effect of Nitride Sidewall Spacer Process on B Dose Loss in Ultra Shallow Junction Formation", Submitted (after revision) J. Vacc. Sci and Tech. (2004).
2. P. Kohli, S. Chakravarthi, A. Jain, H. Bu, M. Mehrotra and S. K. Banerjee, "Fundamental Characterization and Modeling of the effect of Different Nitride Sidewall Spacer Processes on B Dose Loss in Ultra Shallow Junction Formation", in Preparation, to be submitted to Transactions on Electron Devices.
3. P. Kohli, S. Chakravarthi, A. Jain, H. Bu, S. T. Dunham and S. K. Banerjee, " Interactions of B Dopant Atoms and Point Defects with SiO_2 Films During Annealing for Ultra Shallow Junction Formation", in Preparation, to be submitted to J. Appl. Phys.

4. P. Kohli, S. Ganguly, T. Kirichenko, Hong-Jyh Li, S. K. Banerjee, E. Graetz and M. Shvelev, “Microwave Annealing for Ultra Shallow Junction Formation”, J. Elect. Mat. 31 (3), March 2002.
5. P. Kohli, A. Jain, H. Bu, S. Chakravarthi, C. Machala, S. T. Dunham, and S. K. Banerjee, “Effect of Nitride Sidewall Spacer Process on B Dose Loss in Ultra Shallow Junction Formation”, Ultra Shallow Junction-2003, California, April 2003.
6. P. Kohli, S. Ganguly, T. Kirichenko, Hong-Jyh Li and S. K. Banerjee “Advanced Annealing for Ultra-Shallow Junctions”, Ultra Shallow Junctions-2001, Napa, California, April, 2001.
7. P. Kohli, Hong-Jyh Li, S. Ganguly, T. Kirichenko, B. Murto, E. Graetz, P.Zeitzoff, M.Pawlik, P.B.Merrill and S. K. Banerjee “Co-implantation and High Ramp Rate Rapid Thermal Annealing for Ultra-Shallow Junctions” 197th Electrochemical Society Conference, Toronto, Canada., March 2000.
8. Hong-Jyh Li, P. Kohli, S. Ganguly, T. A. Kirichenko, S. Banerjee and P. Zeitzoff, " B Diffusion in Silicon in the Presence of Other Species" Appl. Phys. Lett. Vol. 77, No. 17, pp.2683-2685, 23 Oct. 2000.
9. Hong-Jyh Li, P. Kohli, S. Ganguly, T. Kirichenko, P. Zeitzoff, K. Torres and S. K. Banerjee, "B Diffusion and Activation in the Presence of Other Species" IEDM 2000 Technical Digest pp.515-518.
10. Hong-Jyh Li, P. Kohli, S. Ganguly, T. Kirichenko, P. Zeitzoff, K. Torres and S. K. Banerjee, "B Diffusion and Activation in the Presence of Other

Species" International Conference on Computational Nanoscience, South Carolina March, 2001 (ICCN 2001) (Invited).

Permanent address: C/II/2351 Vasant Kunj,
N. Delhi, India -110070

This dissertation is typed by the author.